TAMPEREEN TEKNILLINEN YLIOPISTO
TAMPERE UNIVERSITY OF TECHNOLOGY

Jukka-Pekka Raunio

Quality Characterization of Tissue and Newsprint Paper based on Image Measurements; Possibilities of On-line Imaging

Julkaisu 1270 • Publication 1270

Tampere 2014

Tampereen teknillinen yliopisto. Julkaisu 1270
Tampere University of Technology. Publication 1270

Jukka-Pekka Raunio

Quality Characterization of Tissue and Newsprint Paper based on Image Measurements; Possibilities of On-line Imaging

Thesis for the degree of Doctor of Science in Technology to be presented with due permission for public examination and criticism in Festia Building, Auditorium Pieni Sali 1, at Tampere University of Technology, on the 12th of December of 2014, at 12 noon.

Tampereen teknillinen yliopisto - Tampere University of Technology
Tampere 2014

ISBN 978-952-15-3416-4 (printed)
ISBN 978-952-15-3459-1 (PDF)
ISSN 1459-2045

Abstract

The paper industry is at a turning point worldwide. The consumption of printed products is assumed to decrease significantly because of electronic gadgets and the internet. Furthermore, the importance of forests and woods in the global warming issue is significant and causes limitations to papermakers to produce cheap products. However at the same time the end users demand high quality products at reasonable prices. Therefore, the cost-efficiency in papermaking process will play a more significant role in the future.

This thesis proposes a set of image analyses and methods which can be implemented in present on-line imaging systems, without a massive effort. The imaging systems can measure the paper accurately and in a versatile manner which improves the control of the paper machine and thus enhances the cost efficiency of the papermaking process.

The creping process which generates the wavy microstructure to tissue paper - a creping pattern - mainly determines the quality properties of the tissue paper. This thesis applied the photometric stereo method with 2D spectral analysis to characterize the versatile properties of creping pattern. The creping process also affects the free fiber ends and pinholes in tissue paper. The free fiber end detection method was based on the number of shadows of fibers. The shadows were made visible by removing the creping pattern from the images of tissue paper with photometric stereo method. The pinhole detection method was based on the linearly polarized light transmitted through paper and the camera with rotating polarizer. It is anticipated based on the thesis that the characteristics of creping patterns and the number of pinholes are possible to be measured on-line by using existing imaging technology in paper machines.

The web inspection systems installed on paper machines measure the web-wide light transmittance of paper. At present they detect and classify defects such as holes and dirt particles and estimate some simple paper characteristics such as light transmittance and formation. This thesis proposed methods to utilize the on-line transmittance images more versatile in newsprint grade. The cross directional shrinkage profile and the small scale structural characteristics such as the light transmittance, formation, length scale of formation and orientation parameters of paper were estimated based on the statistical measures and the features of frequency distribution in the 2D spectrum. The uncertainty of basis weight estimate approximated from the transmittance images was studied with correlation analysis and the Kubelka-Munk equations. It was noticed that the initial quality of the on-line images was insufficient for evaluating formation characteristics and basis weight reliably. However capturing a complete set of calibration and reference images will also enable the formation and basis weight estimation of paper and thus increasing the value of web inspection system significantly.

Preface

The motto in my life has been that everything is possible if you try really hard. This thesis is one proof of the power of that sentence. After I accomplished my diploma thesis in 2006 I thought that I am not a researcher kind of fellow at all and I went to a company to do "real" work. However, after one year I heard about the open vacancy in University and I thought that I give a shot. Now seven years later my thesis is ready. It took a little bit longer than I expected but it doesn't matter because I have enjoyed significantly of these years and at the moment I couldn't imagine a better way to spend that time.

I have been learning a lot of scientific world during these years. The most important reason for learning has been my supervisor Professor Risto Ritala. He has patiently fixed my unscientific sentences from my publications and at the same time he has guided my thoughts in more scientific and systematic direction. Another important person for learning has been my supervisor's counterforce laboratory engineer Heimo Ihalainen. He has suggested several extraordinary (unscientific and scientific) ideas for my thesis and a couple of those have been brilliant. Some of these ideas Heimo suggested when I was sitting on his office's rocking chair. The swinging motion obviously eases the reception of strange ideas. Anyway, everyone should sit on his rocking chair at least once and discuss about the research, science or something else with Heimo. It is worth trying.

To get this thesis to its final stage has been required a lot of feedback and comments from several people. First, I want to thank Professor Erkki Ikonen from Aalto University and Dr. Steven Keller from Miami University for pre-examining my thesis. Also, I want to thank Dr. Ville Tirronen from the University of Jyväskylä who has helped me in developing of image processing algorithms. Furthermore, I want to thank tissue paper experts Mikko Mäkinen, Henry Skoog, and Clay Campbell from Kemira who have been inventing great research ideas and making my work more concrete. Also, I want to express my gratitude to helpful people in Metso Paper, Metso Automation, and Viconsys who made possible the on-line data collection from paper machines. Without funding this work would not have been possible. Therefore I want to thank Finnish forest cluster, Tekes, Metso Paper, Metso Automation and Kemira for giving me this opportunity.

Next, I want to thank all my colleagues from the Department of the automation science and engineering for giving me mental support during these years. Especially I want to thank Marja Mettänen for making my thesis more readable. Also, I want to thank Matti Jukola and Kalle Marjanen for sharing their know-how of image processing and analyses with me. Last but not least I want to thank the grand old men duo Antti Vehkaoja and Timo Salpavaara for sharing their long post graduate student experience and making my time more enjoyable at work.

Finally, I want to thank my whole family for supporting me during this thesis. Especially I want to thank my lovely kids, Iisa and Aapo, who can turn my thoughts from work topics to more relevant things immediately when I open the front door at home. Last I want to thank my wife for her unconditional love and trust during these years. Our journey is just about to begin.

Tampere, December 2014

Jukka-Pekka Raunio

List of publications

I Raunio, J.-P. and Ritala, R. (2009): Analysis of paper structure based on light transmittance and basis weight measurements, *In CD-Proceedings of Papermaking Research Symposium 2009*, Kuopio, Finland, 2009, 11 pages.

II Raunio, J.-P., Tirronen, V., Ritala, R., Nironen, I., Rossi, T. and Kärkkäinen, T. (2010): Web-wide diagnostics of paper properties based on fault detector system images, *In CD-Proceedings of Tappi Papercon2010*, Atlanta, USA, 2010, 13 pages.

III Raunio, J.-P. and Ritala, R. (2010): 2D basis weight estimation based on light transmittance imaging, *In CD-Proceedings of Control Systems 2010*, Stockholm, Sweden, 2010, 6 pages.

IV Raunio, J.-P. and Ritala, R. (2012): Simulation of creping pattern in tissue paper, *Nordic Pulp and Pap. Res. J.*, Vol. 27, No. 2, pp. 375-381.

V Raunio J.-P., Tirronen, V., Lehtoranta, I. and Ritala, R. (2013): Web-wide imaging of paper; Analyzing the potential of on-line light transmittance measurement in quality control and diagnostics of paper, *Nordic Pulp and Pap. Res. J.*, Vol. 28, No. 1, pp. 137-146.

VI Raunio, J.-P. and Ritala, R. (2013): Potential of full-web imaging in measuring web structure on-line, *J-For*, Vol. 3, No. 1, pp. 10-16.

VII Raunio, J-P and Ritala R. (2013): Method for detecting free fiber ends in tissue paper, *Meas. Sci. Technol.*,Vol. 24, No. 12, pp. 1-6. 125206

The publications IV, VI, and VII are related to characterization of the tissue paper. Similarly, the publication II, III, and V are all related to on-line imaging of newsprint paper.

Contents

List of abbreviations

MD	Machine direction. Running direction of paper in the paper machine.
CD	Cross direction of paper machine. Perpendicular to the machine direction.
1D	One-dimensional
2D	Two-dimensional
LED	Light-emitting diode
CCD	Coupled charged device. A light sensitive sensor.
WIS	Web-inspection system. Camera-light system which measures the light transmittance of paper.
QCS	Quality control system. A point based measurement system which travels across the paper web in CD.
CP	Chemical pulping
MP	Mechanical pulping
TMP	Thermomechanical pulping
PGW	Pressurized ground wood pulping
UV	Ultraviolet radiation
IR	Infrared radiation
OTF	Optical transform function
MTF	Modulation transfer function
SSE	Summed squares of errors
RMSE	Root mean square of errors
FPGA	Field programmable gate arrays
VCA	Variance component analysis

1. Introduction

Paper products have an important role in the everyday life of billions of people. The first piece of paper was made in Chine approximately 2000 thousands year ago as a platform for writing (Basbanes 2013). Since then, paper has been the most important storage of data and information. Paper is also applied in a versatile manner as a packaging and a sanitary product. However, during the past five decades the role of paper as a platform of writing and data has significantly decreased because of the development of digital media and internet. Thus the paper industry is at a turning point: at present the main goal of paper manufacturers is to increase significantly the cost-efficiency of the papermaking processes, to increase the quality of paper, and to develop and focus on profitable paper products other than conventional printing papers. This thesis aims to contribute to this area by proposing novel image-based measurement systems, and new analysis methods for current image-based measurements to improve the accuracy of current measurement systems and thus increase the quality of paper.

1.1 Status of paper industry in the world and in Finland

During the past hundred years the manufacturing of paper has been strongly upscaled and automated. While paper was fully handmade in the early days, at present the personnel costs compose only a minor part of the total costs of the papermaking (FIFF 2013). The average yearly consumption of paper products was 54 kg per capita in 2011 being over 150 kg in developed countries, such as in North America, western Europa and Japan, and under 10 kg in Africa (FAO 2013). The consumption of paper products in the world has increased continuously by an average 2.6 % rate per annum, and thus the total consumption has increased 50% from the 80's (FAO 2013). In Finland the production of paper has almost doubled since the 80s being 10.7 million tons in 2013 (FIFF 2013). However, during the last decade the growth has happened only in Asia and Latin America. For example in China the total consumption of paper products has increased 25% during the last four years (FAO 2013). In Japan the consumption has saturated and in Western Europa and North America the consumption of paper has even decreased by 5% during the last four years (FAO 2013). Furthermore, high manufacturing costs and the remoteness of Finland from the global markets has caused paper machine closures and workforce reduction as manufacturing has been moved to countries of lower costs. In Finland over 30 paper manufacturing lines have been closed and over 4000 people have been laid off during the past five years. However, the paper and pulp industry still employs directly 22000 people in Finland (FIFF 2013).

The demand of newspaper and magazine papers is not predicted to increase in the developed countries anymore because of the increased use of Internet, e-books and e-magazines. However, increase is still predicted in Asia, in Latin America and in Africa. Furthermore, the consumption of sanitary and household paper (=tissue paper), packaging paper and boxboard is increasing worldwide. Also new paper products, such as the products made of nano

cellulose or paper as a substrate for printable electronics, may open new use for wood fibers and new markets for current paper manufacturers.

1.2 Research problem

"The value of paper products depends on both their performance and their visual appeal" (Farnood 2009). The quality of paper is evaluated with several measurement devices on-line at the paper machine and off-line after the paper manufacturing process. The assessment of quality depends significantly on the paper grade. In household and sanitary paper the physical properties such as the softness and the water absorption determine the quality. Whereas, in magazine paper the quality is determined based on the visual appeal and the runnability of paper in printing machines.

The quality of the tissue paper is determined based on softness, wet strength, absorption and dry strength of the end-product. At present, the uniformity of quality of tissue paper is controlled based on the on-line basis weight, moisture, filler content, and thickness measurements. However, the relevant properties of tissue paper such as the wet strength, the dry strength, and the absorption are measured off-line. The softness is not necessarily even measured because of the high uncertainty of current softness measurement devices. The creping process which generates the wavy microstructure in tissue paper mainly determines the quality properties of the tissue paper (Oliver 1980; Pawlak and Elhammoumi 2011). Creping also affects a number of fibers extending from the paper – called free fiber ends - which are known to affect especially the surface softness of paper (Patterson 2013).

The quality measurement of printing paper is focused on the performance and the visual appeal of the paper. The variation in paper roughness or thickness decrease the printing quality and can cause breaks in printing machines. Furthermore, the uneven gloss and opacity properties of paper may appear annoying to end-users. At present the visual appeal and the structural properties of paper are measured with a scanner based measurement system. The scanner is a measuring device which travels over the running paper web across the paper machine. The uncertainty of web-wide estimate based on such scanner is rather high due to the small number of points actually measured. However, the scanner measurement has maintained its position in paper industry: systems consisting of multiple detectors are not used mostly because of high costs. During the last few years, the price, speed and performance of cameras and devices providing the illumination have achieved a level which enables high-resolution imaging of paper on-line at a reasonable price. The fast LEDs (light-emitting diode) and camera technologies are already applied in paper machines in web inspection systems (WIS), which detect and classify defects such as holes and dirt particles in the paper web and estimate some simple paper characteristics such as light transmittance and formation.

The research problem of this thesis can be formulated as the following *research questions*:

- How the image measurement can be applied in the evaluation of the creping pattern characteristics, the number of free fiber ends, and the amount of pinholes in tissue paper?
- How the on-line light transmittance (WIS) images can be applied in the analysis of small scale paper structure, the estimation of CD shrinkage profile, and the estimation of basis weight in newsprint paper?
- How the present scanning and web-wide on-line imaging systems must be modified to improve the estimation of tissue paper and newsprint characteristics?

The *hypothesis* of the thesis is that by utilizing the state-of-the-art on-line imaging devices in paper machines – scanning or web-wide – the characteristics of paper can be measured more accurately and in a more versatile manner. The increased information improves control of paper machine and thus the cost efficiency of the papermaking process can be enhanced.

1.3 Contributions

The scientific and technological contributions of this work are:

- An image measurement applying photometric stereo principle for evaluation of the creping pattern characteristics and the number of free fiber ends in tissue paper.
- An analysis method to estimate the magnitude of basis weight, the variability of basis weight, the in-plane orientation distribution of a fiber network, and the CD shrinkage profile of web in newsprint grade based on the online light transmittance images.
- An uncertainty analysis of basis weight estimate for newsprint based on light transmittance images.

The thesis contains seven publications. Based on the research, two patent applications have been filed. The publications including the author's contribution are summarized below.

Publication I *Analysis of paper structure based on light transmittance and basis weight measurements* studies the scale dependency of the statistical relationship – correlation – between light transmittance and basis weight. Correlation was analyzed and a model developed based on the layered Kubelka-Munk theory for light transmittance in paper. The measurement data was provided by Metso Paper Inc. The author was responsible for the analysis of the results, and wrote the article.

Publication II *Web-wide diagnostics of paper properties based on fault detector system images* presents the calibration analysis for on-line imaging systems consisting of several adjacent cameras. The calibrated image data was applied in the estimation of cross-direction (CD) shrinkage of paper web. The measurement data was provided by Viconsys Inc. The calibration analysis was developed and written together with PhD Ville Tirronen, University of Jyväskylä. The author was responsible for the shrinkage analysis and for the writing of the main parts of the article.

Publication III *2D basis weight estimation based on light transmittance imaging* studies the uncertainties affecting basis weight estimation based on offline transmittance images and/or on online transmittance images captured at running paper machine. The measurement data was provided by Viconsys Inc. The calibration analysis for on-line imaging systems was developed together with the co-authors. The author was responsible for the analysis of the results, and wrote the article.

Publication IV *Simulation of creping pattern in tissue paper* presents the method to simulate the structure of creping pattern in tissue paper. The planar creping pattern was described with 2D Gaussian in the wave vector space, which enables presenting the planar structure of creping with only three parameters. The tissue samples were provided by Kemira Inc. The author was responsible for developing the method and for the writing of the manuscript. The patent application was made before the publication and it describes the imaging method and the analysis method of crepe frequency. The author was responsible for the analysis of the results, and wrote the article.

Publication V *Web-wide imaging of paper; Analyzing the potential of on-line light transmittance measurement in quality control and diagnostics of paper* studies the uncertainties affecting basis weight estimation based on online transmittance images captured at running paper machine. The measurement data was provided by Viconsys Inc. The calibration analysis for on-line imaging systems was developed together with co-authors. The author was responsible for the analysis of results and for the writing of the manuscript.

Publication VI *Potential of full-web imaging in measuring web structure on-line* studies the potential of on-line transmittance measurements in paper structure estimation. The paper introduces a method to estimate the structure based on the power spectrum of image. Furthermore, the article presents a method to apply directed antenna principle to separate the diagonal variations caused by the headbox of paper machine. The idea to apply directed antenna principle to detect diagonal variations was developed earlier by Prof. Risto Ritala and MSc Johanna Ylisaari and it is not a contribution of this thesis. The author was responsible for the analysis of the results and for the writing of the manuscript.

Publication VII *Method for detecting free fiber ends in tissue paper* presents the imaging method to detect the fibers extending from the surface of tissue paper. The method was based on the detection of the shadows of fibers from the difference of the original reflectance image and the reconstructed reflectance image estimated with photometric stereo. The patent application related to the measurement system was made before publishing the article. The author was responsible for the invention and for developing the method and for the writing of the manuscript.

1.4 Structure

The dissertation is organized as follows. Chapter 2-3 present the application context of the thesis whereas Chapters 4-5 summarize the measurement methods developed in this thesis. In Chapter 2 the papermaking process in newsprint machine and tissue machine is described briefly. Chapter 3 reviews the factors affecting to the interaction between the light and the paper. Chapter 3 scrutinizes the paper structure, properties of light and the Kubelka-Munk theory which provides a simple model to describe the propagation of light in paper. It also reviews the state-of-the-art in optical and image based measurements applied in paper quality estimation. Chapter 4 presents the novel methods to analyze the characteristics of tissue paper from surface gradient field estimated from off-line reflectance images. Chapter 4 also describes the pre-processing of reflectance images applied in the gradient field estimation. Chapter 5 presents the methods to characterize the structure of newsprint paper based on on-line images. Chapter 5 also discusses the limitations of on-line imaging. Chapter 6 discusses the main outcomes of the thesis and provides the author's answers to the research questions. Finally, Chapter 7 concludes about the measurement opportunities online and web-wide, on-line and scanning, and offline, and presents future challenges.

2. Papermaking process

Paper is a sheet-like product manufactured continuously at speeds as high as 40 m/s. The width of the manufactured paper web in paper machine can be up to 10 meter (Paulapuro 2008). The overall production rate when producing normal 80 g/m^2 copy paper can be up to 80 tons/h. Thus, even a 1% increase in net production can have €5.3 million impact on the annual level (value of copy paper = 800 € / ton). This chapter describes briefly the papermaking process and introduces the main parts and functions of conventional newsprint machine and dry crepe tissue paper machine.

Papermaking process consists of several sub-processes: the fibers are separated from the wood and processed to the pulp, the produced pulp together with water, fillers, and chemicals is fed to the paper machine, the web is formed and finally the web is dried and the surface of the paper is finished. Figure 1 presents the main sections of the process in paper machine. The detailed structure of these processes depends on the desired properties of the final paper. Usually the paper manufacturing line is built only for a specific end product (Paulapuro 2008). The paper/board products can be divided into six major classes: newsprint, printing/writing paper, tissue paper, packaging paper, boxboards, and containerboards. This thesis focuses on the newsprint and tissue papers.

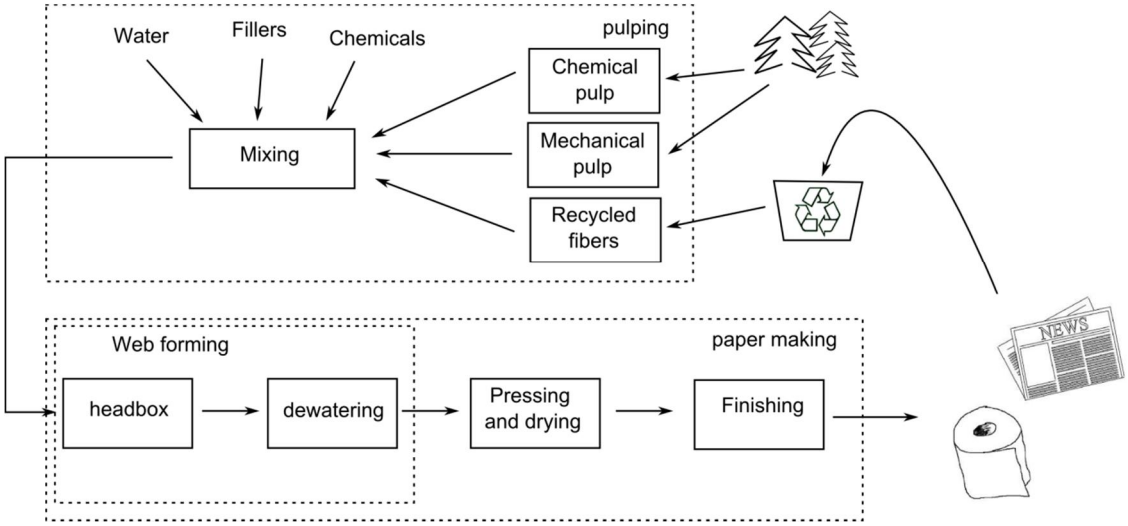

Figure 1. The main sections of the papermaking process

2.1 Pulping

The main raw material component of paper is pulp. In pulp manufacturing the fibers are separated chemically or mechanically from wood. In chemical pulping (CP) the wood chips are cooked and by the effect of heat and chemicals the lignin and other ingredients which are not desired in papermaking are separated from the fibers (Gullichsen and Fogelholm 1999). In the chemical pulping process approximately only half of the wood material is utilized for

papermaking (Stenius 2000). However, the lignin and other discarded ingredients can be burnt as a fuel oil substitute making the modern chemical pulp mill a net energy producer (Paulapuro 2008). The strength of the paper made of chemical pulp is high because of the large number of long fibers. The removal of lignin improves the brightness of the end product.

In mechanical pulping (MP) the wood chips are ground or refined to small particles until they are reduced to fibers (Sundholm 1999). The mechanical pulping can be further divided into two major types: thermomechanical pulping (TMP) and pressurized ground wood pulping (PGW). In mechanical pulping the whole wood material except bark is utilized. However, the energy consumption of grounding and refining is high. The strength of the paper made of the mechanical pulp is low because of the fiber size distribution is dominated by short fibers. The mechanical pulp provides high opacity and good printability of the end product. However, the lignin present in mechanical pulps interacts with light making the end product eventually yellowish.

Pulp can also be made from recycled paper. Approximately half of the raw material of paper products is produced from recovered paper (FAO 2013). The origins of fibers in recovered paper differ significantly and therefore the characteristics of fibers can vary. Thus the recycled fibers are not used in grades where the requirements for the properties of paper are strict. The wood fibers can be re-used a maximum of 3-5 times. Thus, the collection of recycled paper is normally sorted to writing/newsprint papers including small amount of recycled fibers and to paperboard/boxboard products including large amount of recycled fibers. However, sorting depends strongly on the culture and the country.

2.2 Approach system and headbox

The raw material consisting of several pulps is diluted with water and mixed with chemicals and fillers. Such pulp is called furnish and is fed to the headbox. The main function of the headbox is to distribute the furnish on the wire/between the wires evenly across the width of the paper machine. A furnish distributor is a channel that runs across the whole headbox width and distributes the furnish to small pipes. The purpose of pipes is to generate turbulence to the flow and thus break the fiber flocks in the furnish. After the pipes the flow enters to the headbox nozzle which generates the final web forming jet. The planar material layer on the wire/between the wires is called paper web. The amount of material in paper web is described by its basis weight, which is the most profound quality characteristic of paper. The purpose of quality control in headbox is to generate paper web in which the basis weight variation is minimal across the width of the paper machine and over time.

The travel time of furnish flow inside of the headbox manifold from one edge of the headbox to the other edge is approximately 2-3 seconds. The speed of the jet should be similar in each location of cross directional headbox nozzle. Thus the pressure drop in furnish is compensated by a pressure rise which is achieved by decreasing the sectional area of the furnish distributor. This is possible because the volumetric flow along the channel decreases which is due to the furnish entering into the pipes and nozzle. The nozzle accelerates the

furnish flow and spreads it on the wire. The nozzle consists of top and bottom lips: the opening between the lips determines the thickness of the jet. The uneven feed of CD distributor may generate some flow components in the nozzle which may cause quality problems in the final product. Thus the opening of the lip can be controlled to adjust the outflow and thus a basis weight at a certain position in CD. The distance between the screws which adjust the opening is usually 100-150 mm in CD. The uneven feed of the CD distributor can also be compensated with dilution flows. In such a design the water is added to the headbox flow to compensate the CD basis weight variation in the web formed. The water is usually added to each pipe exiting from the CD distributor (Paulapuro 2008). The advantage of dilution control compared to adjustment of lip opening is the higher resolution (smaller than 50 mm in CD) of basis weight control. However the fast consistency variation entering into the headbox cannot be compensated with such controlling units because of the slowness of the actuators and because of the delay time of paper web (= 30s – 120s) from headbox to basis weight measurement (Leiviskä 2009). Thus the consistency variation may produce e.g. diagonal basis weight variation to the final product (see Fig. 2).

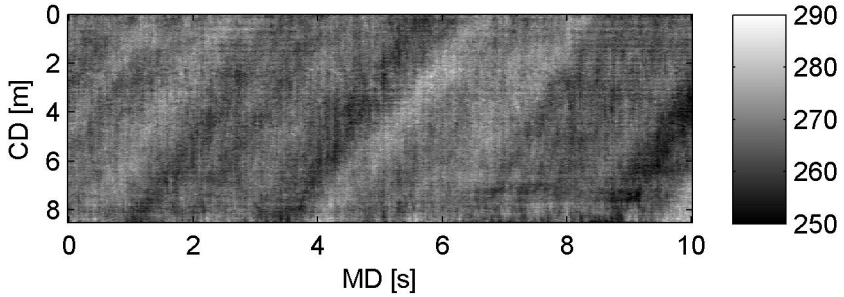

Figure 2. Light transmittance image of newsprint paper. The consistency variation of pulp entering into the headbox causes diagonal waves (Publication II). The speed of the paper was 27 m/s. Gray scale shows the pixel intensity (10 bit image).

2.3 Newsprint paper machine

The typical furnish in newsprint is 70-100 % mechanical pulp and 30-0 % chemical pulp, which is because of the requirements of good runnability in printing machines and of high opacity in the end product (Paulapuro 2000). The pulp made of recycled fibers can be used as such in newsprint grade. The proportion of fillers in newsprint is usually 0-15% of total material. The purpose of fillers is to improve the printability, the opacity, the gloss and the brightness of end-product (Neimo 1999). Chemicals are used in newsprint to improve the runnability of the process and the strength of paper.

The basis weight range in newsprint is usually 40-49 g/m^2. The speed of a typical newsprint machine is 33 m /s and the width can be 10.6 meters. A modern newsprint machine has cross-directional dilution control in the headbox, a press section with two shoe presses, a drying section equipped with re-moisturiser, soft calenders and reeling. In the wire section the fibers and fillers are filtered on the wire or between two wires while the water is removed through the wire by stationary pressure, suction, and pressure pulses. After the wire section the paper web is pressed mechanically between two felts in the press section, or between a felt and a

roll. In the press section only the water and small particles are moving in the paper web. The rest of the water is removed by evaporating it from the paper with several hot drying cylinders or radiation dryer. The paper may be finished after drying by using a calender, which makes the surface of paper glossy and smooth. Finally, the dry paper is rolled up to a reel-up drum (Paulapuro 2008).

2.4 Tissue paper machine

The pulp mix in tissue paper depends highly on the desired properties in end use (see Table 1). The properties of fibers impact the softness, the dry strength, the wet strength and the absorption of tissue paper. The important characteristics of toilet paper, softness and dry strength, are achieved with a mix of recycled fibers and chemical pulp. In contrast, the important characteristics of kitchen towel, wet strength and absorption, are achieved with an appropriate mix of virgin chemical and mechanical pulp. The mixture of pulp in tissue paper depends also on the types of fibers available on a local basis, including the availability of recycled fibers. However, most of the tissue manufacturers have premium grades in which the mixture of pulp and fibers are strictly specified. The filler content in tissue paper is 0-15% of total material. The fillers are used in tissue paper to decrease the cost of the final product and to improve the brightness. Chemicals are used in tissue paper to increase the softness and the strength of tissue paper. The strength of tissue usually decreases when recycled fibers are used.

Table 1. The properties of tissue paper required in various products

Product	Softness	Dry strength	Wet strength	Absorption	Appearance properties
Toilet paper	x	x			
Kitchen towel			x	x	
Facial tissue	x				x
Napkin		x			x
Hand towel			x	x	

The web formation process in a tissue machine is similar to that in newsprint machines. The basis weight of tissue paper varies usually between 12-24 g/m^2 but can be up to 50 g/m^2 in some special towels. The speed of the tissue machine can be 33 m/s or even higher and the width can be 7.5 meters. The web forming and dewatering are rather similar to those in newsprint machines. The vast majority of the tissue machines are dry-crepe machines in which the most common press configuration is to use one press roll. Such an arrangement enables the high thickness and softness in the sheet. This thesis studies the tissue grades made on dry crepe machines.

The drying in dry crepe machines differs significantly from the newsprint machine. The sheet is adhered to a Yankee cylinder which dries the sheet completely by heating the water out of the paper. Yankee cylinder is a large steam-heated drum with iron surface whose diameter can be as large as 7 meters (Ramasubramanian 2011) (see Fig. 3). The Yankee cylinder not

only supplies the required energy for the drying but also transports the sheet during the drying and provides the base for the creping process. The adhesion between the sheet and the Yankee cylinder is controlled with a coating sprayed directly on the cylinder. The coating consists of several components e.g. organic components, phosphates, modifiers, adhesive and release agents (Oliver 1980). The phosphates and organic material reduce the blade wear, protect the surface of the Yankee cylinder, and impact the adhesion in coating. The modifiers affect the softness of coating. The duty of adhesive agents is to hold the sheet against the Yankee cylinder (Nordman and Uggla 1977; Furman and Su 1993). However, as a result of adhesive agents the crosslink between the sheet and the Yankee is so strong that the control of detaching would be difficult and web release would cause holes to the sheet and breaks of the web. Therefore the release agents are added to the coating to weaken the adhesion between the sheet and the Yankee cylinder (Furman and Su 1993). The key phenomenon in tissue production in dry crepe machines is the creping mechanism which generates the softness and other desired properties to tissue paper. The dry sheet is scraped off from the cylinder with a blade. The scraping process is called creping as it forms crepe folds in the sheet. Finally, the creped sheet is pulled to the machine reel. As the creping contracts the sheet in the running direction, the speed is lower at the machine reel. The speed ratio between the Yankee cylinder and the machine reel is called the crepe ratio. The crepe ratio generally falls within the 1.1-1.25 range (Hollmark 1983) in typical tissue grades.

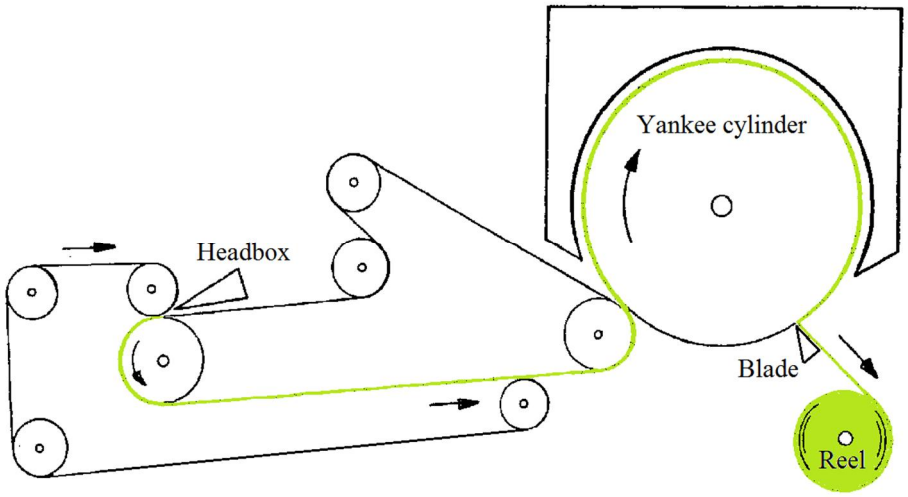

Figure 3. A schematic drawing of dry-crepe tissue machine (Hermans and Hada 2004). The green color shows the path of the paper web.

The sheet adhesion impacts the width of the crepe folds in MD. Low adhesion produces typically wide crepe folds and high adhesion produces narrow ones if the other factors in creping are kept constant (Stitt 2007). The wide crepe folds increase the thickness of the tissue paper. However, the creping does not explain the thickness differences entirely as also the basis weight before the Yankee cylinder and the gap size between the blade and the Yankee cylinder impact the final tissue thickness.

The angle between the top surface of the blade and the surface of Yankee cylinder defines the ratio of macro and micro folds in tissue paper (Hollmark 1972; Oliver 1980). The length scale of micro folds is usually between 40 μm and 100 μm. A macro fold consists of a pile of micro folds making the length scale larger. The blade angle with respect to cylinder tangent can vary from 40 to 100 degrees being usually in the range of 80-90 degrees (Oliver 1980). At small angles the micro folds are piling up after creping thus forming a single macro fold (see Fig. 4, left). Such super creped tissue sheets are rather unusual and they may have crepe ratio higher than 1.5. At large angles the macro folds are not necessarily formed or the size difference between the macro and micro folds is minor. The forming of micro folds at large angle is illustrated in Fig. 4, right.

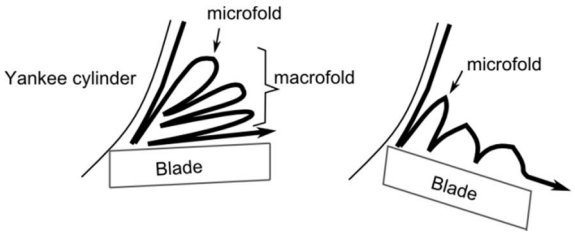

Figure 4. The impact of the angle between the Yankee cylinder and the top surface of the blade in creping. Left: The angle is small. Right: the angle is large. (Hollmark, 1972; Oliver, 1980).

The detailed forming mechanism of crepe folds is the following (Hollmark 1972; Sun 2000; Ramasubramanian 2011). The tissue sheet starts to buckle when the sheet hits the blade. The buckling happens because the force which presses the sheet against the blade overcomes the adhesion which connects the sheet and the Yankee cylinder. The buckling continues until the sheet collapses completely and forms the crepe fold. At this point the formed crepe fold moves toward the machine reel because of the pulling force of the reel and as a result the adhered sheet behind the crepe fold hits the blade. The adhered sheet starts to buckle and the entire cycle is repeated and as a result a rather regular creping pattern is generated to the sheet (see Fig.5).

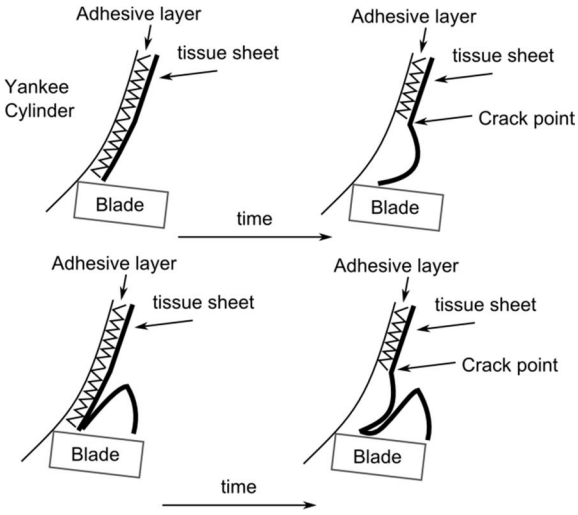

Figure 5. The propagation of creping (Publication IV).

The angle between the surface of the blade and the Yankee cylinder, the adhesion, and the structure of the sheet (e.g. thickness, basis weight) defines the crack point (see Fig. 5, bottom right) in the creping process. Finally, the creped tissue paper is rolled on the reel. The reels are transported to the converting factories in which the tissue paper achieves its final treatment e.g. laminating, embossing and/or printing before the end use.

3. Interaction between light and paper

The behavior of light on the paper surface and inside the paper depends on the physical properties of the paper. This chapter outlines how light interacts with paper. Section 3.1 describes the paper structure and how the structure is modeled. Section 3.2 presents the general properties of light and electromagnetic waves, relevant for understanding the interaction with paper. Section 3.3 introduces the interaction between the light and the paper. Sections 3.4 and 3.5 review the state-of-the-art of the optical and the image based measurements, respectively, applied in the estimation of paper quality.

3.1 Paper structure and its measurement at paper machine

The thickness of paper web varies according to the product grade typically between 30 µm and 200 µm (see Fig. 6). Paper consists of a random arrangement of wood fibers and smaller particles such as mineral pigments, and chemicals. The diameter of fibers varies between 15 µm and 40 µm, which means that paper usually consists between a few fiber to some 20 layers of fibers in the thickness direction. The wood fibers are usually several times longer than the thickness of paper and thus the fiber network is almost two-dimensional. Therefore many paper properties can be analyzed with two-dimensional structure estimation.

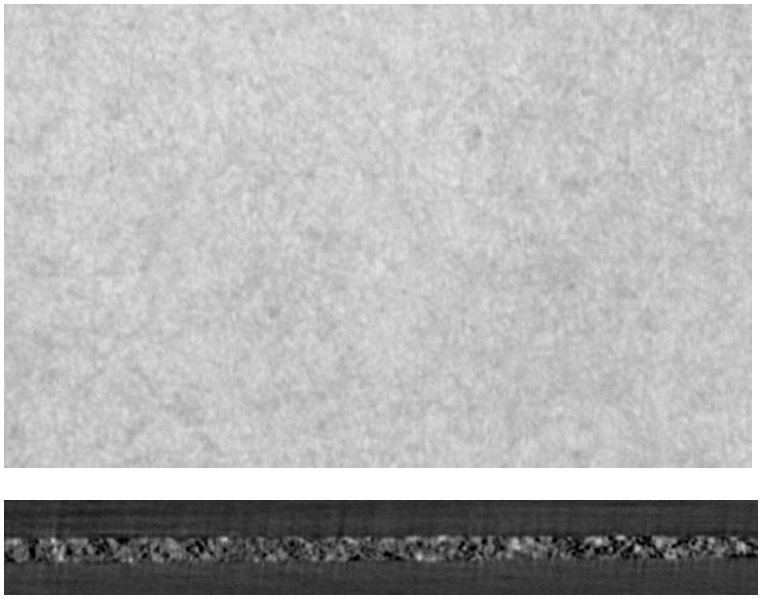

Figure 6. The x-ray tomograph of the paper (top) and the cross-section of the same paper (bottom). The resolution of the images is 3.8 µm and the width of both the images is 3.3 mm. The paper was a normal print paper whose basis weight was 77 g/m^2 and thickness 100 µm.

The planar non-uniformity of the distribution of material is called formation. One widely used definition of formation is the planar small scale basis weight variation of paper. Formation is commonly summarized by its length scale and magnitude (Norman and Wahren 1974). Even paper has a small magnitude of formation. Small length scale of variation means grainy paper (the opposite being cloudy paper). The length scale of basis weight variation accounted for formation is usually assumed to be smaller than 40 mm. Formation depends on several factors in papermaking process, e.g. the properties of the pulp, the properties of the suspension flow inside of the headbox, and the dewatering process in the wire section.

The in-plane orientation distribution of the fiber network is characterized by the anisotropy of fiber orientation and the dominant orientation direction of fibers, i.e. the direction of fibers with the highest probability. The orientation of fibers in paper depends on the several forces impacting the web forming (Parker 1972). The most important is the speed difference between the wire and the jet which produces a shear field and rotates the fibers towards machine direction. Thus the orientation distribution of fibers is anisotropic. Furthermore, the orientation of fibers depends on the direction and the turbulence of the suspension flow. (Paulapuro 2008).

The discrete number of fiber layers in paper plane implies that the number of fibers - also called coverage - in a certain location is Poisson distributed (Corte and Kallmes 1961):

$$P(k) = \frac{\lambda^k e^{-\lambda}}{k!}, \tag{1}$$

where k is the number of fibers and λ is average number of fibers. The mean and the standard deviation of Poisson distribution are both determined by the parameter λ and thus mutually dependent: the standard deviation of Poisson distribution is proportional to the square root of the mean value of Poisson distributed data (Draper and Smith 1998). Thus the planar material measurement results on paper, e.g. the basis weight, would be Poisson distributed with this interdependence between the mean and variance. When comparing samples with different average basis weight this may be an unwanted. However, the variance can be stabilized. In the case of Poisson distribution the variance can be stabilized sufficiently with square-root function (Draper and Smith 1998). As a result the mean and stabilized variance can be considered independent. In this thesis the square root of light transmittance measurements was computed to stabilize the variance so that samples with different basis weights can be compared.

The paper structure can be measured on-line at the end of the paper machine before the reeling or off-line in a paper laboratory. The on-line estimates of e.g. basis weight variations in paper in scales larger than formation are determined with a scanning measurement (Kjaer et al. 1995; Leiviskä 2009). The scanner is a measuring device which travels over the running paper web across the paper machine and forms web-wide profile estimate based on several measurement points in CD. The travel time from one edge of the web to the other edge is typically 20-30 seconds. The resolution of such a system is typically 15 mm/sample in CD. The resolution in MD is approximately 0.5…2 m/sample, i.e the web travels this distance in

MD while the scanner measures one CD sample. The interval at a CD location between the samples in MD varies locally from 0.05 s to 60 s because of the zigzag shaped scanning path as a function of time (see Fig. 7).The uncertainty of such web-wide estimate is rather high due to the small number of points actually measured with the scanner.

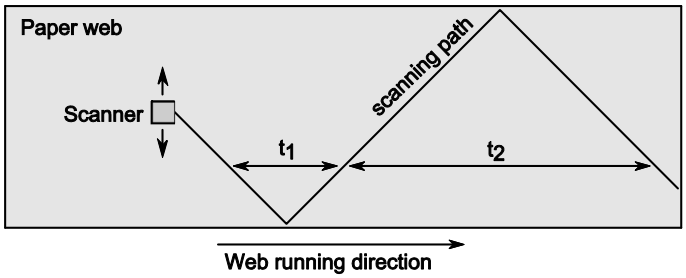

Figure 7. An example of scanning path over the paper web. The intervals t_1 and t_2 illustrate the uneven sampling time in the MD caused by the zigzag shaped scanning path (Publication V).

The on-line analyzer measures several properties including:

- basis weight of paper based on absorption of beta radiation (Norman and Wahren 1974; Keller and Pawlak 2001; Keller et al. 2004)
- filler content based on absorption of x-ray radiation (Arendt 1974; Mercer 1987)
- moisture based on absorption of IR (infrared) radiance(Sturm 1984; Kuusela 1990; Figiel et al. 2010)
- thickness of paper based on the laser triangulation measurement (Graeffe 2010)
- porosity of paper based on the pressure of air (Gockel et al. 1986; Komulainen 2004)
- formation of paper based on the light transmittance (Avikainen et al. 2004).

Most of the paper properties are measured with point based sensor meaning that the small scale 2D structure of paper cannot be detected, and although the sensor were 2D, the paper structure is measured only from few locations of paper because of the characteristics of the scanning measurement.

The off-line paper structure measurement systems are usually two-dimensional and the operational principle is similar to that in on-line measurements. However, off-line measuring is time consuming because of the larger number of measurement points and the handling of individual paper samples.

3.2 Properties of light

Light has a dual wave-particle nature. The particles are called photons which explains how the light interacts with electrons such that, for example, the color arises. In this work the light is considered as an electromagnetic wave which simplifies the treatment of polarization phenomenon and the absorption and scattering properties of light (Hecht 2007). The electromagnetic radiation consists of electric and magnetic field oscillation (see Fig. 8). The simplest way to describe the three dimensional electromagnetic wave is the plane wave in

free space. The magnetic and electric fields are perpendicular to the direction of the propagation of the wave and to each other. The plane wave ψ can be presented as

$$\Psi(\mathbf{r},t) = A\cos(\mathbf{k}\cdot\mathbf{r} - \omega t), \qquad (2)$$

where **k** is the wave vector which determines the direction of the wave and the wave number of the wave and **r** is the position vector which defines a point in three-dimensional space and t is time. The A and ω are constants that define the amplitude of the wave and the angular frequency of the wave, respectively.

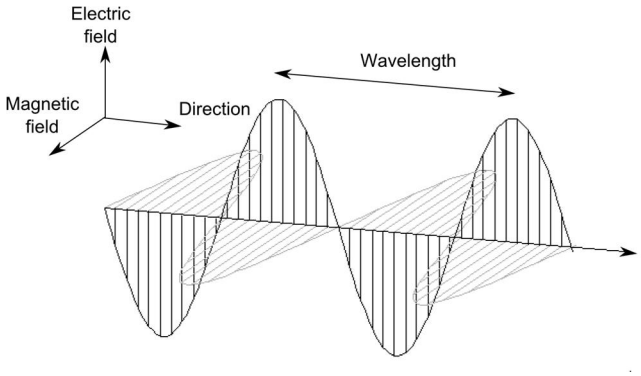

Figure 8. The electromagnetic wave.

The number of wave oscillations per second is called frequency and the wavelength is inversely proportional to frequency. The electromagnetic radiation is classified based on the wavelength of the radiation (see Fig. 9). The radiation between the wavelengths of 380 nm and 760 nm is visible light. The wavelengths shorter than 380 nm are called ultraviolet radiation (UV) and higher than 760 nm are called infrared radiation (IR).

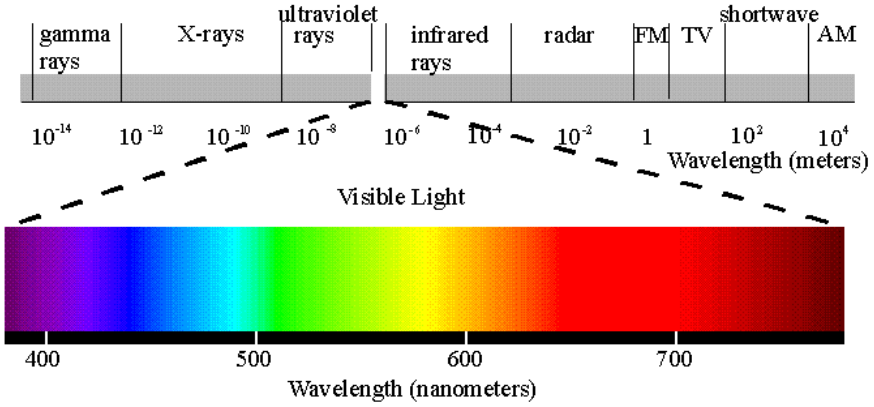

Figure 9. Electromagnetic spectrum (Nasa 2014).

Polarization is the orientation of electric/magnetic fields in the plane perpendicular to the direction of propagation. Most sources of electromagnetic radiation contain a large number of atoms or molecules which emit the photons (Hecht 2007). The orientations of electric fields produced by such emitters are usually not correlating. Thus the natural light emitted e.g. from the sun is not polarized as all polarizations are present with same probability. Similarly the LEDs and most of the human made light sources excluding lasers emit unpolarized light.

When describing the polarization, usually only the electric field is presented and the magnetic field ignored because the two fields are always perpendicular. The unpolarized light propagating in z-direction can be described by letting $\mathbf{E}(z,t)$ be the sum of two perpendicular electric fields as follows

$$\mathbf{E}(z,t) = \mathbf{E}_x(z,t) + \mathbf{E}_y(z,t), \tag{3}$$

where

$$\mathbf{E}_x(z,t) = \hat{\mathbf{i}} E_{ox} \cos(kz - \omega_x t) \;\; and \;\; \mathbf{E}_y(z,t) = \hat{\mathbf{j}} E_{oy} \cos(kz - \omega_y t + \varepsilon) \,. \tag{4}$$

In Eq. (4), ε is the relative phase difference between the two waves and **i** and **j** are the vector components. The sum of two waves is linearly polarized if the frequency of the waves is the same ($\omega_x = \omega_y$) and the phase difference is 0 or integer multiple of $\pm\pi$. Thus, the direction of the electric field of the resulting vector is constant. Figure 10 (left) shows the linearly polarized wave $\mathbf{E}(z,t)$.

The linear polarized light is special case of elliptical polarization. In elliptically polarized light the resultant electric vector rotates and changes the magnitude at the same time. In such case the endpoint of E vector will draw an ellipse around the wave propagation axis (Hecht 2007). Figure 10 (right) shows the sum of two fields whose relative phase difference is $\pi/2$ (circularly polarized).

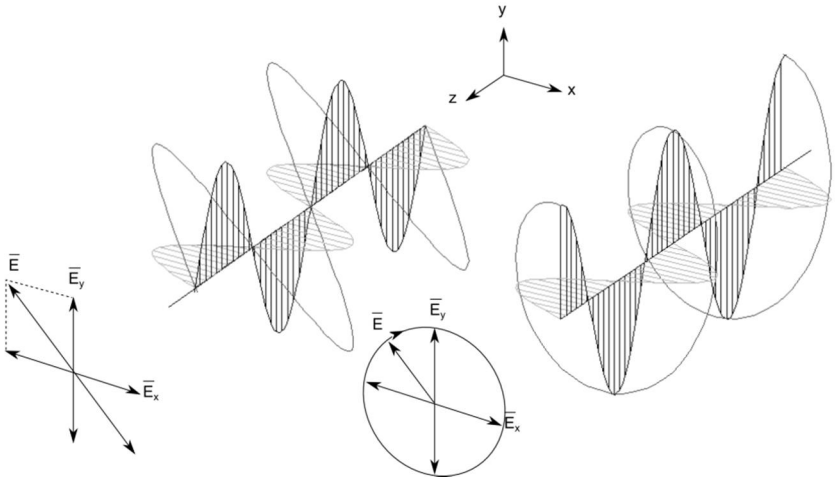

Figure 10. The linearly polarized wave E (gray solid line) on the left and the circularly polarized wave (gray solid line) on the right. Both waves were generated as a sum of waves E_x (gray wave) and E_y(black wave).

An optical device whose input is unpolarized light and the output is some form of polarized light is called a polarizer. Unpolarized light can be expressed as the superposition of two linearly polarized, orthogonal waves with equal amplitude whose phase relation is not constant. The polarizer separates these two components by removing one wave and passing through the other one. Circular and elliptical polarizers are based on the same idea to separate two components of unpolarized light and adjust the phase difference to the desired one.

3.3 The propagation of light in paper

Light is reflected or scattered from paper, absorbed to paper or transmitted through paper (see Fig. 11). In specular reflection the surface of paper acts as a mirror. In scattering the light penetrates to the material, is reflected several times from fibers and pigments and finally out of the paper (Pauler 2002). The light which is not transmitted through paper or scattered back is absorbed to paper. The surface of material in which the reflected intensity is independent of the viewing direction is called diffuse (Lambert 2001). There exist diffuse reflection and diffuse transmission. On paper surface the reflection is typically a combination of specular, diffuse reflection and transmission because the light reflects from the surface of paper and from the inner parts of the paper (Borch et al. 1984).

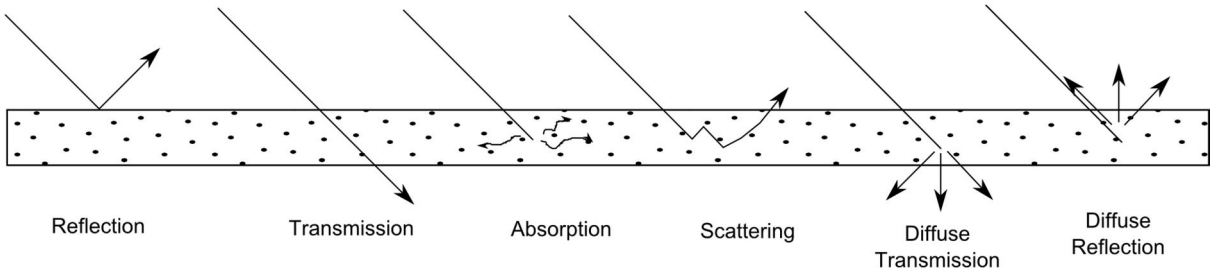

Figure 11. The interactions between the light and the paper.

Kubelka and Munk described the light propagation in a homogenous material in which randomly distributed particles absorbing and scattering light are much smaller than the thickness of material itself (Kubelka1948; Kubelka 1954). Such material can be considered as a continuum and thus simplifying the three-dimensional light propagation into material with two one-dimensional streams which describe the forward and backward scattering of light. The optical material properties are condensed to two parameters: absorption (K) and scattering (S) coefficients.

The connection between the coefficients S and K and the reflectances R_0 and R_∞ is determined as follows

$$R_\infty = 1 + \frac{K}{S} - \sqrt{\frac{K^2}{S^2} + 2\frac{K}{S}} \tag{5}$$

and

$$R_0 = \frac{e^{SW\left(\frac{1}{R_\infty} - R_\infty\right)} - 1}{\frac{1}{R_\infty} e^{SW\left(\frac{1}{R_\infty} - R_\infty\right)} - R_\infty}, \tag{6}$$

where R_∞ represents the reflectance of an opaque pile of homogenous paper and R_0 is the reflectance of a single sheet with black, totally absorbing, background. W is the basis weight of the material. The light transmittance of the material is given as a function of light absorption and scattering coefficients and R_∞ as (Kubelka 1948; Pauler 2002).

$$T = \frac{\left(1 - R_\infty{}^2\right) e^{-\frac{1}{2} SW\left(\frac{1}{R_\infty} - R_\infty\right)}}{1 - R_\infty^2 e^{-SW\left(\frac{1}{R_\infty} - R_\infty\right)}} \tag{7}$$

Figure 12 shows the theoretical relationship between the basis weight and light transmittance computed by eq. (7). The light scattering and absorption coefficients were set to S = 49 m^2/kg and K =5.5 m^2/kg, typical to newsprint paper.

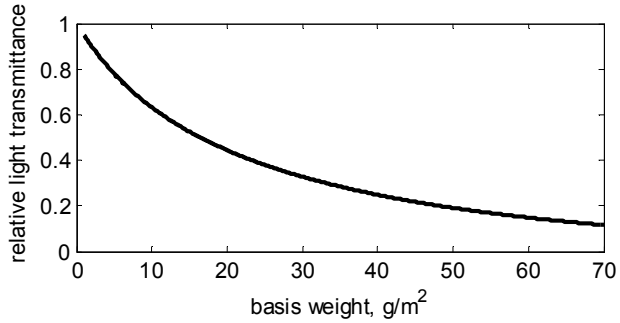

Figure 12. The theoretical relationship between the basis weight and light transmittance.

In paper pulp, the light scattering coefficient (S) varies typically between 15 m^2/kg and 70 m^2/kg, and the light absorption coefficient (K) between 0.05 m^2/kg and 40 m^2/kg (Niskanen 1998; Pauler 2002). However, the post-treatments of paper such as the surface coating, surface sizing and calendaring may affect significantly on the final light scattering and absorption coefficients. Furthermore, the uneven filler and moisture distribution in paper plane can cause local variation to coefficients.

Many paper grades consist of several layers e.g. two coating layers and one base paper layer. The light transmittance and reflectance for multilayer material can be obtained from the Stokes equations for scattering (Kubelka 1954). Figure 13 illustrates the reflectance and transmittance of a two-layer material, when reflectance R_i and transmittance T_i at each layer i is known. (Kubelka 1954).

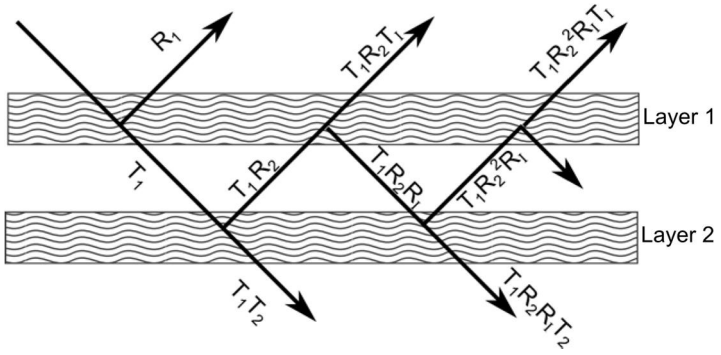

Figure 13. The adding method of the reflected and transmitted light in two-layer material

The transmitted light through the two-layer material is the sum of T_1T_2, $T_1R_2R_1T_2$, etc. which can be denoted shortly as follows (Kubelka 1954)

$$T_{1,2} = T_1T_2\left(1 + R_1R_2 + R_1^2R_2^2 + \ldots\right) = \frac{T_1T_2}{1 - R_1R_2} \tag{8}$$

The reflectance of two-layer material can be written as

$$R_{1,2} = R_1 + T_1T_1R_2\left(1 + R_1R_2 + R_1^2R_2^2 + \ldots\right) = R_1 + \frac{T_1^2R_2}{1 - R_1R_2} \tag{9}$$

The equations for *n*-layer material can be obtained similarly using the adding method described in Fig. 13 recursively. The transmittance and reflectance for n-layer material are as follows

$$T_{1,2,3,\ldots,n} = \frac{T_1T_{2,3,\ldots,n}}{1 - R_1R_{2,3,\ldots,n}} \tag{10}$$

$$R_{1,2,3,\ldots,n} = R_1 + \frac{T_1R_{2,3,\ldots,n}}{1 - R_1R_{2,3,\ldots,n}} \tag{11}$$

where $T_{2,3,\ldots,n}$ and $R_{2,3,\ldots,n}$ can be computed recursively based on equation (8) and (9).

Obviously Kubelka-Munk theory is a crude approximation of propagation of light in paper as the paper sheet is not homogenous. However, the theory is simple and sufficiently accurate to approximate the light propagation in paper for purposes of this work and is widely used in paper industry (Niskanen 1998; Pauler 2002; Farnood, 2009). Furthermore, the theory can be applied in the interpretation of the relative importance of material property variations (filler, moisture, fibers, chemicals) to light scattering and absorption coefficients and further to light reflectance and transmittance of paper.

3.4 Optical measurements of paper

At present, the optical quality of paper is evaluated with whiteness, brightness, color, opacity and gloss which are all measured through reflectance and transmittance. The on-line measurements are point based which means that the measurement system consists of a device providing an illumination and one light sensitive sensor. In offline conditions such optical properties can be estimated also from 1D measurement or 2D images.

Whiteness of paper is determined as high luminous diffuse reflectance R_∞ along the visible light spectrum (ISO 11475 2004). Usually, the whiteness in papermaking process is controlled by bleaching, adding blue dye to the substrate and controlling the removal of lignin (Ganz 1976).

Brightness is defined as the reflectance R_∞ of blue light at wavelength 457 nm (PAPTAC standard 1990). The brightness is related to Kubelka-Munk theory through Equation (5). However, the brightness does not sufficiently describe the whiteness and reliable whiteness value can be estimated only with spectrum wide color measurements described in (ISO 11475, 2004).

Opacity defines the ability of a single sheet to hide the background. Opacity is determined as a ratio of the reflectance of a single sheet and the reflectance of an opaque pile of sheets R_0/R_∞ and the reflectances are measured at wavelength of 577 nm (ISO 2471, 2008). The opacity is connected to Kubelka-Munk theory with Equations (5) and (6). Inverting the light scattering and absorption coefficients of material can be obtained through brightness and opacity data.

Gloss is determined as the intensity ratio of the specular reflection of a sample and the incident light (Bosch 1984, Farnood 2009). Gloss is the property of paper surface because the light which goes inside the paper reflects several times from fibers, fines and fillers, and loses directionality. Therefore, gloss depends on the surface smoothness of paper and the gloss of paper is controlled with the properties and the thickness of coating layer particles. The small coating particles fill the pores of the base paper and smooth the surface of papermaking the paper glossier (Alince and Lepoutre 1980).

3.5 Image based measurements of paper

The 2D image measurement and 2D analysis of paper started approximately 35 years ago (Sara 1978; Komppa and Ebeling 1981; Taylor and Nixon 1981). At first the image based measurements in paper industry were applied in the measurement of optical characteristics of paper presented in Section 3.4 and in the indirect measurement of characteristics of paper such as basis weight offline (Sara 1978; Ferguson 1997) and 2D structure of paper (Kropholler et al. 1981). The benefit of imaging measurements is that they are able to capture the texture of paper not attainable in the 1D and point based optical measurements.

Image based measurements are applied in analysis of formation and flock size (Avikainen et al. 2004; Ihalainen et al. 2012; Marjanen et al. 2009), regular marking of paper (I'anson 1995a; I'anson 1995b), paper CD shrinkage (Raunio 2006; I'anson et al. 2008), paper roughness (Ihalainen et al. 2012; Kuparinen 2008), fiber orientation (Erkkilä and Pakarinen 1998; Shakespeare 2009), printability (Mettänen 2010; Vartiainen 2007; Sadovnikov 2010), and other properties related to the texture of paper such as cracking (Leppänen 2007). Usually, imaging measurements are applied offline and therefore they are mainly a research and development tool. The first web inspection systems (WIS) which detected the defects of paper web-wide were published in the late 90's (Ferguson 1997; Chen 1998; Chen et al. 1998; Pfeifer et al. 1998). Since then the technology has been in use in paper machines and nowadays the resolution of online images starts to be enough high to measure i.e. the roughness (Ihalainen et al. 2012) and fiber orientation in paper (Shakespeare 2007).

Image based measurements are not only applied at the wavelengths of visible light. The properties of paper can be measured also with IR-radiation which is mainly applied in moisture and temperature measurements in paper machines (Metso IQ 2011). During the past two years the IR-radiation has also been applied in the basis weight measurement of fibers (Metso IQ 2011) and in the weight measurement of low weight tissue paper (Lang 2012, Meijer et al. 2012).

3.5.1 Imaging measurement system

The image measurement system can be characterized by its impulse response, also called point spread function in optics. The optical transfer function (OTF) or the frequency response of the system is the Fourier transform of the impulse response. The absolute value of the OTF is called modulation transfer function (MTF) and it describes how the different frequencies are filtered in the imaging system.

The sampling rate of the image is called spatial frequency, in units of dots per mm. The imaging system can be considered as a 2D low pass filter in which the pass/transition band ends at the half of the spatial frequency (=Nyquist frequency). In imaging system the finite size of pixels in image sensor, the shape of the lens aperture and the aberrations in the lens impact on the MTF. Figure 14 shows an example of the radial part of the MTF (black) estimated from a typical image measurement system (kit lens, f-number: 8, focal length 50 mm). Figure 14 shows also the ideal MTF curve of the imaging system (gray) including lens in which the theoretical diffraction limited maximum of the circular aperture is defined as (Johnson 1972)

$$MTF(f) = \frac{2}{\pi}\left(\arccos(f/f_0) - (f/f_0)\sqrt{1-(f/f_0)^2}\right) \qquad (12)$$

where f is the spatial frequency and f_0 is the cutoff frequency which depends on the aperture diameter (D), the focal length (F) and the radiation wavelength (λ) as follows $f_0=D/F\lambda$.

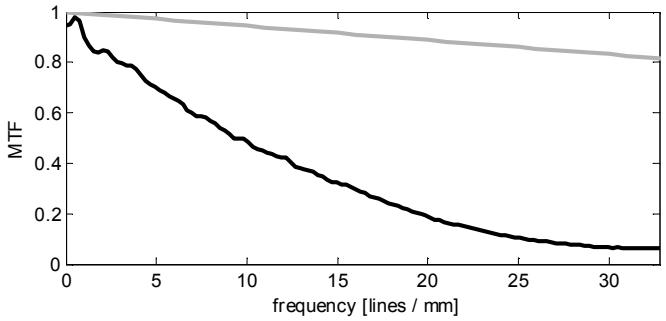

Figure 14. The MTF curve of kit lens (black line) and the theoretical maximum MTF curve(gray line).

The finite pixel size attenuates the MTF more at frequencies closer to the Nyqvist frequency. Furthermore, it can be seen that even the perfect lens attenuates the high frequencies and thus such low-pass phenomena must be taken into account especially when the frequency response is applied as an analysis tool of images. Furthermore, the MTF of a real life imaging system

is not ideally zero at Nyqvist frequency (black curve). Thus, the frequencies higher than Nyqvist frequency are aliasing to lower frequencies and distort them.

3.5.2 Photometric stereo

The 3D surface variation of paper is traditionally measured with a profilometer which detects the height of the surface mechanically with a stylus or indirectly by measuring the reflection of laser light. However, the profilometers which detect the surface with high accuracy and high speed are rather expensive and apply line cameras which do not provide complete information about the 2D texture. Photometric stereo is a method based on stereo imaging where two or more images are captured from a surface illuminated from the different directions (Woodham 1978). Photometric stereo method estimates the surface normal assuming that the surface is ideally diffusive (Lambertian), i.e. the brightness of the surface point is independent on the observation angle. The Lambert's law for an ideal diffusively reflecting surface states that the pixel intensity i at the point (x,y) is

$$i = \rho E \mathbf{l}_{3x1}^{T} \mathbf{n}_{3x1}, \tag{13}$$

where ρ is the surface albedo describing the reflectivity of surface, E is the intensity of the light source, $\mathbf{n}$ is the unit normal of the surface and $\mathbf{l}$ is the unit vector toward the light source. The term ρE can be estimated from the calibration images captured from the flat surface whose reflectivity is equal to estimated surface. The unit normal of the surface is a three dimensional unit vector therefore two equally bright light sources are enough to solve the unit normal from (13) (Woodham 1978). The Lamberts law can be represented in matrix form as follows

$$\mathbf{i}_{mx1} = \rho E \mathbf{L}_{mx3} \mathbf{n}_{3x1}, \tag{14}$$

where m is the number of light sources, $\mathbf{i}$ is the intensity vector of light sources, $\mathbf{L}$ is the matrix consisting of 1x3 unit vectors towards each light source, and $\mathbf{n}$ is the unit normal of the surface. In this thesis four or more equally bright light sources are applied to decrease the uncertainty of the surface normal estimate. In that case the problem is over determined and can be solved by minimizing the square of error. The Lambert's law is applied to each image pixel separately and the result is a surface normal field. The gradient fields can be obtained from surface normal by dividing the x component by the z component (x-gradient) and the y component by the z component (y-gradient).

The 3D surface is reconstructed by integrating the gradient fields. The surface is not usually ideally Lambertian and thus the bias of surface normal is cumulated during integration distorting the result. Thus several methods have been developed to integrate the gradient fields (Frankot and Chellappa 1988; Simchony et al. 1990, Hansson and Fransson 2004; Hansson and Johansson 2000).

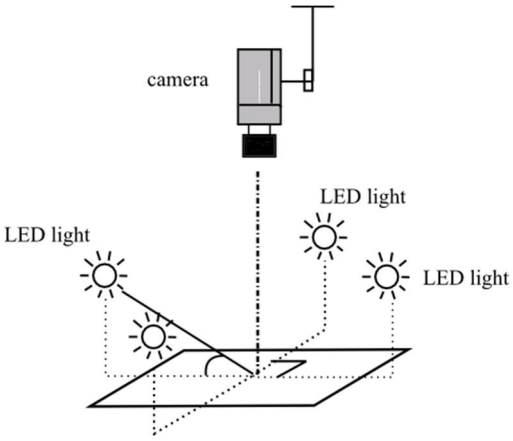

Figure 15. The imaging setup of photometric stereo with four lights.

When the surface is moving with high speed the images for photometric stereo must be taken with extremely fast imaging and illumination, or by using several wavelengths at the same time in the illumination, and taking only one image with a camera sensitive to several wavelengths (Woodham 1994, Smith and Smith 2005). Such method is applied currently in paper roughness and orientation measurement system (Ihalainen et al. 2012; Metso IQ 2013).

4. Evaluating characteristics of tissue paper from off-line images

During the past three decades the image measurements have been applied little in tissue paper industry. Hollmark (1972) was the first who studied the creping mechanism from experimental point of view by imaging the process with high speed cameras, and developed a description of the creping process. Furthermore, imaging has been applied off-line to characterise the crepe frequency from images (McConnel 2004; Archer et al. 2010; Raunio and Ritala 2012). This Chapter presents the novel analysis methods to estimate the 2D characteristics of creping pattern and the number of free fiber ends in tissue paper (Publication IV, Publication VII). Chapter 4 describes also the pre-processing method for the reflectance images applied in tissue paper analyses.

4.1 Pre-processing of off-line images

The assessment of the creping characteristics and counting of free fiber ends from the tissue paper are based on the gradient fields estimated with the photometric stereo method discussed in Section 3.5.2. The reflectance images must be pre-processed to decrease the distortion of surface normal estimates.

The tissue paper was measured off-line. Thus the camera and the target were aligned accurately and the perspective distortion was insignificant. However, the imperfectness of camera lenses causes radial distortion to the images. The radial distortion can be classified to negative distortion (also called barrel distortion) and positive distortion (also called pincushion distortion) (see Fig. 16).

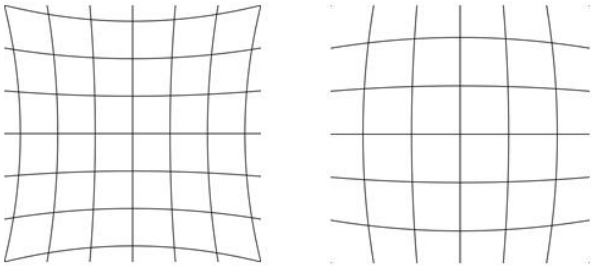

Figure 16. Typical radial distortions. The negative distortion on the right and positive distortion on the left.

In negative distortion the locations of points are moved towards the center of the image when viewed through the lens system, whereas positive distortion moves the points away from the center of the image. The radial distortion can be removed with two common methods (Mikhail 2001). The first method stores the reference radial distances (reference target e.g. chessboard with known square dimensions) and the corresponding distortion values, and the

image coordinates can be corrected by a lookup table and interpolation. Another way to correct the radial distortion is to describe it as a polynomial function of odd powers of distance from the center as follows

$$d_r = k_1 r^3 + k_2 r^5 + k_3 r^7 + \ldots \quad (15)$$

where d_r is the radial distortion, r is the distance of the point from the center of the image, and $k_{1,2,3,\ldots}$ are the radial distortion coefficients. The radial distortion coefficients can be determined from the image of a reference target.

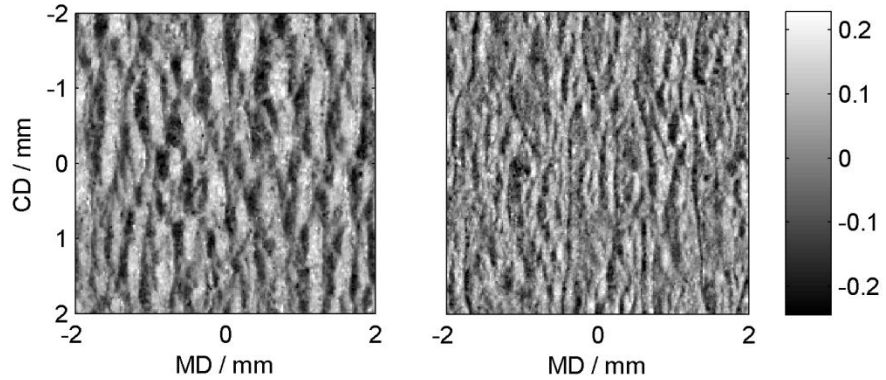

Figure 17. MD gradient fields estimated from bath tissue (left) and kitchen towel (right). The gradient fields were computed with photometric stereo method (Publication IV). Gray scale shows the magnitude of gradient.

The ridges of crepe bars are orientated in the CD of tissue paper. Thus the gradient field in MD was estimated with photometric stereo method (see Fig. 17). The computation of surface normals with photometric stereo is based on the reflected intensity variation of the sample surface. The photometric stereo assumes that the light arriving to the sample surface is collimated (= the unit vector toward the light source are equal in every spatial location of sample surface). However, this is not the case in our measurement system because the distance between the light source and the sample is small and the physical size of the LED light source is small. Thus the beam pattern of the light source on the sample surface depends on the intensity of the LED, and the location and the beaming of the LED.

The reflected intensity variations caused by the intensity of the LED and the beaming of the LED are compensated by a 2D second order polynomial. The polynomial is fitted on the calibration image which is captured from a surface that is flat and whose reflectance properties equal to those of sample surface. The second order polynomial was selected because the intensity of the light reflected from the sample decreases quadratically with the distance from the center of the LED beam. The 2D model can be defined as follows

$$i(x,y) = ax^2 + by^2 + cxy + dx + ey + f\,, \quad (16)$$

where x and y are the coordinates of each pixel in the image and the $i(x,y)$ describes the intensity of the pixels of the original image. The parameters from a to f are the polynomial

coefficients which are solved by minimizing the least squares of the error. The fitting was based on all the pixels in the calibration image. To compensate for the illumination variation on the surface, the original reflectance image is divided pointwise by the 2D polynomial. Figure 18 shows an example of the original reflectance image, the 2D second order polynomial model of the intensity variation, and the compensated reflectance image.

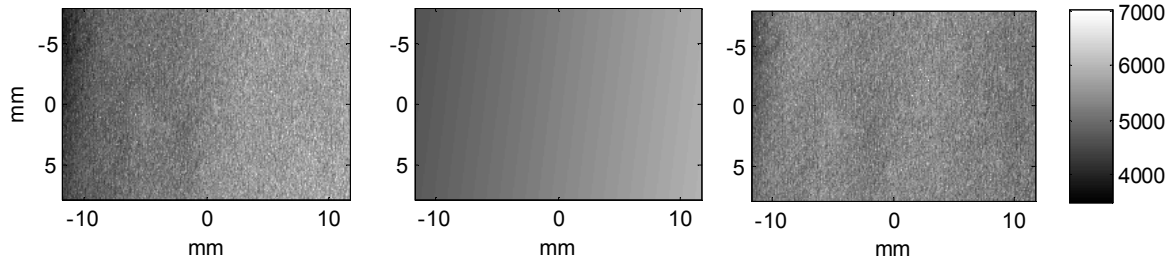

Figure 18. Effect of 2D second order polynomial compensation. Original reflectance image on the left, fitted second order polynomial in the middle and compensated reflectance image on the right. Gray scale shows the pixel intensity (12 bit image).

The orientation of the light beam arriving from the LED varies between the locations of the sample surface. Therefore, based on the Lamberts law the sample side closer to the light source should be brighter because of the steeper angle of the light beam. However, such variation was already removed above in the 2D second order polynomial compensation. Therefore, these variations must be reconstructed based on the known location of LEDs in our measurement system. Such compensation matrix is computed by dividing the height of the light source (z_{light}) by the distances (**d**) between each image pixel and the light source as follows.

$$C_{i,j} = \frac{z_{light}}{\mathbf{d}_{i,j}} = \frac{z_{light}}{\sqrt{\sum \left(\mathbf{x}_{light} - \mathbf{x}_{i,j}\right)^2}} \qquad (17)$$

The $\mathbf{x}_{\text{light}}$ is the (x,y,z) -vector containing the coordinates of the light source. The $\mathbf{x}_{i,j}$ is the (x,y,z) -vector containing the coordinates of the point on the sample. The i and j are the matrix indices. The result C is the cosine of angle between the z_{light} and **d**. To complete the preprocessing, the polynomial corrected reflectance image is multiplied pointwise by the matrix (17).

4.2 Methods to analyse the characteristics of tissue paper

Creping structure is essential for the functional physical properties of tissue paper: strength, absorption and softness. This chapter introduces the imaging methods to characterize the creping pattern of tissue paper, the number of free fiber in tissue paper, and the amount of pinholes in tissue paper which all are assumed to affect relevant properties of tissue paper. In this thesis these characteristics are measured off-line, and thus come late from control perspective. However, the developed image measurements are based on light transmittance and photometric stereo methods which both are already successfully applied at running paper

machine (Williams et al. 1996; Metso IQ 2013). Thus the image measurement methods developed in this thesis can be applied present on-line systems directly or only slightly modification is required.

4.2.1 Characterization of creping pattern

Creping provides softness for tissue paper. The structure of the creping pattern has usually been described with a single parameter which tells the average number of crepe folds per unit length in MD (Archer at al. 2010; McConnell, 2004). However, such a parameter ignores the 2D characteristics of the creping pattern. In this chapter, 2D power spectrum is applied to characterize the creping pattern (Publication IV). The 2D power spectrum was computed from MD gradient field estimated with the photometric stereo method presented in Section 3.5.2. The measurement system is a laboratory device which consists of a digital systems camera and four LEDs. The angle between the LEDs and the sample surface normal was 35º and the horizontal angle between the LED locations was 90º.

The two-dimensional Fourier transform converts the MD gradient field into the frequency domain. The Fourier transform of $f(\mathbf{x})$ is denoted as $F(\mathbf{k})$ and it describes the amplitude and phase for each frequency and orientation of 2D sinusoidal so that when summed they produce $f(\mathbf{x})$. Let $\mathbf{x}$ be the point (x_{CD},y_{MD}) in 2D spatial space and $\mathbf{k}$ the point (k_{CD},k_{MD}) in 2D dimensional frequency space. Then

$$F(\mathbf{k}) = \int_{\Re^2} f(\mathbf{x}) \exp(-i2\pi(\mathbf{x}\cdot\mathbf{k}))d\mathbf{x} \tag{18}$$

The power spectrum which is the squared amplitude at each frequency is

$$S(\mathbf{k}) = |F(\mathbf{k})|^2 . \tag{19}$$

The power spectrum computed from a single image contains a significant amount of noise and the estimates derived are uncertain. To reduce the uncertainty the 2D Welch spectrum estimate was computed by averaging 15 power spectra from one image area and by taking their average as the spectrum estimate (Welch 1967). The size of each spectrum was 1/2 from the height and 1/3 from the width of the original image, the overlaps of the spectra were 50% in both x and y direction. Before computing the power spectrum each image was Hamming windowed (Lim 1990). This decreases the image edge effects that produce spectral side lobes in finite-sample Fourier transforms. Fig. 19 shows as examples the Welch spectra computed from the two CD gradient fields in Fig. 17. Furthermore, the spectra are transformed into polar coordinates (see Fig. 20) in which the variation in angular space can be seen more clearly. In this representation wavenumbers are pairs of angle ϕ and distance k from the origin.

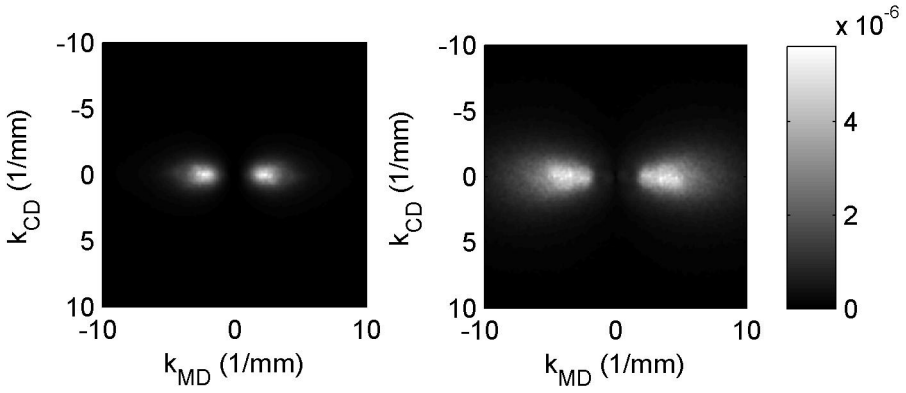

Figure 19. The Welch spectra computed from the bath tissue (left) and from the kitchen towel (right). Gray scale shows the magnitude in the spectrum (Publication IV).

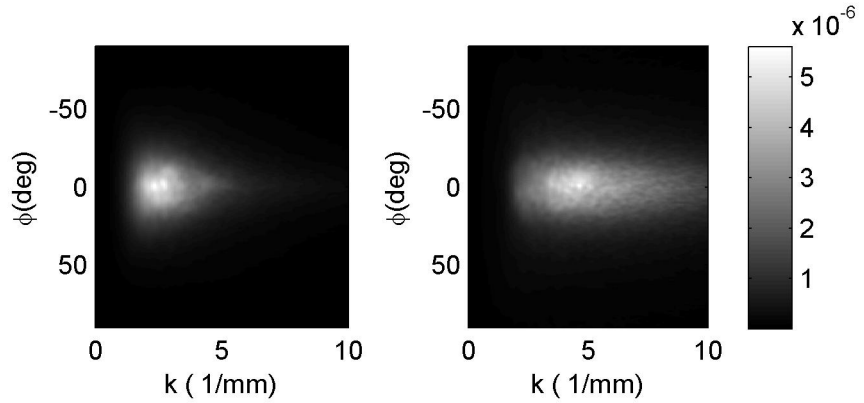

Figure 20. The Welch spectra of the bath tissue (left) and the kitchen towel (right) transformed to polar coordinate system (Publication IV).

It can be seen that the intensity of Welch spectra concentrates around certain MD frequencies, which is due to the creping pattern in the tissue samples. The 2D shape of the high intensity area in the Welch spectrum in polar coordinate system is approximated with a 2D Gaussian function. Note that in the publication IV the 2D Gaussian approximation was done in Cartesian coordinate system whereas in this chapter the approximation is done in polar coordinate system. The Gaussian function was fitted by using trust-region optimization algorithm (Polak 1997). The intensity function is obtained as follows

$$I(\mathbf{s}_i,\mathbf{s}_0,W,Q)=\exp(-\frac{1}{2}(\mathbf{s}_i-\mathbf{s}_0)^T\Sigma^{-1}(\mathbf{s}_i-\mathbf{s}_0)),\ \text{where}\ \ \Sigma=\begin{bmatrix}W^2 & 0\\ 0 & Q^2\end{bmatrix}. \qquad (20)$$

It was assumed that the Σ is diagonal matrix. Thus the intensity function can be obtained as the multiplication of two 1D Gaussian functions as

$$I(\mathbf{s}_i,\mathbf{s}_0,W,Q,A)=A\exp(-\frac{(\mathbf{s}_i-\mathbf{s}_0)^2}{2W^2})\exp(-\frac{(\mathbf{s}_i-\mathbf{s}_0)^2}{2Q^2}).$$

The parameters W and Q determine the spread of the intensity function in k and ϕ directions in polar transformed power spectrum. The W describes the width variation of crepe folds in MD and Q describes the waviness. The location of the Gaussian function is $\mathbf{s_0}$ denoted as *(k_0*

$,\phi_0)$ where ϕ_0 is zero and k_0 is the average number of crepe folds in MD. The $\mathbf{s_i}$ is the point (k,ϕ) in 2D dimensional wave number-angle space. Coefficient A is the peak amplitude of the Gaussian distribution.

The fitted parameters of bath tissue grade (see Fig. 20 (left)) were k_0=2.9 1/mm, W = 1.2 1/mm, and Q = 16.5º and k_0=5.8 1/mm, W = 2.2 1/mm, and Q = 17.4º in towel grade (see Fig. 20 (right)). The average wave number 2.9 1/mm corresponds to wavelength of 0.35 mm in bath tissue grade and 5.8 1/mm corresponds to wavelength of 0.17 mm in towel grade (see Fig. 17). Furthermore, small W in bath tissue grade indicates that the wavelength of the crepes folds is quite constant in MD which can be seen in Fig 17 (left and right). The waviness Q of creping patterns was roughly equal in the samples.

The intensity distribution can be approximated also with other functions, e.g., with a product of 1D Gaussian distribution in ϕ direction and χ^2-distribution in k direction which mimics the shape of the creping pattern in k direction better than the Gaussian distribution. Figures 21 and 22 show the 1D profiles summed over the angle and the wave number direction. Figures also show the fitting results by using Gaussian-Gaussian and Gaussian- χ^2 fitting.

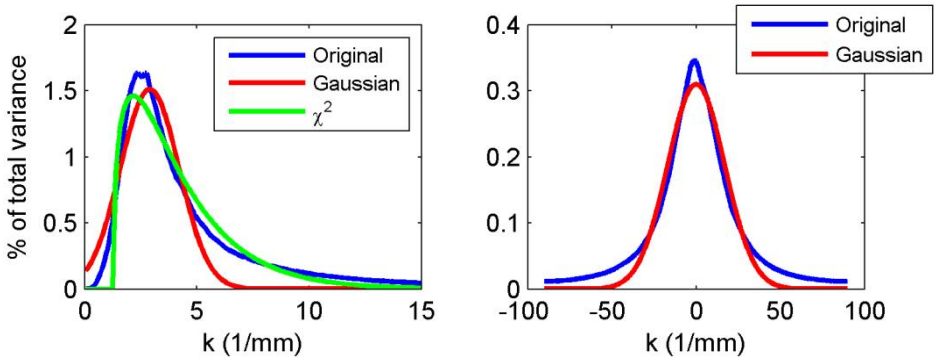

Figure 21. Fit visualization in Bath tissue grade. Wavenumber profiles on the left and angle profiles on the right.

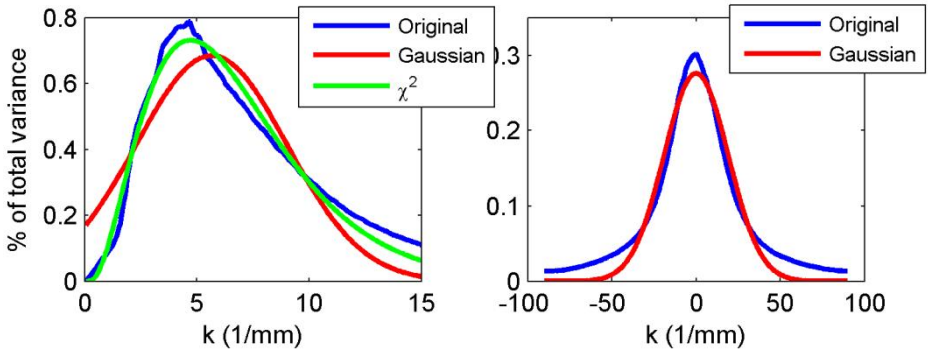

Figure 22. Fit visualization in Kitchen towel grade. Wavenumber profiles on the left and angle profiles on the right.

In χ^2-distribution the optimized parameter is degree of freedom d. The k_0 was approximated by using definition of mode (k_0=d-2) in χ^2-distribution. The W can be estimated with the variance defined in χ^2-distribution as $W = 2d$. In bath tissue grade the W (standard deviation) and k_0 (mode) estimated with χ^2-distribution were W= 6.2 1/mm and k_0=2.2 1/mm. In towel

grade the values were W= 12.9 1/mm and k_0=5.0 1/mm. The goodness of fit between the two functions is compared in table 2 below.

Table 2. The goodness of fit statistics

	1D Gaussian * 1D Gaussian			1D Gaussian * 1D χ^{2-} distribution		
	SSE	R^2	RMSE	SSE	R^2	RMSE
Kitchen towel	0.598	0.878	0.062	0.053	0.989	0.018
Bath tissue	5.97	0.805	0.195	1.82	0.940	0.108

A SSE denotes the summed squares of errors (the lower the better), R^2 is the square of the correlation between the original and the model (range 0..1, higher the better), and RMSE means the root mean squared error (the lower the better). It can be seen that the product of 1D Gaussian and χ^2-distribution fits better than the product of two 1D Gaussians in both bath tissue and kitchen towel grade.

4.2.2 Estimating the number of free fiber ends

One shortcoming in the current tissue softness measurement devices is that they do not detect the smooth surface feeling of tissue. One cause for smooth surface feeling are the fiber ends which are pointing out on the paper surface. Hollmark and Ampulski (2004) suggested that the artificial robotic fingers studied in medical applications (Howe and Cutkosky 1992; Howe and Cutkosky 1993) could be applied also in the measurement of surface softness of tissue paper. However, the online application of such measurement device is not currently realistic because of the required contact between the sample and the device.

In this thesis an image based measurement method was developed (Publication VII) which detects fibers extending from the surface (=free fiber ends) of tissue paper based on the shadows of the fibers. The patent application related to the measurement system and the invented measurement method was filed in 2013. The shadows become detectable after the creping pattern is removed from the image of the tissue paper. The detection method presented in this Chapter utilizes the photometric stereo method presented in Section 3.5.2 in which the target is illuminated from 12 horizontal locations and the surface normal at each image pixel is estimated (Woodham 1978). The vertical angle between the LED and the sample surface normal was 30º. The measurement system is a laboratory device which consists of a digital systems camera, LED, the sample holder and two linear polarizers. The unwanted effect of specular reflection was reduced by crossing the polarizers placed in front of the LED and in front of the camera lens (Saito et al. 1999; Wolff 1990). The light source was attached to a supporting arm (see Fig. 23). The supporting arm rotates around the sample. Thus the sample located on the sample holder can be illuminated from various angles. Figure 23 shows a schematic drawing of the measurement device and the measurement procedure.

First, the surface normal vectors for each pixel were estimated based on photometric stereo. The photometric stereo method summarizes the pixel information from 12 reflectance intensities to a three dimensional surface normal vector and thus averages out any discontinuity points caused by shadows or specular reflections. The computation of surface normal vector is based on minimizing the square of errors and thus e.g. the effect of a shadow

visible only in one reflectance intensity is small compared to the other 11 reflectance intensities in which the shadow is not present. The Lambert's law (Lambert 2001) was then applied to reconstruct the reflectance image from the estimated surface normals. The difference between the reconstructed reflectance image and the original reflectance image was computed, in order to capture image features not contributing to the surface normal estimates. The difference image includes discontinuity points which the Lamberts law was unable to recover (see Fig. 24 (c)). The discontinuity points caused by the abnormal reflection can be seen as noise whereas the shadows can be seen as long and thin dark colored objects.

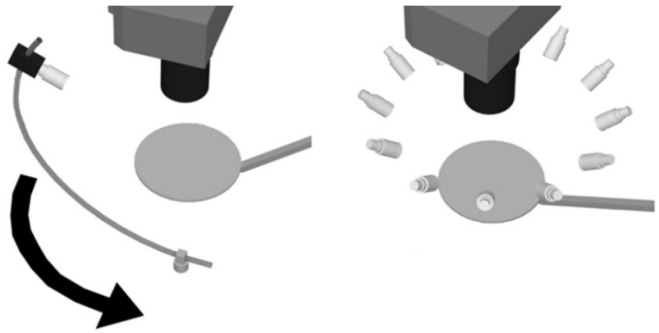

Figure 23. Schematic drawing of the measurement device. The device consists of a digital systems camera, LED, and sample holder. Each location of the LED during imaging is drawn to same image on the right (Publication VII).

The difference image was processed with *orientated means* -method (Galun et al. 2007). The method computes the mean for each pixel location and orientation of line. The shadows are darker than the rest of the variation in paper and thus the minimum orientation value is selected for the resulting image. The typical width of the wood fiber is 20 µm and the length of fiber varies typically between the 200 µm and 1000 µm (see e.g. Paulapuro 2008). However, the length of the shadows varies depending on the angle and the extension of free end of the fiber being shorter than the actual fiber. Thus, the width and the length of the line objects detected from image are set in this method to 20 µm and 100 µm, respectively. If the object width is 10% wider (narrower) the number of found objects decreases (increases) around 10%. The 10 % increase (decrease) in the fiber length increases (decreases) the number of found objects around 20% thus being more sensitive for the change than the width. Furthermore, when the length of the object is larger than 700 µm the count starts to decrease. The percentage changes in this sensitivity analysis depend on the analysed tissue grade, however the given values are well representative. Figure 24 shows a small portion of the original reflectance image illuminated from the direction of the lower edge and the reconstructed image from the same area computed with the method described above. Figure 24 shows also the difference image between the original and the reconstructed reflectance images and this image filtered with the *orientated means* -method.

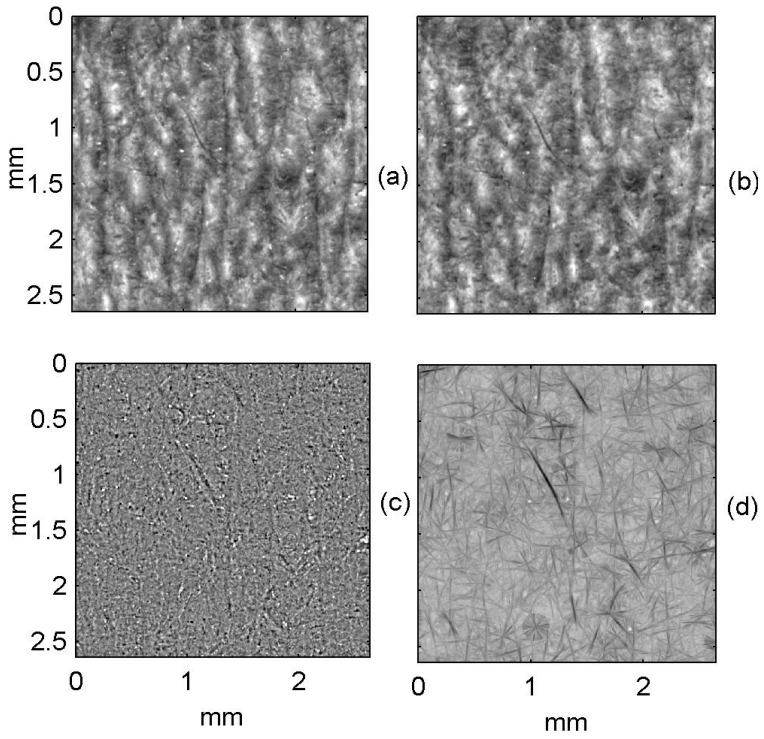

Figure 24. Close-up from the original image (a), the reconstructed image (b), the difference between the images (c), and the image (c) processed with *orientated means* - method which amplifies the shadows (d) (Publication VII).

The shadow objects can be detected from processed image (d) by thresholding. First, the histogram which shows the distribution of pixel values was computed. The threshold limit was set to 0.2%. The threshold limit was selected based on the fiber counts of the reference measurement system introduced in (Pawlak and Elhammoumi 2011). By setting the threshold limit 10% higher increases the number of found objects about 10%. Similarly the 10% lower threshold limit decreases the object about 10%. In the binary image only objects whose length is larger than 100 μm are accepted. Furthermore, the shape of the object should be elongated. Therefore the lengths of the minor and major axes of an ellipse fitted to the each object were calculated. The ellipse fitting algorithms are based on the 2D Gaussian function fitted to the coordinate points (Fitzgibbon et al. 1999). The objects whose major axis was at least five times longer than the minor axis, i.e. those with eccentricity larger than $2\sqrt{6}/5$, are accepted in the final binary image.

The performance of the image based measurement method was compared with a reference measurement similar to the one introduced by Pawlak and Elhammoumi (2011). The reference measurement procedure is as follow: the tissue paper sample was folded over an edge and the image of the folded edge of the tissue paper was captured with a digital camera. Figure 25 shows the image of the folded tissue paper. The long fibers extending from the surface can be seen clearly.

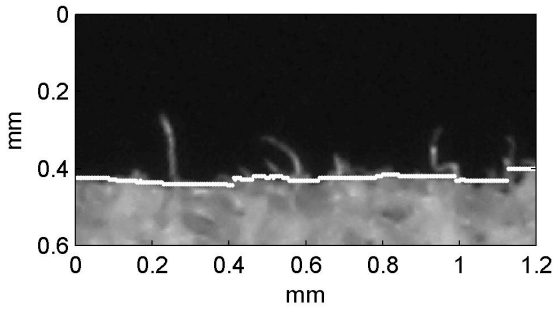

Figure 25. Surface of folded tissue paper. The estimated surface boundary is drawn on the image with white dots (Publication VII).

The surface boundary was estimated by computing the difference of the pixel vector in the y-direction for each x location. The maximum difference in y-direction was obtained and the mean value from the neighboring surface boundary points in the x-direction was computed. Fibers whose location was more than 50 μm above the estimated surface boundary were considered to be free fiber ends (see Fig. 25, white curve). The width of the folded edge was approximately 2 mm and this width was used to estimate the density of free fiber ends per area (numbers / cm^2). The adjustable parameters in the shadow based imaging method—the length of shadows considered to be shadows of the free fiber ends and the threshold level in conversion from gray scale to binary image—were chosen to minimize the difference between the two independent measurements. Both free fiber end counts (reference and imaging method) were measured from the same samples (sample area 10 cm x 10 cm) but not from the same location.

It can be seen that the results of the shadow based imaging method are in reasonable accordance with the results of the reference method (see Table 3). The samples rank in the same order in both measurements. Furthermore, the standard deviations are significantly smaller in the shadow based imaging method, which is mostly because of the larger measurement area. The area from which the shadow of free fiber ends are counted is 7.8 times larger than in reference method which indicates that the standard deviation should be reduced by a factor of $\sqrt{7.8} \approx 2.8$. However, the standard deviations are a somewhat higher in the new method than this straightforward argumentation predicts.

The stability of the results in Table 3 was studied with sensitivity analysis. It was noticed that the 50 % decrease in the fiber length limit in the developed imaging method decreased the total free fiber end count by 5% when the shadow threshold limit was kept constant. The 50% increase in the fiber length limit increased the total free fiber end count by 10%. The effect was equal in each tissue grade analysed in this thesis. The 50% increase in the shadow threshold limit increased the final free fiber end count by 25% and the effect was equal in each tissue grade. However the 50% decrease in the shadow threshold limit decreased the free fiber end count from kitchen towel by 20% whereas in other grades the decrease was around 40%.

The small count difference between the measurements can be explained with the different measurement technique: the reference method counts particularly the extending fibers whereas the shadow based imaging method counts the shadows of fibers. It is possible that the slant angle of a fiber is so small that the reference method ignores the fiber in its count whereas the novel imaging method may still detect the shadow of such a tilted fiber. Furthermore, the folding of tissue paper may straighten up certain fibers that otherwise lie flat on the surface, and thus cause the difference in the counts.

Table 3. The averages and standard deviations of free fiber end densities (number / cm^2) estimated with the reference measurement system (36 measurement points per grade) and the shadow based imaging measurement system (36 measurement point per grade).

	Kitchen towel	High-quality facial tissue	Low-quality facial tissue	High-quality toilet paper	Low-quality toilet paper
$Avg._{reference}$	42.4	124.8	71.6	90.9	41.5
$Std._{reference}$	19.7	25.5	19.8	16.2	18.0
$Avg._{image}$	52.0	127.5	64.1	93.9	43.8
$Std._{image}$	14.0	7.9	7.8	11.1	15.2

4.2.3 Detecting the pinholes from paper

The polarization of light provides relevant information of paper when transmitted through paper or reflected from paper surface. This is because the polarization of light changes when travelling through fibers. This phenomenon is applied e.g. in the consistency measurement of pulp suspension (Madsen and Simms 1979) and in the detection of fiber orientation of paper (Shakespeare 2007) and anisotropy of paper (Linder and Löfqvist 2012). This Section presents a method for detecting pinholes in paper by polarization analysis. The pinholes are small holes in paper which are especially a problem in small basis weight paper products such as tissue papers. A large amount of pinholes deteriorates the absorption and the visual appearance of paper and may increase the probability of fractures in paper.

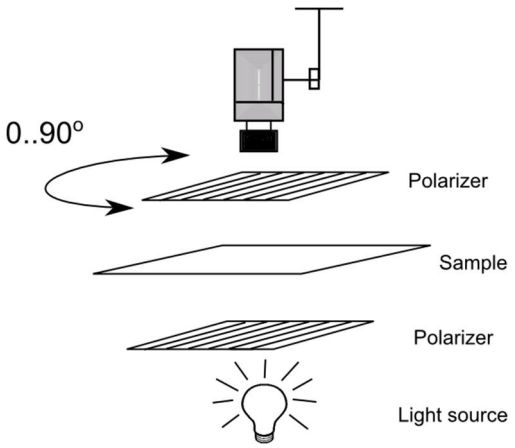

Figure 26. Measurement system to detect the pinholes in paper.

The measurement system which detects the pinholes consists of a camera, two linear polarizers and the light source. The camera measures the light transmittance through the paper. One polarizer is placed between the light source and the sample and the other polarizer between the camera and the sample (see Fig. 26). The latter polarizer can turn 90 degrees.

Two images are captured from the target: one with parallel polarizers and one with crossed polarizers. When the light travels through paper it scatters from fibers and thus the polarization becomes random and the intensity decreases. On contrary when the light travels through holes the polarization and the intensity remain unchanged. Thus when the polarizers are parallel the pinholes appear as bright dots and when the polarizers are crossed the pinholes can be seen as black spots. In locations which are not holes the intensity of light travelled through paper is approximately equal in both images. Furthermore, the difference between the two images was computed. The difference between the images increases the contrast and the pinholes become easier to detect (see Fig. 27 (a),white spots). Figure 27 (b) shows the pixel intensity distribution of the difference image and the threshold limit (gray line). Finally, the difference image is thresholded (c). The threshold limit was selected based on the intensity values in calibration images with the two arrangement of polarizers and captured without a sample. The histogram which shows the distribution of pixel values was computed from the difference of calibration images and the threshold limit was set to pixel value in which 1% of pixel intensities are lower. This limit was applied as a threshold limit in the difference of sample images. The sensitivity of threshold limit is the following: if the limit is increased by 500 units (pixel value) the total area of pinholes decreases by 44 % and if the limit is decreased by 500 units the total area increases by 92 %. The number of pinholes decreased by 46 % and increased by 54% with the same changes.

The introduced measurement system consists of one camera and the rotating polarizer. However, the rotating polarizer can be removed by using two synchronized cameras provided with crossed linear polarization filters. This modification enables also the on-line application of such measurement method.

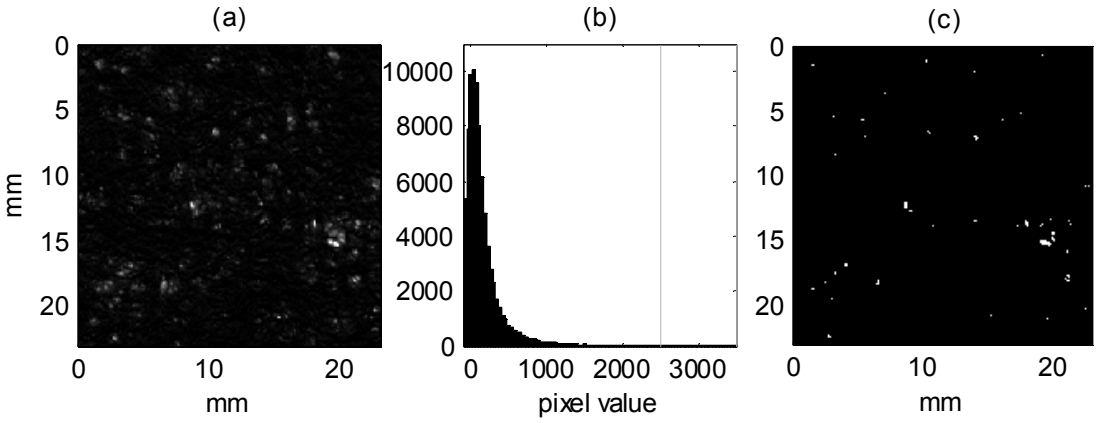

Figure 27. (a) Difference image, (b) the pixel intensity distribution and the threshold limit(gray line), and (c) the threshold difference image.

5. Evaluating the characteristics of newsprint from on-line images

During the last two decades several web-wide measurement systems have been suggested to overcome the fact that the scanning-based measurement provides a rather sparse sample of the entire web. Shapiro et al. (1998) introduced a web-wide measurement system based on the electric properties of the fluid inside of the paper. Hindle et al. (1994) presented the web-wide measurement based on parallel near infrared sensors and transmitters. A commercial system measures the moisture of paper web-wide with parallel IR radiators and sensors (MetsoIQInsight 2013). However, none of these measurements is able to detect the small scale texture of paper. Ferguson et al. (1997) introduced the measurement system consisting of parallel near infrared cameras which could be used with a scanning based measurement system in 2D basis weight estimation. Chen (1998), Chen et al. (1998) and Pfeifer et al. (1998) introduced a measurement system consisting of CCD cameras and light source which measures the whole paper web. However, these 2D measurement systems were not completely successful in paper machines on one hand because the technology for having a large number of parallel sensors is expensive, and on the other hand because calibrating the parallel sensors/cameras in the measurement systems is difficult.

During the last few years, the price, speed and performance of cameras and devices providing the illumination have achieved a level which enables high-resolution on-line imaging of paper at a reasonable price. Such technology is in use in web inspection systems (WIS). In this Chapter the methods to estimate the small scale paper structure characteristics (Publication VI) and the CD shrinkage profile of paper (Publication II) based on on-line images are presented. Furthermore, this Chapter discusses the uncertainty of basis weight estimation from on-line WIS images for CD/MD control and diagnostics applications (Publication V) and the limitations of on-line imaging.

5.1 Modes of on-line imaging

There is a variability in paper from sub millimeter (= fast variation) scale, which is caused e.g. the local fiber and filler variation, to scales of tens of kilometers in MD (slow variation) which is caused e.g. the imperfect function of valves or actuators at the paper machine. The variations are generally divided into three components: a variation in the running direction of paper machine (MD), a variation in cross direction of paper machine (CD) and the residual variation (Chen 1998). From residual variation the variations in CD and MD have been removed and thus its average in CD and MD is zero. The variations can be measured with a single scanning camera or continuous web-wide imaging system.

Scanning camera measurement is usually installed in the current on-line scanning measurement system (see Chapter 3.1.1) in which the scanner moves back and forth across

the paper web. Such camera systems are in use in paper machines and they measure e.g. the orientation of fibers (Metso IQ 2012; Chen 2010), the formation of paper (Metso IQ 2012, ABB OP4255 2013), and the roughness of paper (Ihalainen et al. 2012; Metso IQ 2013). The scanner based measurement system is suitable for estimating paper properties which are slowly varying in time, e.g., the CD shrinkage profile of paper. However, any fast variation of shorter duration than the scan time will escape observation and estimation, and most residual variations cannot be estimated.

Continuous web-wide imaging is based on several adjacent cameras in CD and an illumination panel which is normally implemented with LEDs (see Fig. 28). The imaging areas of adjacent cameras and the areas of consecutive images of a camera in time are overlapping, so that the entire web is captured in CD and MD. At the moment the technology is in use in the web inspection systems, which detect and classify the defects such as holes and dirt particles of paper web based on the light transmittance images of paper (Williams et al. 1996). The system is also applied in the estimation of simple paper characteristics such as light transmittance and formation. The WIS system whose data were available in this thesis consists of eighteen 8-bit cameras capturing approximately 330 images per second. The data rate is 594 Mbytes/s with lossy compression and 1200 Mbytes/s with lossless compression of VGA image. Therefore the pre-processing of images and data compression of images is made by fast hardware circuits e.g. by using field programmable gate arrays (FPGA). At the moment, the WIS detects mainly the defects of paper and saves only the numbers, locations and sizes of the defects. This action compresses significantly the data captured with WIS and enables the visualization of information e.g. showing the defect map and their statistical and CD/MD summaries. If the WIS images were to be applied for controlling the paper machine, the resolution of continuous image data must be decreased significantly. For control purposes the resolution of the data could be e.g. 10 mm in CD (corresponding the resolution in quality control system (QCS)) and 100 mm in MD (333 Hz sampling frequency at 30 m/s web speed) which is enough for diagnosing for example the fast consistency and pressure variation of pulp in headox. The data rate of such compressed data is 1.2 Mbytes/s with lossless compression.

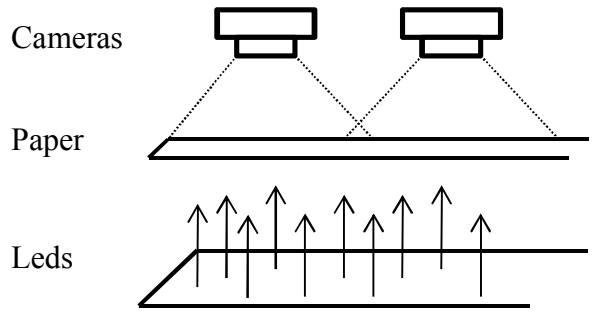

Figure 28. Web-wide imaging which measures the light transmittance. Usually the WIS consists of several cameras which each cover e.g. 50 cm in CD.

Snapshot web-wide imaging means the case in which the full-resolution images captured web-wide are recorded over a period of time, typically 10-100 s, and downloaded from the WIS for pre-processing and off-line analysis. The number of images to be saved depends on

the size of the image buffer available in WIS. The downloading of images is required in high level analysis in which the hardware based on FPGA is not capable. The size of the WIS images studied in this thesis is 640 x 128 pixels (CD x MD). The resolution of the images was 0.83 mm/pixel in both CD and MD. Thus, the size of a single image was 531 mm x 105 mm. Snapshot web-wide imaging can be applied e.g. in the estimation of small scale characteristics of paper and for trouble-shooting purposes in which the high-resolution of images in time and in CD is required.

5.2 Limitations of on-line imaging

The paper characteristics estimated from off-line images are only mildly affected by variations of illumination intensity and geometrical distortions. This is because the paper is not moving and thus the illumination and the orientation of the camera can be adjusted to achieve the best image quality. However, in on-line situation the imaging disturbances are less well controlled. In on-line imaging the target moves and also the illumination conditions may drift over long term. This section discusses the error sources in on-line imaging.

5.2.1 Resolution of the imaging system

The resolution of the imaging system depends on the size of the image sensor, the number of pixels in the image sensor, the focal length of the lens and the distance of the object from the camera. The high imaging rate required in on-line imaging means that the resolution of images tends to be low. Figure 29 shows a schematic picture of two ideal modulation transform functions computed from the image data sampled at two different resolutions in k_y direction. The resolution (=the sampling rate) in measurement 2 is double compared to that in measurement 1. The dashed area shows the difference between the measurements and the dotted line shows the ideal MTF.

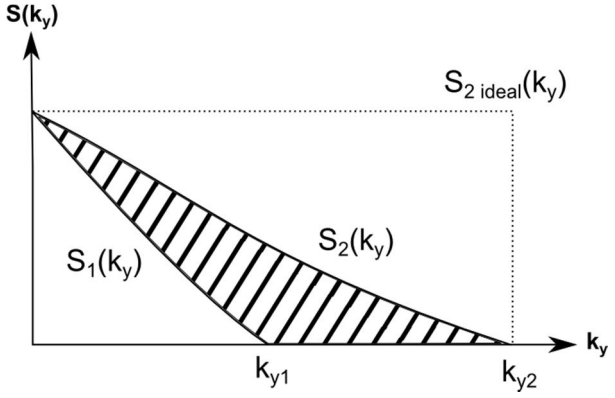

Figure 29. A schematic drawing of two power spectra estimated from the data sampled at two resolutions. The dashed area shows the difference between the spectra (=the difference of variance).

It can be seen that the variance, which is the integral of the spectrum, depends significantly on the resolution of the measurement. Thus the paper characteristics estimated from imaging systems of different resolutions cannot be compared as such. For example, the pixel size of on-line WIS images (0.83 mm) is not sufficient for detecting the small scale constituents such

as smallest scales of formation or individual fibers, which can be detected in high-resolution image based on-line formation measurement (Metso IQ 2012) or in off-line formation measurement based on imaging (Avikainen et al. 2004) or beta radiation (Keller and Pawlak 2001). Thus when calibrating or comparing two measurements of different resolutions, the higher resolution must first be decreased computationally to match the lower resolution.

5.2.2 The movement of the target and the vibration of the camera

The main sources of movement which cause distortion to on-line images are the linear movement of paper and the periodical and random mechanical vibrations of the imaging system. The paper machine consists of heavy rotating elements, such as rolls and reels. Thus the WIS system situated usually before the reeling cannot be completely mechanically isolated from the machine. Furthermore, the exposure times in machine vision cameras may vary to a small degree. These distortions can be avoided by pulsing the light source and keeping the shutter open during a period longer than the light pulse. The length of the light pulse in the WIS studied in this thesis was approximately 5 µs. Figure 30 shows how the movement of paper during imaging depends on the duration of the LED pulse. The relationship is drawn with two machine speeds: 25 m/s (gray) and 36 m/s (black).

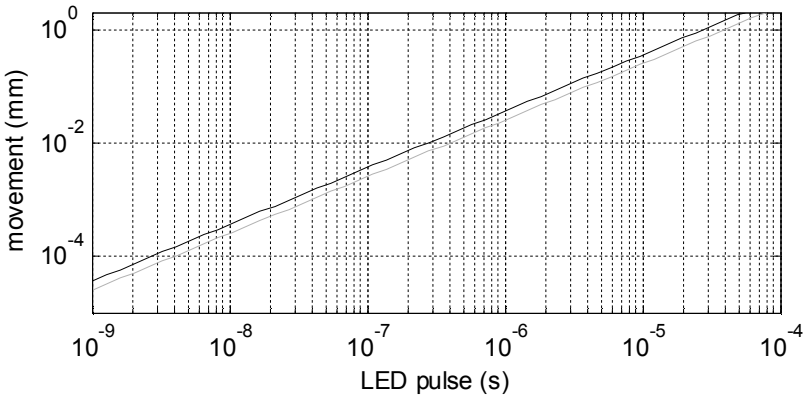

Figure 30. The relationship between the length of the LED pulse and the movement of the target during illumination.

It can be seen that the target movement is 0.125 mm when the length of the LED pulse is 5 µs and the machine speed is 25 m/s. Obviously, the movement is larger, 0.175 mm, when the machine speed is 36 m/s. Figure 31 shows three MD Welch spectra in which the effect of the longer and shorter light pulse is shown. Blue line shows the simulated Welch spectrum in which the effect of 5 µs pulse length is removed with the deconvolution by using Wiener filtering (Lim 1990). Red line shows the original MD Welch spectrum in which the pulse length was 5 µs and green line shows the effect with 10 µs pulse length. The MD spectra were calculated by averaging the values from the 2D Welch spectra over CD.

It can be seen that both the 5 µs and 10 µs pulse lengths act as a low-pass filter in MD by filtering high frequencies. Thus especially the orientation and the length scale of formation estimated from the spectrum do depend on the pulse length.

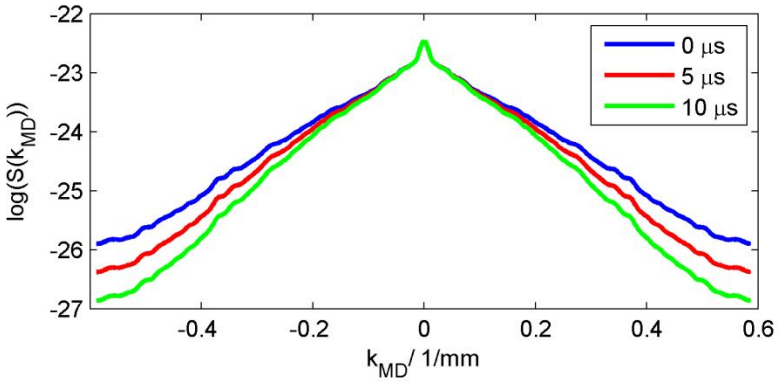

Figure 31. The effect of shorter and longer pulse length on MD Welch spectra. The effect of 0 µs pulse length (blue line), the original Welch spectrum (5 µs pulse length) (red line) and the effect of the 10 µs pulse length (green line).

5.2.3 Illumination effects

During the past decade the illumination with sufficiently short light pulses has usually been implemented with LED panels. Although the quality of illumination panels is increasing constantly the intensity of a single LED may vary, and the electrical components providing the current into the LED are not identical either causing e.g. differences in how fast the LED achieves its maximum intensity. As a result intensity varies in the LED panel. Figure 32 shows a WIS image of a part of the LED panel without a paper. It can be seen that the intensity of the LEDs has strong spatial structure. Furthermore, the joints of plastic covers protecting LEDs cause thin non-transparent areas, the two vertical black stripes.

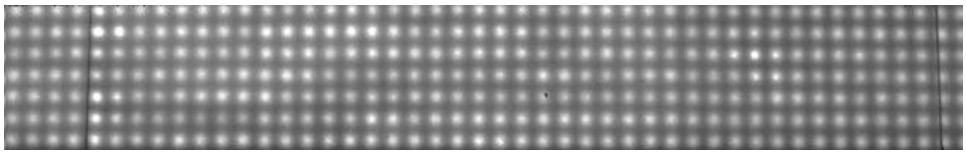

Figure 32. An example image of LED panel (550 mm x 105 mm). The intensity of the LEDs varies locally and the contact surface between the plastic covers on the LED panel forms two black vertical stripes shadowing the LEDs.

The time-independent illumination variations can be compensated as presented in the next chapter. However, the best quality of illumination compensation is achieved with appropriate off-line calibration of the camera system. This can be done with a reference sheet which is imaged at each camera separately. The reference sheet should be located at the same height as the running paper web and the exact location and possible rotation of the reference sheet must be known. The reference sheet must be imaged also with the separate off-line system so that the variation specific to the paper can be separated from the variation caused by the WIS. However, such an ideal calibration arrangement is very tedious and not possible during this thesis because of the loss of highly valuable production time during calibration.

5.3 Pre-processing of on-line images

In online measurements the initial quality of images taken from the paper is usually insufficient for analysis of paper properties directly (see Fig. 33). Each image is acquired through an optical system which consists of illumination, paper and camera. This system causes several forms of geometric and intensity distortions. These distortions must be modeled and compensated for reliable estimation of the variation of paper characteristics. The geometric and intensity distortions can be estimated reliably with a reference image (Asada et al. 1996; Yu 2004). However, in paper machines the paper grade, the illumination conditions or the performance of the cameras may change while the machine is running and therefore the reference images captured when the machine was stopped would be inaccurate as references. Thus the models of intensity and geometric distortions must be estimated from the on-line images (Publication II).

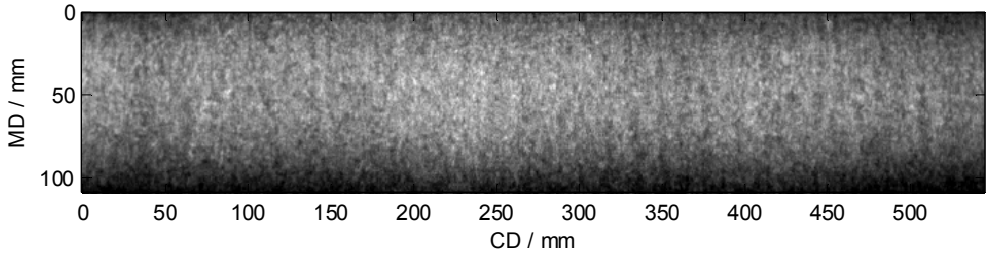

Figure 33. Example of an image captured with web inspection system (WIS).

The radial distortion of the lenses is constant over time and can be estimated from the cameras before installation to the WIS by using the method presented in Chapter 4.1. The perspective distortion caused by the orientation of camera can be determined by studying the overlap areas of the images; the consecutive images in MD are overlapping by 20%. The perspective distortion can be corrected by planar projective transformation when it is assumed that the camera orientation has not changed during the imaging period. Figure 34 shows an example of reference grid and the effect of projective transformation.

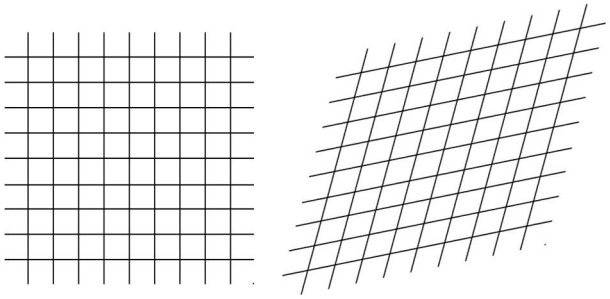

Figure 34. The effect of projective transformation. The reference grid is shown on the left and transformed on the right.

The projective transform can be defined with homogeneous coordinates (Sonka 1998) as

$$\begin{bmatrix} xp' \\ yp' \\ wp' \end{bmatrix} = M \begin{bmatrix} x \\ y \\ 1 \end{bmatrix}, \quad where\, M = \begin{bmatrix} a & b & c \\ d & e & f \\ g & h & i \end{bmatrix} \tag{21}$$

where M is the transformation matrix. The variable i assumes value 1 (Sonka 1998). The $(x,y,1)$ and (xp',yp',wp') respectively are the locations of the corresponding points in the coordinate system of paper and in the homogenous coordinate system. The homogenous coordinates xp', yp' and wp' are transformed to $(x',y',1)$ coordinate system by dividing the xp' and yp' with wp'. Thus the (x',y') coordinates can be written with two equations and eight unknowns.

$$\begin{cases} x' = (ax+by+c)/(gx+hy+1) \\ y' = (dx+ey+f)/(gx+hy+1) \end{cases} \tag{22}$$

To solve the transformation matrix M, theoretically having four corresponding points in the overlapping images is sufficient. However, in order to obtain a reliable estimate at least 50 corresponding points are used here and the transformation matrix is solved in the least square sense. Fig. 35 shows an example of an image pair for which overlapping areas are stitched together from consequent uncorrected images (top), and the bottom part of Fig. 35 shows the projective transformed images.

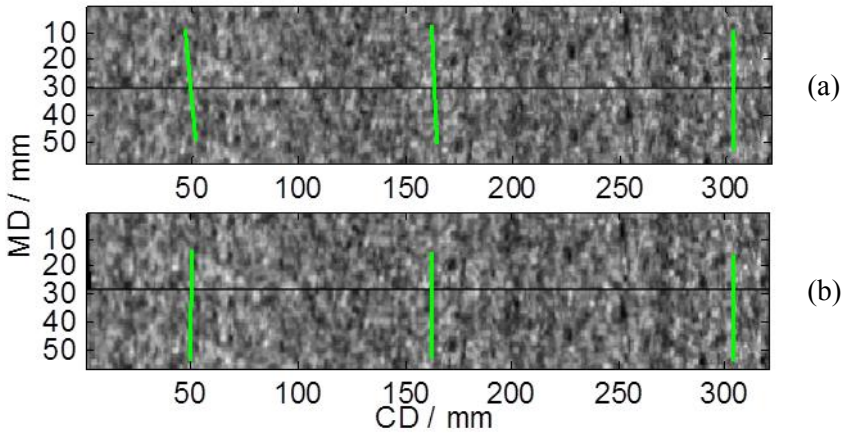

Figure 35. Effect of projective transformation. The overlap areas of consecutive images (a) before and (b) after projective transformation. The green lines illustrate the geometric distortion.

Furthermore, the illumination effects not caused by variations in the web need to be removed. The image is darker near the edges (see Fig. 33) which is because of too small LED panel in MD. Thus the image captured from paper is a product of intensity variation and the true variation of paper as $I(x,y) = Q_{paper}(x,y)\, n_{error}(x,y)$.

It is assumed that the unevenness of illumination is constant in the time scales concerned and the variation in the paper is the only cause for intensity variations from image to image. This constant texture can be uncovered by computing MD average image of N consequent images for each camera located in the WIS. The average image for a single camera is marked as $I_{avg} = \frac{1}{N}\sum_{i=1}^{N} I_i$. It is important to note that the paper may also include constant structure variation in MD, in CD profile, which is removed with the compensation method. Finally each unprocessed image is divided with the average image and the true variation of paper is

reconstructed (see Fig. 36). The division is selected over subtraction because it unifies the variation in the image area.

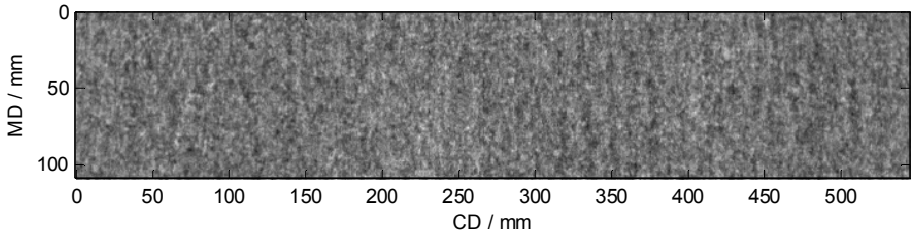

Figure 36. The original image (see Fig. 33) divided with an average image.

Finally, the images are stitched together to form the web-wide transmittance map. Each image is positioned according to the ordering of the images which gives their approximate relation (i.e. before/after or next to) each other. The exact overlap between the images is determined by maximizing the point-wise cross correlation. The typical maximum correlation between the overlap areas was 0.5-0.6 being approximately three times larger than base level correlations. Also, the maximum correlation is achieved only from very small area which indicates that the found maximum reveals the overlap between the images reliably. The imaging rate is equal in each camera which implies that the overlap in MD between the consecutive images should also be equal. However this is not the case. This is because the distance between the cameras and the paper and the focus of the cameras vary. Figure 37 shows the averaged overlap in MD of each camera.

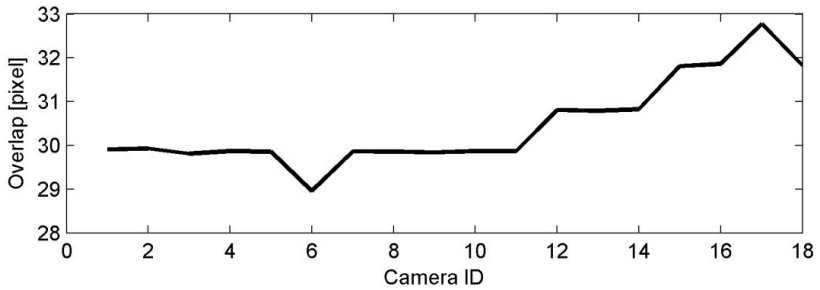

Figure 37. The MD overlap of images in each camera.

The size of the overlap reveals the relative magnification of the cameras which are then compensated in the pre-processing stage. Figure 38 shows an example of the final pre-processed 2D light transmittance map in three different scales.

(a)

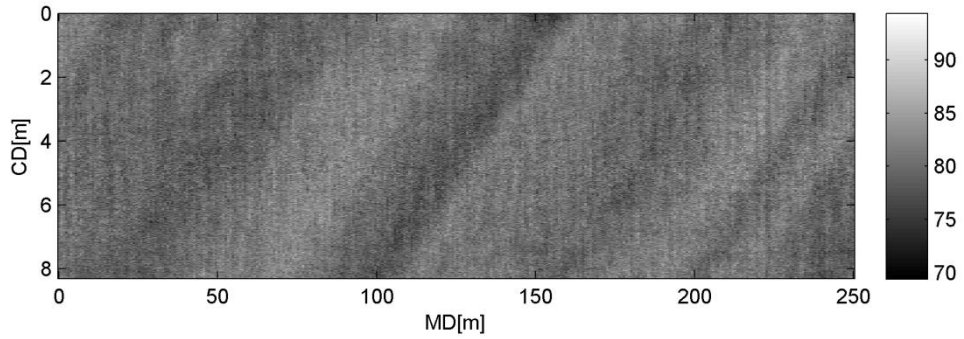

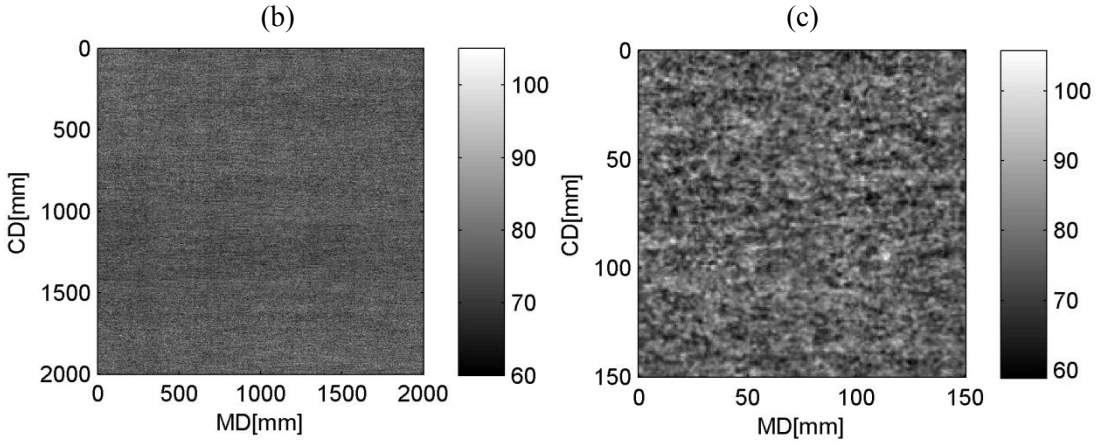

Figure 38. Examples of light transmittance variations shown in various scales. (a) Large scale variation of paper (the image size is 8.3 meters in CD and 250 meters in MD). (b) Medium scale variation (the size of the image is 2 meters in CD and MD). (c) Small scale variation (the image size is 0.15 meters in CD and MD). The resolution in each image is 0.83 mm /pixel. Grayscale shows the light intensity. (Publication II)

5.4 Methods to analyze the characteristics of newsprint

This chapter presents the estimation of small scale structural characteristics in newsprint paper based on WIS images. Furthermore, the method to estimate the CD shrinkage profile of paper is presented and the estimation of basis weight from WIS images is discussed.

5.4.1 Characterization of small scale paper structure

Small scale characteristics of paper are mainly studied with off-line measurements, which means that the data cannot be utilized in the closed-loop control of paper machine. The estimation of microscopic structure for diagnostics and control requires a fast web-wide high-resolution measurement system such as WIS. As discussed in Chapter 3.5 the usability of 2D images has been widely studied based on off-line studies during the last decade. Furthermore, measurement devices which estimate on-line the orientation of fibers and anisotropy of fiber orientation of paper have been studied and patented (Shakespeare and Paavola 2009; Shakespeare 2007). However, such on-line measurement systems do not cover the entire web width and therefore suffer from the same problems as QCS scanner. This Section presents the methods to characterize the small scale structure variation of paper based on WIS images: light transmittance, the magnitude of formation, the length-scale of formation, the anisotropy of fiber orientation and the dominant orientation of fibers. As the entire web is covered by the WIS images, large scale maps of variations in small scale characteristics are computed.

The pixel size of WIS images, 0.83 mm, is not sufficient for detecting the smallest scale constituents such as individual fibers but describes only the characteristics of fiber network at this scale. However, web-wide maps of paper characteristics can be constructed at a resolution of an individual image as follows. The intensity of light transmittance value I for

images is computed by averaging pixel values of the pre-processed images (Ylisaari and Ritala, 2010):

$$\mu_{m,n} = \frac{1}{N_{cd} N_{md}} \sum_{i=1}^{N_{cd}} \sum_{j=1}^{N_{md}} I(i,j)_{m,n} \quad (23),$$

where the N_{cd} = 640 and N_{md} = 128 are the number of pixels in CD and MD, i and j describe the location of pixels in a single image, and m and n describe respectively the CD location of the camera and the time instant of image. The standard deviation of pixel values from pre-processed images characterizes the formation and hence web-wide formation maps can be computed as:

$$\sigma_{m,n} = \sqrt{\frac{1}{(N_{cd} N_{md} - 1)} \sum_{i=1}^{N_{cd}} \sum_{j=1}^{N_{md}} (I(i,j)_{m,n} - \mu_{m,n})^2} \quad (24)$$

The orientation properties and the length-scale of formation were estimated from the 2D Fourier power spectrum. To reduce the uncertainty the 2D Welch power spectrum estimate was computed by averaging the power spectra of 30 consecutive images in MD and by taking their average as the spectrum estimate. There are narrow high intensity areas in the power spectrum, see Fig. 39 (a). These spectral peaks are due to periodic transmittance variations in paper, caused e.g. by the structures in felts, wires or rolls of the paper machine.

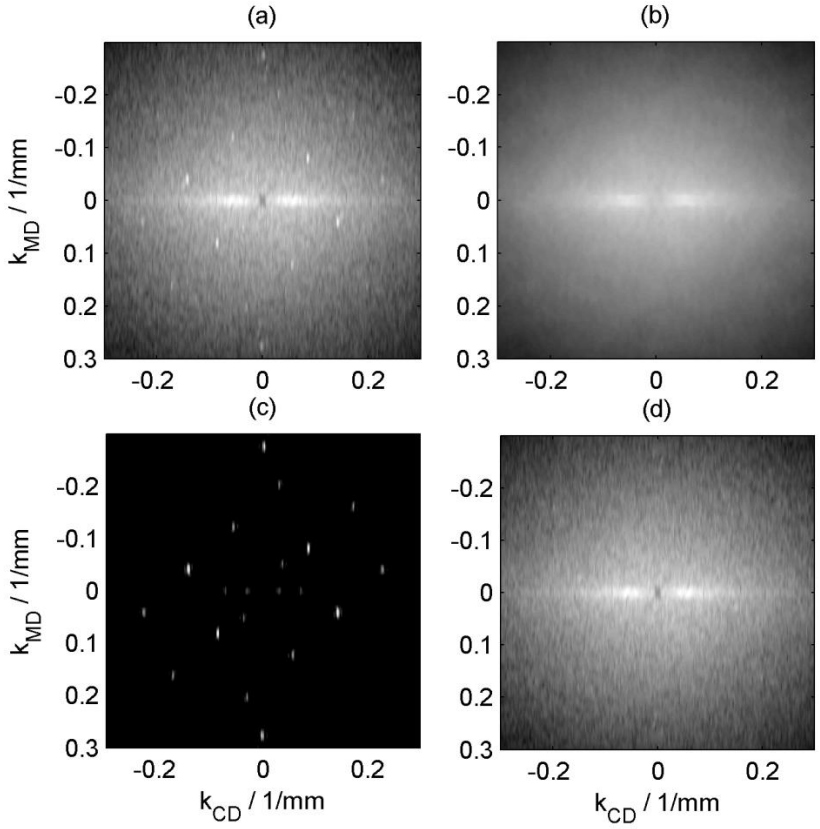

Figure 39. Averaged power spectrum computed over 30 power spectra (a). The median filtered power spectrum (b), the result (c) when (a) is divided by (b), and the power spectrum with spectral peaks removed (d).

When the characteristics of paper are analyzed, the peaks must be removed from the power spectrum because they are not properties of the forming process but rather those of the dewatering and drying elements. The shape of the ideal spectral peaks can be computed by taking the Fourier transform of the windowing function. The windowing function was Hamming and the size of window corresponds to the size of the transmittance image. The locations of the peaks in the power spectrum are determined as follows. First the power spectrum is 2D median filtered to remove the narrow peaks (Sonka 1998)(see Fig. 39 (b)). The size of the ring-like median filter was obtained based on the size of the ideal peak (see Fig. 40).

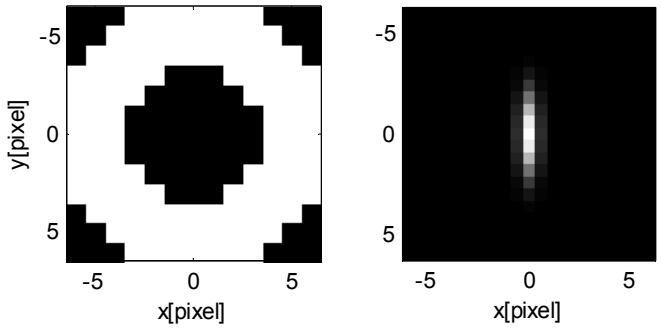

Figure 40. The ring-like median filter applied in peak removing method (left). The values in median filter are selected from the white areas. Ideal spectral peak based on the size and the shape of the Fourier transform of the windowing function (right).

Then the point-wise ratio of the initial spectrum to the median-filtered spectrum is computed, as presented in Fig. 39 (c). In the ratio the intensities of peaks are pronounced so that their areas can be identified by thresholding. The threshold level is determined based on the random image, which is a matrix containing independent random values from a Gaussian distribution. The random image was chosen to simulate the 2D texture which does not include any regular pattern. The Welch spectrum of the random image is median filtered and the filtered spectrum is divided pointwise by the unfiltered spectrum. The histogram which shows the distribution of pixel values was computed and the 90 % percentile values of the histogram were estimated. This value was used as a threshold limit. Increasing or decreasing the percentile value by 5 percentage point did not change the number of found spectral peaks. The holes in the thresholded binary image (=the area of peaks) are widened with dilation operation and finally the areas of holes are replaced with the values of spectrum in its neighborhood. The power spectrum with peaks removed is presented in Fig. 39 (d).

The 2D power spectrum is computed in the Cartesian coordinate system (k_{CD}, k_{MD}). Next, the spectrum is visualized in the polar coordinate system where the coordinates are represented as (k, ϕ). The angle ϕ is respect to MD [-90…+90]. Figure 41 shows the power spectrum of Fig. 39 (d) transformed into the polar coordinate system.

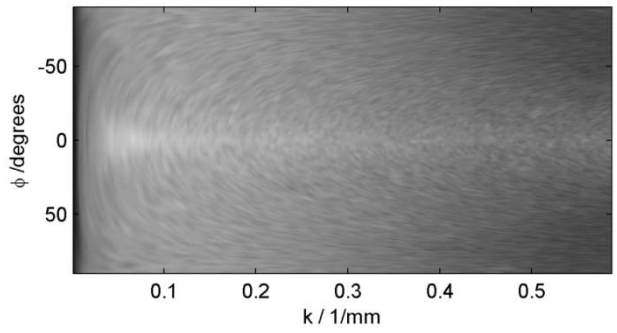

Figure 41. Power spectrum transformed to polar coordinate system.

It can be seen that due to the anistropic nature of paper a significant amount of the variation is orientated in MD. The length-scale of formation is estimated from the normalized spectral distribution of wave number. The normalized spectral distribution of wave number is computed by summing the power spectrum values in polar coordinate system over the angle direction and dividing the resulting vector with the sum of power spectrum values as follows

$$S_{norm}(k) = \frac{\sum_{\phi} S_{Polar}(\phi,k)}{\sum_{k,\phi} S_{Polar}(\phi,k)} \qquad (25),$$

where $S_{Polar}(\phi,k)$ is the power spectrum in polar coordinate system. The average wavelength describes the length-scale of formation. It is defined as the inverse of the product of normalized spectral distribution $S_{norm}(k)$ and the wave number k integrated over k as follows.

$$\lambda_{m,n} = \frac{1}{\sum_{k} S_{norm}(k)k} \qquad (26)$$

In this thesis the anisotropy of fiber orientation is determined as the ratio of average wavelengths in CD and MD. Value 1 corresponds to isotropic paper and value 0 to anisotropic paper where all the flocks are orientated to MD. The average wavelengths are estimated from the CD and MD spectra. The CD and MD spectra are computed by summing the values of 2D spectrum over MD, respectively CD:

$$S_{MD}(k_{MD}) = \sum_{k_{CD}} S(k_{CD},k_{MD}), \quad S_{CD}(k_{CD}) = \sum_{k_{MD}} S(k_{CD},k_{MD}) \qquad (27)$$

The average wavelength is the inverse of the expectation value of the wave number. Thus the anisotropy of fiber orientation is

$$\left[\frac{\lambda_{CD}}{\lambda_{MD}}\right]_{m,n} = \frac{(\sum_{k_{CD}} S_{CD}(k_{CD})k_{CD})^{-1}}{(\sum_{k_{MD}} S_{MD}(k_{MD})k_{MD})^{-1}} \qquad (28)$$

The dominant orientation of fibers is estimated from the normalized spectral distribution of angle. The normalized spectral distribution of angle is computed by summing the power spectrum values in polar coordinate system over wave number direction and dividing the resulting vector with the sum of the power spectrum values

$$S_{norm}(\phi) = \frac{\sum_{k} S_{Polar}(\phi, k)}{\sum_{k,\phi} S_{Polar}(\phi, k)} \tag{29}$$

The dominant orientation of fibers is determined as (Fisher 1993).

$$\theta_{m,n} = \arg\left(\sum_{\phi=0}^{2\pi} \exp(i\phi) S_{norm}(\phi) \right) = \arg\left(\sum_{\phi=0}^{2\pi} \cos(\phi) S_{norm}(\phi) + i \sum_{\phi=0}^{2\pi} \sin(\phi) S_{norm}(\phi) \right) \tag{30}$$

Figure 42 shows the 2D maps estimated from WIS images based on the definitions above; light transmittance (a), standard deviation of light transmittance (=magnitude of formation) (b), length scale of formation (c), anisotropy of fiber orientation (d) and the dominant orientation of fibers (e). The zero angle in (e) means strict machine direction and positive angle means counter-clockwise rotation. Each property was estimated per a WIS camera in CD (18 points) and 3300 in MD (the number of images in 10 seconds).

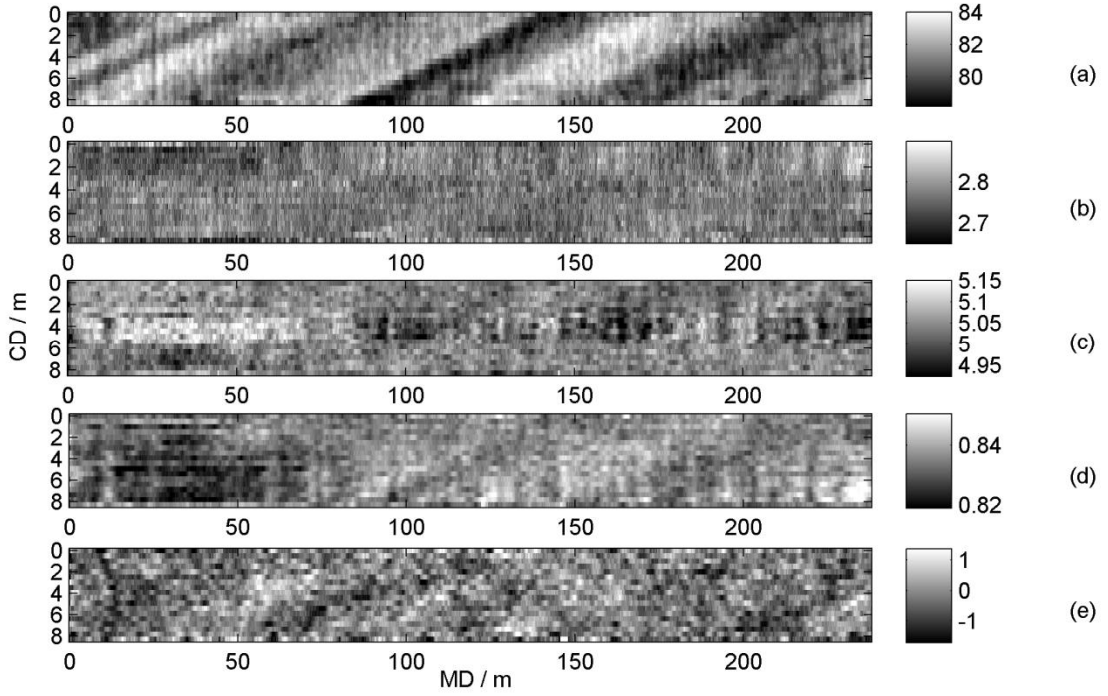

Figure 42. 2D maps of the light transmittance (a), standard deviation of light transmittance (b), length scale of formation (c), anisotropy of fiber orientation (d) and the dominant orientation of fibers (e). Units: gray level values represent the pixel values (a), standard deviation of pixel values (b), mm (c), anisotropy (d), and degrees (e).

The variation in 2D maps was divided to CD, MD and residual variation with variance component analysis (VCA) (Dunn and Clark 1974). Table 4 shows the variances of 2D maps separated to CD, MD and residual variances.

The CD variances are insignificant because the CD profiles were removed from the 2D maps in the pre-processing stage, as discussed in Chapter 5.3. The proportion of MD variation is higher than 15% in light transmittance, length-scale of formation, and in anisotropy of fiber orientation whereas in other characteristics the residual variation is dominating overwhelmingly.

Ylisaari and Ritala (2010) showed based on the web-wide image data that the consistency variation in headbox inflow forms diagonal waves such that delay between edges is 2-3 s. Furthermore, they suggested applying the directed sensor array principle (Naidu 2001) for separating the diagonal waves from other variation in paper. In this thesis the same approach is utilized for other small scale paper characteristics. It can be seen that the diagonal waves, obvious in the light transmittance map of Fig. 42 (a), can be seen also in the dominant orientation angle of fibers (e) and anisotropy of fiber orientation (d) maps although their contribution to overall variation is much smaller.

The delayed 1D signal (z) was obtained from the 2D map (I) as follows

$$z(a) = \sum_{n} I(m - \frac{a}{N_{CD}} n, n) \tag{31}$$

where a is the delay, N_{CD} is the amount of data points in CD, n is the CD and m is the MD location of the data point. Finally, the variances of such signals were computed as a function of delay a. The range for delay was [-5s, +5s].

Delay describes the time difference between the front and the back end of the paper web (see Fig. 43). Zero delay corresponds to strict machine directional variation which indicates that the cause for variation is the jet flow properties in the headbox nozzle or/and the interactions between the jet and the wire. Positive delay corresponds to variation tilted to the direction of the diagonal waves. Negative delay corresponds to variation tilted opposite direction than diagonal waves. Thus, at negative delays there should not exist any high variance component.

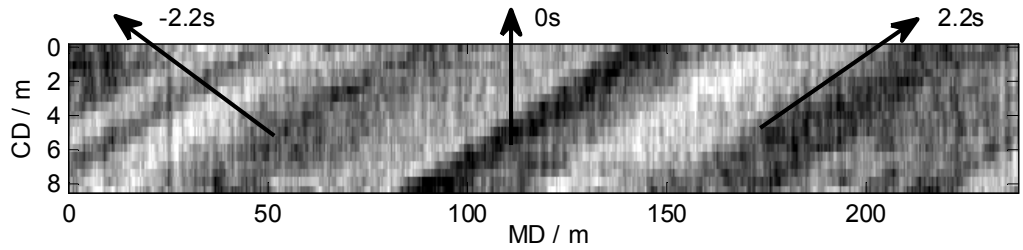

Figure 43. The illustration how the delay in seconds corresponds to angle of tilted variation.

Table 4 shows the variances of 2D maps from which the variation orientated in the angle of diagonal waves (see Fig. 42 (a)) has been removed. The reduction in total variance after the diagonal wave removal shows the proportion of variance caused by diagonal waves. In the light transmittance, the diagonal waves constitute almost 70% of the total variance whereas in other characteristics their effect is below 30%.

Table 4. CD, MD, and residual variations computed with the VCA. The table shows the variances from original 2D maps and 2D maps from which the variations orientated in angle of diagonal waves have been removed (wr). The μ is the light transmittance, σ is the magnitude of formation, E[λ] is the length scale of formation, $E[\lambda_{CD}]/E[\lambda_{MD}]$ is the anisotropy of fiber orientation and θ is the dominant orientation of fibers.

	CD (% of total)	MD (% of total)	Res (% of total)	Tot. var(σ^2)
μ	-0.03	15.18	84.85	0.000232
μ (wr)	0.20	19.95	75.62	0.000061
σ	0.06	7.57	87.48	0.001344
σ (wr)	0.16	8.01	86.97	0.001231
E[λ]	0.22	18.89	76.61	0.001782
E[λ] (wr)	0.30	12.85	82.25	0.001503
$E[\lambda_{CD}]/E[\lambda_{MD}]$	0.66	39.67	56.51	0.000029
$E[\lambda_{CD}]/E[\lambda_{MD}]$(wr)	2.75	13.92	78.92	0.000018
θ	0.11	6.74	88.22	0.230379
θ (wr)	0.30	4.39	90.27	0.196443

Figure 44 shows the variances of 2D maps in various delays. It can be seen from Fig. 44 (a) that in the map of the light transmittance, the local maximum occurs at delay 2.2 s. The diagonal waves in the anisotropy of fiber orientation (d) and in the dominant orientation (e) suggest that the orientation properties may have a connection to consistency variation. However, anisotropy variation strictly in MD is also high which is consistent with the fact that the one reason for anisotropy of fiber orientation is the MD speed difference between the wire and the jet and the turbulence in the jet (Parker 1972). The variation of length-scale of formation is orientated more in MD than in tilted angle which suggests that such variation visible in 2D maps is formed because of the differences in flow properties in the headbox nozzle and the differences between the jet and wire MD speed which is well in accordance with the pre-existing knowledge (Paulapuro 2008). The variation of magnitude of formation does not show any clear MD or tilted phenomena as more than 90% of the variance is in residual variation.

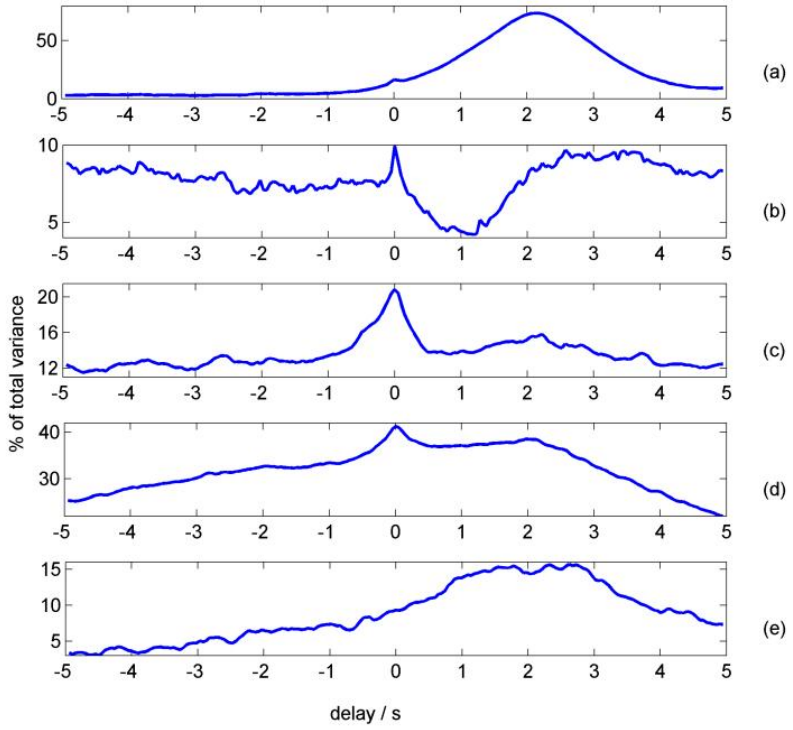

Figure 44. The variances in various delays. Light transmittance (a), magnitude of formation (b), length scale of formation (c), anisotropy of fiber orientation (d), and dominant orientation direction of fibers (e).

5.4.2 Estimation of the CD shrinkage profile

The paper web shrinks during the drying. The paper web shrinks most when the solids contents is above 40%, i.e. in the end of the press section and in the drying section of paper machine. The shrinkage occurs mainly in cross direction and the paper tends to shrink more near the edges and thus forms a CD profile (Niskanen 1998). The shrinkage affects many physical properties of paper. It has been shown firstly that high shrinkage at the edges of the paper machine can cause blockings and stops in printing presses, and secondly that the

dimensional stability changes when paper web shrinks, making the paper weak (Viitaharju and Niskanen 1993). Therefore the optimal trim cutting of paper reel based on the shrinkage profile brings economic benefit to papermakers. Furthermore, with shrinkage profile the CD actuator responses of the headbox are more accurately mapped to the dry end. The estimation of shrinkage profile from off-line paper images has been studied in a multiple articles (Viitaharju and Niskanen 1993; Raunio 2006; I'Anson et al. 2008). In most cases the estimation is based on wire marking. Wire marking is a regular pattern caused by wires in wire and press section where the paper web is subject to structure changes. Usually the marking is so faint that the observation of marking is possible only with Fourier methods such as Welch spectrum.

Here the marking from suction rolls or cylinders was studied. This is because the spatial resolution of WIS images was 0.83 mm / pixel. This is insufficient for finding marking produced by wires, whose marking scale is the distance between yarns in a wire, typically from 0.2 mm to 0.5 mm. The distance between suction elements vary from 5 mm to 15 mm. The marking from rolls and cylinders is more delicate than the wire marking and therefore the high amount of image data in MD is required to find the regularity of roll marking from paper web images. The Welch power spectrum was computed similarly by averaging 30 consecutive power spectra in MD and the variation caused by other than regular patterns was removed based on the method presented in Section 5.4.1 and in Fig. 39. The exact locations of the spectral peaks were estimated by fitting a second order 2D polynomial to each identified peak area in the original spectrum and detecting the location of the maximum of the polynomial. These peak positions were determined at subpixel accuracy.

The shrinkage is not the only deformation of paper in paper machine. Paper also shears and stretches. All these deformations change the periodic strcture of the marking and thus move frequency peaks in the spectrum. The changes can be specified by a linear transformation matrix M, which defines scaling, shearing and rotation (Sonka 1998). Scaling represents the shrinkage or stretching of paper web, and shearing represents the distortion of paper web in CD or MD. In wire marking the CD shearing represents the sum of distortions from CD yarn and paper web (I'anson et al. 2008), but because the suctions rolls are not deformed the only possible distortion is caused by the deformation of paper web. Furthermore, the paper can shear only in machine direction. As the camera in a fault detection system may be rotated compared to paper web causing an error to shrinkage estimation, the rotation is also identified in the analysis. The spatial transformations can be combined into an overall transformation matrix by taking the product of the three individual transform matrices. The resulting transformation matrix M is

$$M_{scale,shear,rotate} = T_{scale} \times T_{shear} \times T_{rotate} = \begin{bmatrix} S_{CD} & 0 \\ 0 & S_{MD} \end{bmatrix} \begin{bmatrix} 1 & 0 \\ H_{MD} & 1 \end{bmatrix} \begin{bmatrix} \cos\theta & \sin\theta \\ -\sin\theta & \cos\theta \end{bmatrix} = \begin{bmatrix} S_{CD}\cos\theta & S_{CD}\sin\theta \\ H_{MD}S_{MD}\cos\theta - S_{MD}\sin\theta & H_{MD}S_{MD}\sin\theta + S_{MD}\cos\theta \end{bmatrix} \quad (32)$$

The four unknown parameters S_{CD} (=CD shrinkage), S_{MD} (=MD shrinkage), H_{MD} (=MD shearing), and θ (=rotation) can be solved on the basis of spectral peak positions. The reference position of peaks is chosen to be that in the middle of the paper web in CD. The peak positions [k_{x0}, k_{y0}] in the reference spectrum and the peak positions [$k_{xshrinkage}$, $k_{yshrinkage}$] in the shrinkage-deformed spectrum at other locations are related through

$$\begin{bmatrix} k_{x\,shrinkage} \\ k_{y\,shrinkage} \end{bmatrix} = M_{shear,scale,rotate} \begin{bmatrix} k_{x0} \\ k_{y0} \end{bmatrix} \quad (33)$$

Because of the finite resolution of the WIS image, the position of the spectral peak has always some uncertainty. Therefore the transformation is estimated from several frequency peaks in the least-square sense increasing the robustness of results.

The shrinkage and the shearing profiles estimated above determine the relative profiles (see Fig. 45). However, the width of the entire paper web can measured e.g. with the web-inspection system and as the jet width, taking account the cut edges, flowing out of the headbox is known, the absolute shrinkage profile can be estimated by multiplying the relative shrinkage profile with a correction term. The correction term is the ratio between the width of the jet and the width of the paper in the dry end.

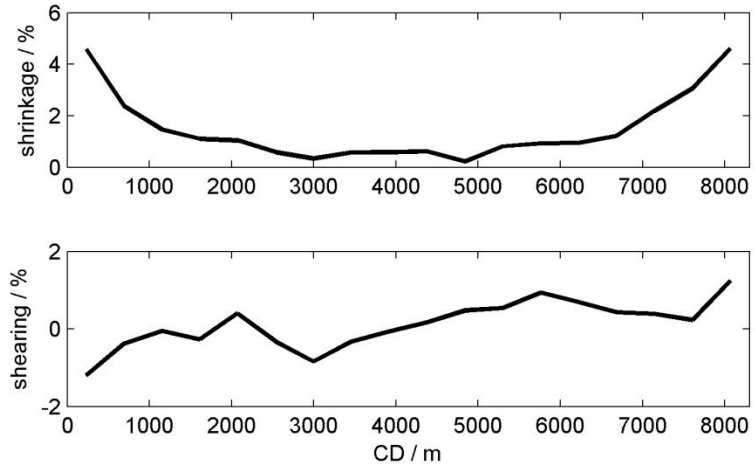

Figure 45. The relative shrinkage and the shearing profile occurred at the paper machine estimated from the suction roll marking from WIS images available in this thesis.

It can be seen that the shrinkage is almost 5% higher near the edges than in the middle. The magnitude of shearing is small as it was assumed.

5.4.3 Estimating basis weight by light transmittance measurement

The WIS measures the light transmittance which provides indirect information about basis weight. This relationship has been widely studied from paper physics perspective off-line (Sara, 1978; Komppa and Ebeling 1981; Raunio and Ritala 2009) and on-line (Ferguson 1997; Publication III; Publication V). In this thesis it was observed that the correlation between the light transmittance images and the 2D basis weight maps is approximately 0.7 in the studied uncoated printing paper in length scales higher than 0.1 mm (Raunio and Ritala 2009). The correlation between the basis weight and light transmittance between the 1D signals is approximately 0.9 in the studied uncoated uncalandered paper grades in length scales higher than 5 m (Publication V). Therefore, the on-line web-wide transmittance images would provide high resolution information about basis weight of paper, potential for 2D control of paper machine and for diagnostics of paper quality variations.

To minimize the uncertainty of light transmittance based basis weight estimates the illumination distortion in WIS images must be compensated, which is done most reliably with reference images. Capturing of images from a reference sheet at a full-scale paper machine is difficult and requires exceptional circumstances, for example a production break. Furthermore, the reference images must be updated quite frequently because the aging of LEDs, moisture, dust, and heat change slowly the imaging conditions. If the paper machine includes on-line scanning basis weight measurement system (see Chapter 3.1.1) the updating interval can be increased. This can be done by evaluating and compensating the changed image conditions based on the on-line basis weight and WIS data. However, the updated reference images are still required.

The on-line transmittance data, the on-line basis weight data, the off-line basis weight data and off-line transmittance data were compared in order to assess the uncertainty of basis weight estimation based on WIS transmittance measurement. The data from on-line basis weight measurement systems was collected over a period of 30 h, representing 2894 km of paper as the machine speed was 26.8 m/s. The WIS data was collected from 10 sample instants covering totally 13 km of paper in MD. Samples for off-line analysis were taken at two sampling instants for which WIS data was also available. The samples were cut across the web on the top of a paper reel, each sample consisting of 30 crosscut stripes covering 330 meter of paper in MD. Thus the off-line measurement covers paper total of 660 m in MD. The on-line and off-line measurements were aligned based on the time stamps of the systems and the reel ID and change information. The time alignment between the on-line measurements was accurate. However, the reel change times were estimates and it is possible that uncertainty in time alignment is over 10 minutes between the off-line and the on-line measurements. Therefore averages over MD (=CD profiles) were compared rather than individual profiles. The averages over MD were computed from the two time instants for which all on-line and off-line measurement data was available. The on-line basis weight CD profiles covers 8000 m of production, the on-line light transmittance CD profiles 1000-3300 m of production, and off-line CD profiles 660 m of production. Finally, The CD profiles at two sample instants were further averaged in MD to find the generalized behavior of profiles. The CD resolution of the profiles is 0.81 mm in WIS data, 12 mm in off-line analyzer and 14

mm in QCS scanner. Thus the profiles were resampled to the QCS scanner data resolution for point-wise correlation analysis. Furthermore, the imperfect compensation of illumination variation in WIS image may generate distortions to long wavelengths and thus the wavelengths longer than 200 mm were filtered out from the CD profiles.

The estimation of basis weight based on light transmittance measurement requires the determination of the sensitivity of light transmittance to basis weight and to variations due to other paper properties via the scattering and absorption coefficients of the material. This is done by applying the Kubelka-Munk theory, see Section 3.3.1. The scattering and absorption properties are affected by e.g. moisture and filler content of paper. The moisture itself does not affect significantly to the Kubelka-Munk parameters (Niskanen 1998). However, the weight of water naturally causes variation to basis weight. Figure 46 (b) shows that the online moisture, measured with QCS, varies between 7.7 % and 9.3 %. Thus the maximum variation is 1.6 % (=9.3 % -7.7 %) from the basis weight.

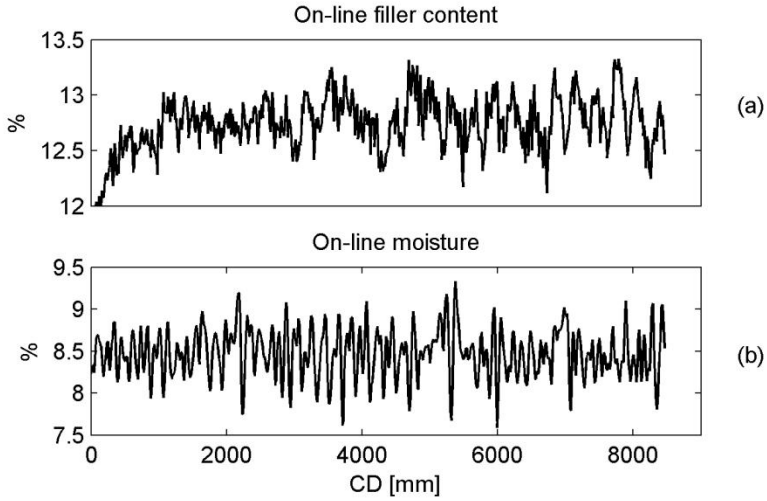

Figure 46. The CD profiles of (a) on-line filler content and (b) on-line moisture.

Furthermore, the magnitude of disturbance caused by the filler variation is small because of small average amount of fillers and thus small variation of basis weight contribution of fillers (maximum variation is 1.3 % =13.3 % - 12 %) (see Fig. 46 (a)). Thus, the fiber content is main reason for light transmittance variation in this paper grade and the linerization around the nominal point of this paper grade, W = 0.045 kg / m^2, S = 49 m^2 / kg, K = 5.5 m^2 / kg, is reasonable (Niskanen 1998; Pauler 2002). The linearized relationship is the following.

$$\hat{T} = 0.218 - 0.257\frac{(W-0.045)}{0.045} - 0.196\frac{(S-49)}{49} - 0.077\frac{(K-5.5)}{5.5} \quad (34)$$

Thus one percent relative change in basis weight yields a change of transmittance by 0.0026 units in newsprint grade. The same change at constant basis weight is produced by 1.3 % relative change in scattering coefficient or by 3.4 % relative change in absorption coefficient. The light scattering and absorption coefficients of typical filler (Clay, $CaCo_3$) in paper are

approximately S = 170 m^2 / kg and K = 1 m^2 / kg. Furthermore, the average filler content in the paper measured in this thesis was 12.7 % (see Fig. 46 (a)). Thus one percentage point increase in filler content increases the light scattering coefficient by 2.7 % and decreases the light absorption coefficient by 0.9% yielding a total change of transmittance by 0.0048. The standard deviation in off-line filler content in this paper grade was 0.14 % which means 0.1 g/m^2 (=0.25 %) deviation in basis weight in 45 g/m^2 paper. The standard deviation in off-line basis weight profile was 0.9 g/m^2. Thus, it can be said that the variation in filler content is not disturbing significantly the Kubelka-Munk parameters or transmittance in (34).

The correlation coefficients between the off-line and on-line measurements are shown in Table 5. The interpretation of the correlation coefficients is based on the following:

1. The off-line data was considered as the ground truth for variations, and for the correlation between the basis weight and the transmittance.
2. The correlation between the off-line transmittance and off-line basis weight shows the minimum uncertainty when the basis weight profile is estimated via light transmittance
3. The on-line basis weight is studied in order to solve the accuracy of time alignment and to study the usability of on-line basis weight information in the calibration of on-line transmittance data.
4. The off-line transmittance is studied in order to study the success of pre-processing of on-line images.

Table 5. The correlations between on-line and off-line CD profiles. The wavelengths longer than 200 mm have been filtered out.

	On-line transmit.	On-line basis weight	Off-line basis weight	Off-line transmit.	On-line filler content
On-line transmittance	1.00	-0.47	-0.44	0.45	0.01
On-line basis weight		1.00	0.79	-0.74	0.03
Off-line basis weight			1.00	-0.93	0.06
Off-line transmittance				1.00	-0.06
On-line filler content					1.00

It can be seen that the maximum correlation that can be achieved between the basis weight and transmittance profiles is ρ = -0.93, i.e. between the off-line basis weight and the off-line transmittance. The high correlation indicates that in newsprint grade the light transmittance provides quite accurate information about the basis weight variation and the 2D data of transmittance could be utilized when controlling of paper basis weight in CD. The correlation between the off-line basis weight and the on-line basis weight is ρ = 0.79 indicating that the on-line basis weight measurement may include uncertainties and that the time alignment in MD may not be correct. The correlation between the on-line basis weight and the off-line transmittance is even smaller being ρ = -0.74.

The off-line and on-line basis weight (W_{off}, W_{on}) can be modeled with off-line transmittance (T_{off}) and off-line basis weight as follows

$$W_{off} = aT_{off} + b + \varepsilon_1 \quad , \quad W_{on} = W_{off} + \varepsilon_2 \qquad (35), (36)$$

where ε_1 is the error between the model and the off-line basis weight and ε_2 is the error between the on-line basis weight and the off-line light basis weight. The Eq. (36) is substituted to Eq. (35) and then

$$W_{on} = aT_{off} + b + \varepsilon_1 + \varepsilon_2 \qquad (37)$$

The variance of residual error (σ_ε^2) when the W_{on} is explained with Eq. 36 can be determined with the correlation coefficient $\rho^2_{T_{off},W_{on}}$ and the variance of on-line basis weight $\sigma^2_{W_{on}}$ as follows

$$\sigma_\varepsilon^2 = (1 - \rho^2_{T_{off},W_{on}})\sigma^2_{W_{on}} \qquad (38)$$

Furthermore, the variances of ε_1 and ε_2 are assumed to be independent and thus the total error between the on-line basis weight and the off-line transmittance can be written by using the sum of two error variances as follow

$$(1 - \rho^2_{T_{off}W_{on}})\sigma^2_{W_{on}} = \sigma^2_{\varepsilon_1+\varepsilon_2} = \sigma^2_{\varepsilon_1} + \sigma^2_{\varepsilon_2} = ((1 - \rho^2_{T_{off}W_{off}}) + (1 - \rho^2_{W_{on}W_{off}}))\sigma^2_{W_{on}} \qquad (39)$$

The off-line correlation between basis weight and transmittance was -0.93 and the correlation between the off-line basis weight and on-line basis was 0.79. Thus by using the (39) the correlation between the off-line transmittance and the on-line basis weight should be -0.699 ($((1-(1-0.93^2)-(1-0.79^2))^{1/2} = 0.699$). Combining this fact with the correlation between the off-line transmittance and on-line basis weight ρ=-0.74 it can be said that the correlation achievable with current temporal alignment of data sets between on-line basis weight and transmittance should be at least -0.699.

However the correlation between the on-line basis weight and the on-line transmittance is only ρ = -0.47. Thus the correlation was studied for 18 locations in CD corresponding imaging areas of adjacent cameras. Figure 47 shows the camera specific correlation in CD. It can be seen that correlation varies significantly between the camera views. The theoretical minimum correlation is achieved in cameras 1, 2, 6 and 14. However, at the rest of the camera areas the correlation is so small that the cameras would require appropriate calibration.

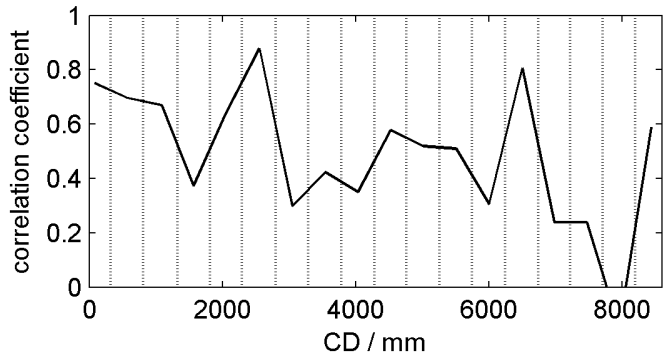

Figure 47. The camera specific absolute correlations. The dashed vertical lines describe the borders of two adjacent cameras.

The results of this section indicate that the on-line transmittance data cannot be utilized as such in basis weight estimation. This is because in the on-line imaging illumination or geometrical distortions may not have been accurately corrected – due to not having reference images - in the pre-processing stage. However, the calibration which is easily manageable although tedious task would increase the value of WIS significantly and enable the more accurate 2D diagnostic and the 2D control of paper machine in newsprint machines.

6. Discussion

Image measurements have the advantages of capturing of the 2D texture, reasonable low price of technology, and the implementation possibilities in on-line processes. This thesis has studied the possibilities of imaging technology and 2D analyses in assessment of newsprint and tissue paper characteristics.

At present, the imaging technology is applied little in quality characterization of the tissue paper, mainly because of the supposed minor financial benefit of more accurate and versatile measurement systems. However the demand of the tissue paper is predicted to increase worldwide during the next decades and thus the financial benefit of more optimal control of tissue machine will also increase. Therefore, the first research question dealt the possibilities of image measurements and analysis in the characterization of the tissue paper.

> *How the image measurement can be applied in the evaluation of the creping pattern characteristics, the number of free fiber ends, and the amount of pinholes in tissue paper?*

The characteristic of creping pattern is usually described with one parameter – the crepe frequency – ignoring several characteristics of creping pattern. In this thesis the method which determines the pattern with three parameters – the crepe frequency, the waviness of the creping pattern, and the irregularity of the creping pattern – was developed. The characteristics of creping pattern were evaluated from the MD gradient fields estimated with the photometric stereo method. The MD gradient enforces the features orientated in CD such as the creping pattern. The MD gradient was analyzed with the Welch spectrum in frequency domain. The creping pattern generates high intensity area to the Welch spectrum whose location, dimensions, and shape were represented with Gaussian and χ^2 –functions. The combination of the functions was fitted to the high intensity area in order to estimate characteristics of creping. The MD location of the maximum of this representation provides the crepe frequency, the width in MD tells the regularity of the creping pattern and the height the waviness of the creping pattern. The method is designed for tissue papers which does not contain embossing, lamination, printing or other structures generated in converting. It is expected that the converting usually increases the uncertainty of creping characteristics.

Until now *the number of free fiber ends* on the tissue paper is measured with the folding method not suitable for on-line applications. In this thesis a method based on photometric stereo which counts the free fiber ends was developed. The free fiber ends were detected from the reflectance images based on the shadows of free fiber ends. The shadows were detected by constructing tissue surface with photometric stereo and finally subtracting it from the original reflectance image. It was noticed that the shadow based method is in accordance with the results of the folding method and the uncertainty was smaller. The adjustable parameters in the developed method—the length of shadows and the threshold level in conversion from grayscale to binary image—were chosen based on the free fiber ends counts

between the reference and the shadow based imaging method: two parameters were estimated based on the measurements from five tissue grades. However, the length of the fibers and the optical characteristics of the tissue surface may change significantly between the grades. Thus the selected parameters may not perform optimally in all five grades and may not work at all in other grades. However, the parameters could be optimized to several tissue grades which would decrease the uncertainty. Furthermore, the converting of tissue paper increases the uncertainty of free fiber end count causing for example the shadows and black object to surface of tissue which could be mixed up to shadows of fibers.

Pinholes are undesired artefacts in paper. In this thesis the pinhole detection method, based on light transmittance and two linear polarizers, was developed. Two images were captured from the target: one with parallel polarizers and one with crossed polarizers. Thus, when the polarizers are parallel the pinholes can be seen as bright dots and when the polarizers are crossed the pinholes can be seen as black spots. Finally, the pinholes were detected from the difference of the two images which increases the contrast making the pinholes more visible. The difference image was thresholded to be able to count the amount and the area of pinholes. The selected limit in the thresholding affects naturally both values. In this thesis the limit was selected based on the intensity values in calibration images with the two arrangement of polarizers and captured without a sample. However, if such pinhole detection technique is applied the reference pinhole measurement is required to calibrate and select the threshold limit more accurately.

In printing paper business the image measurements have been applied already for two decades in on-line applications. The systems have been mainly point-wise in which the camera is stationary or travels across the paper web. However, the price of imaging and illumination technology has decreased constantly and thus the web-wide imaging systems have been installed increasingly to paper machines. At the moment such systems detect mainly artefacts such as holes, from the paper, rather than the small scale structure or the large scale characteristics of paper. Therefore the second area of interest in this thesis was to study the possibilities of on-line imaging in characterization of newsprint paper

How the on-line light transmittance (WIS) images can be applied in the analysis of small scale paper structure, the estimation of CD shrinkage profile, and the estimation of basis weight in newsprint paper?

At present, *the small scale structure of paper* is measured off-line, or on-line with the scanning based measurement system. Such systems include uncertainties (on-line) or come late for hours in control perspective (off-line). This thesis presented the method to characterize the small scale structure of paper based on the on-line light transmittance images. The small scale structural characteristics such as the light transmittance, formation, length scale of formation and orientation parameters of paper were estimated based on the statistical measures and the features of frequency distribution in the 2D Welch spectrum. The pixel size in WIS images was 0.83 mm x 0.83 mm which means that the computed characteristics do not tell anything about the objects smaller than 0.83 mm. Furthermore, the analysis was based on preprocessed image from which the MD stripes (caused by the LED

panel or normal variation in paper) were removed. Thus estimated characteristics evaluated from such images may give unexpected results. However, the origin of MD stripes would be studied in future studies.

The high shrinkage at the edges of the paper machine can deteriorate the paper quality and cause blockages and stops in printing press. This thesis presented the method to *estimate the CD shrinkage profile* of paper based on the markings formed by the suction rolls and the cylinders at the paper machine. The marking formed by the rolls and cylinders is faint and thus high amount of image data was required to distinguish the marking. The shrinkage of paper was estimated based on the transition of the frequency peaks between the edges and the middle of the paper web. The shrinkage results were well in accordance with the pre-existing knowledge.

At present the *basis weight of paper is estimated* with the scanning measurement system. Such system includes uncertainties because of the small numbers of points actually measured. The relationship between the two paper properties was studied in the basis of CD profiles. It was noticed that the correlation between the on-line transmittance and the basis weight was rather low which was because of the illumination variation in the light source which could not be compensated in the preprocessing stage. However, it was noticed that the correlation between the basis weight and light transmittance in certain cameras was as high as expected which means that calibrating of each camera in WIS would enable the basis weight estimation from transmittance images on-line.

The present on-line imaging systems serve the front line machine vision technology which should be utilized in a more versatile manner. In the beginning it was assumed that the quality of on-line images and the configuration of imaging systems as such do not provide the performance required for the methods developed in this work. Therefore, the third area of interest in this thesis considered the shortages of present imaging systems and suggested possible modification to them.

> *How the present scanning and web-wide on-line imaging systems must be modified to improve the estimation of tissue paper and newsprint characteristics?*

The assessment of tissue characteristics was based on photometric stereo (creping characteristics and free fiber end count) and light transmittance (pinholes). The creping characteristics were estimated with 4-light configuration in which the angle between the sample surface normal and the light source was 35 degrees which was noticed to be enough to illuminate major part of the valleys in creping structure in various grades. In present on-line photometric stereo configuration (Metso IQ 2013) the angle is larger indicating that the light rays may not reach the bottom of steep valleys which causes shadows to reflectance images and thus increasing the uncertainty of analyses. However, the present on-line photometric stereo method estimates of the order of one hundred gradient fields per second which enables the use of statistical methods for decreasing the uncertainty caused by the impropriate illuminating angle. Thus, the imaging system technology for assessment of creping characteristics exists. Furthermore, the present on-line scanning system can be also

utilized as such in the estimation of CD shrinkage. The resolution of images in such system is enough to detect the roll and wire marking from paper. Also, the large amount of data available in on-line system increases the accuracy of estimation.

The free fiber end count method was based on 12 reflectance images from the same target. The 12 reflectance images were selected because the higher amount of images did not affect the results. On the contrary, the uncertainty of analyses increases when the number of reflectance images is decreased for example in on-line application. However, similarly than in the assessment of creping characteristics, the amount of data obtained with on-line systems is high which enables the use of statistical methods to decrease the uncertainty of analysis. The on-line free fiber end – detection system is possible to develop with reasonable effort but requires multi wavelength cameras or extremely short exposure times, short light pulses and high accuracy alignment of images.

The detection of pinholes was based on two light transmittance images captured from the same location of paper. The light transmittance imaging technology is commonly used in WISs so the developed method can be applied as such to on-line. The on-line system would require two synchronized cameras which are imaging the same location from target. The light transmitted through paper must be linearly polarized and both cameras are provided with linear polarization filters: one parallel in respect of light source polarizer and one crossed in respect of light source polarizer.

Evaluating the characteristics of newsprint was based on the on-line transmittance images captured with WIS. It was noticed that the initial quality of the images was insufficient for evaluating paper characteristics. The focus of cameras, the orientation of cameras, the location of cameras and the intensity of illumination vary locally in CD. The distortions can be divided into the focus distortion, the geometric distortion, and the illumination distortion. The geometric distortion of images caused by the camera orientation and location was removed. In this thesis the radial distortion could not be removed because of the lack of calibration images causing distortion especially to the corners of images. The radial distortion causes uncertainty to CD shrinkage estimation widening the spectral peaks in frequency domain and to estimation of length scale of formation enlarging/downsizing the length scale near the corners. However, it was assumed that the radial distortion is constant between the camera lenses in WIS and thus relative variation of properties could be studied in CD. The geometric distortions can be accurately estimated and thus compensated by capturing images from known calibration target (Zhang 1999; Heikkilä and Silven 1997).

The main reason for uneven illumination was too small illumination panel in MD. The light intensity near the top and bottom edges was approximately 50% of the intensity in the middle of the image. Also, the efficiency variation between the LEDs, the broken LEDs and the joints of plastic covers protecting LEDs cause intensity variation to images. The imaging condition may change slowly in paper machines. Thus the estimated characteristics related to light intensity such as the basis weight and the characteristics related to variance of light intensity such as the magnitude and the length-scale of formation were rather uncertain.

However, removal of long-term CD profile revealed the relative variation in residual and machine direction and thus such profiles were analyzed in this thesis.

The reference images for calibration must be captured off-line with a reference sheet which is imaged at each camera in WIS separately. The reference sheet should be located at the same height as the running paper and the exact location and possible rotations of the reference sheet must be known. The reference sheet must be imaged also with the separate off-line system so that the variation specific to the paper can be separated from the variation caused by the WIS.

7. Conclusions and Future Work

The cost efficiency of the papermaking process plays an important role in the paper industry. One way to enhance the cost efficiency is to measure the paper more accurately and in a more versatile manner than the present measurement systems and thus improve the control of the paper machine. The imaging systems provide a technology for the improved measurements however such technology is not fully utilized in the paper machines at the moment. Therefore this thesis proposed a set of image analyses and methods which can be implemented in present on-line imaging systems.

The creping process forms the creping pattern to the tissue paper which mainly determines the quality properties of the final product. The creping process also affects the free fiber ends and pinholes. This thesis applied the photometric stereo method with 2D spectral analysis to characterize the versatile properties of creping pattern. The pinhole detection method was based on the linearly polarized light transmitted through paper and the camera with the rotating polarizer. It is anticipated based on the thesis that the characteristics of creping patterns and the number of pinholes are possible to be measured on-line by using existing imaging technology in paper machines.

The image measurements and analyses developed for tissue paper were tested for various tissue grades manufactured in Northern Europa and US. However, the properties of tissue paper grades change significantly from country to country. Thus one goal in future studies is to test the current methods for completely different grades and to update methods if necessary. The measurements of creping pattern characteristics, the number of free fiber ends and the pinholes are useful from the production management point of view. However, the end-user of the tissue paper evaluates the product based on the softness, the absorption and the strength. Therefore, the more precise relationship between the estimated tissue characteristics and the physical properties relevant to the end-users will be studied in the future work.

At present the most of the newsprint paper properties are measured on-line with a scanning method or off-line after the paper is made. The on-line scanner measurement has maintained its position in paper industry and it has been widely applied in the control of the paper machine. The scanning technique works well when slowly varying quality characteristics are measured and controlled. However, the uncertainty of the web-wide estimate based on such scanner is rather high due to the small number of points actually measured.

During the last few years, the price and performance of imaging and illumination technology have achieved a level which enables the measurement of paper on-line at a reasonable price. Such technique is in use in web inspection systems which measure the light transmittance of the entire web which enables fast and accurate control of paper quality characteristics. In this thesis the small-scale structure, the CD shrinkage, and the basis weight of newsprint paper

were estimated based on the web-inspection images. It was noticed that the initial quality of the on-line images was insufficient for evaluating small scale formation characteristics and basis weight reliably. However, it was noticed that capturing a complete set of calibration and reference images will enable the formation and basis weight estimation of paper and thus increasing the value of WIS significantly.

The newsprint grade studied in this thesis is not coated nor calandered. Both finishing methods affect significantly on the optical properties of paper and thus it is likely that the analyses developed in this thesis cannot be applied as such to other paper grades. Therefore one direction for future studies is to generalize the analyses to cover a wide range of paper grades including optically challenging ones. In such study, the Kubelka-Munk theory would provide a simple model for optically layered materials such as the coated and calandered paper grades.

The results of this thesis indicate that image measurements have vast potential in the tissue and newsprint paper business. Furthermore, the thesis showed that the potential can be easily utilized by using the present on-line imaging systems in the paper machines. This encourages to further study the possibilities of applying image measurements in papermaking and various other business areas.

Bibliography

ABB, The Optical Properties Measurement OP4255 (2013), Available at: http://www.abb.com/industries/db0003db001873/c12570c30026b34185256aa4006fe526.aspx (visited in 2013, May 31).

Alince, B. and Lepoutre, P. J. (1980): Porosity and optical properties of clay coating structure, *Coll. int. Sci.* Vol. 76, No. 1, pp. 439-444.

Archer, S., Furman, G. and Von Drasek, W. (2010), Image analysis to Quantity crepe structure, *PaperCon 2010*, Atlanta, USA, 2010.

Archer, S. and Furman, G. (2005): Embedded sheet Structures- Impact on tissue properties, *Tissue World*, Nice, France, April 4-7, 2005.

Arendt, F.P. (1974): Determination of paper ash content by X-ray absorption analysis, U.S. Patent 3904876 A, (Issued Sep 20, 1974).

Asada, N., Amano, A. and Baba, M. (1996): Photometric calibration of zoom lens systems, *Proc. 1996 Pattern Recognition 13th 10 International Conference on*, Vienna, Austria, 1996.

Avikainen, M., Markkanen, M. and Erkkilä, A.-L. (2004): Comparison of different average flocsize and scale parameters of paper formation, *Proc. Progress in Paper Physics Seminar*, Trondheim, Norway, 2004.

Bailey, A. L. and Lamont, L. J. (1993): A standard procedure for accelerated testing and measurement of yellowing by light in papers containing lignin, *Tappi J.*, Vol. 76, No. 9, pp.175-180.

Basbanes, N. A. (2013): *On paper, the everything of its two-thousand-year history*, Random House LCC, New York, USA.

Bird, G.R. and Parrish, M. (1960): The wire grid as a near-infrared polarizer, *J. Opt Soc. Am.,* Vol. 50, No. 9, pp. 886-891.

Bosch, J., Lyne, M.B., Mark, R. and Habeger, C.C. (1984): *Handbook of Physical Testing of Paper*, Marcel Dekker Inc., New York, USA.

Chen, Y. (1998): *Image Analysis Methods for Paper Formation Evaluation*, Master's thesis, University of Toronto, Toronto, Canada, 1998.

Chen, S.-C. Subbarayan, R., Kristinsson, K. and Snyder, R. (1998): Paper machine applications with fullsheet imaging measurement, *Control Systems '98 Conference*, Porvoo, Finland, 1998.

Chen, S.-C. (1998): Analysis of Two-dimensional sheet variations from a non-scanning measurement, *proceedings from the IFAC Workshop on Adaptive Control and Signal Processing*, Glasgow, Great Britain, 1998.

Chen, S.-C. (2010): Improving sheet dimensional stability to reduce paper rejects, *International paper world*, No. 10-11, 2010, pp. 22-24.

Clark, H. C. and Ramsay, H. L. (1965): Predicting optical properties of coated papers, *Tappi J.*, Vol. 48, No. 11, pp. 609-612.

Corte, H. and Kallmes, O.J. (1961): Statistical geometry of a fibrous network, *Trans. 2nd Fund. Res. Symp.*, Oxford, 1961, (Bolam, F., ed.), FRC, UK, 1961, pp. 13-46, 1961.

Draper, N. R. and Smith, H. (1998): *Applied Regression analysis*, John Wiley & Sons, 292-293, New York, USA.

Dunn, O.J. and Clark, V.A. (1974): *Applied statistics: analysis of variance and regression*, Wiley, New York, USA.

Erkkilä, A.-L., Pakarinen, P. and Odell, M. (1998): Sheet forming studies using layered orientation analysis, *Pulp and Paper Canada*, Vol. 99, No. 1, pp. 81–85.

FAO (2013): Food and Agriculture Organization of the United Nations, forest products statistics, Available at: http://www.fao.org/forestry/statistics/ (visited May 30, 2013).

Farnood, R. (2009): Optical properties of paper; theory and practice, *Trans 14th Fund Res Symp*, Oxford, (I'anson, S.J., ed.), FRC, UK, pp. 273-352, 2009.

Ferguson, K.H. (1997): Full sheet imaging system becomes control reality, *Pulp & Paper*, Vol. 71, No. 10, pp. 75-81.

FFIF, (2013): Finnish forest Industries Federation, Available at: www.forestindustries.fi (visited May 30, 2013).

Figiel, K., Gill, J., MacHattie, R., Nuyan, S., Sturm, S., Tippett, J. (2010): *Measurement systems and product variability, Paper machine quality control systems (QCS)*, Tappi press, 27-33 and 71-89, Norcross, USA.

Fisher, N. I. (1993): *Statistical Analysis of Circular Data*, Cambridge University press, England.

Fitzgibbon, A., Pilu, M. and Fisher, R. B. (1999): Direct least square fitting of ellipses, *IEEE Trans. Pattern Anal. Mach. Intell.,* Vol. 21, No. 5, pp. 476-480.

Frankot, R. and Chellappa, R. (1988): A method for enforcing integrability in shape from shading algorithms, *IEEE transactions on pattern analysis and machine intelligence*, Vol. 10, No. 4, pp. 435-446.

Furman, G. and Su, W. (1993): A review of chemical and physical factors influencing Yankee dryer coatings, *Nordic Pulp and Pap. Res. J.*, Vol. 11, No. 5, pp. 217-222.

Ganz, E. (1976): Whiteness: photometric specification and colorimetric evaluation, *Applied Optics*, Vol. 15, No. 9, pp. 2039-2058.

Galun, M., Basri, R. and Brandt, A. (2007): Multiscale edge detection and fiber enhancement using differences of orientated means. *Computer vision, ICCV 2007, IEEE 11th international Conference on*, Vancouver, 2007.

Gockel, B., Heins, J.-P., Schmidt, H., Schuster, H.K. (1986): Measuring head for measuring the porosity of a moving strip, U.S. Patent 4672841 A, (Issued Jul 3, 1986).

Graffe, J. (2010): *Optical online measurement of paper thickness*, PhD thesis, Tampere university of technology, Tampere, Finland, 2010.

Gullichsen, J. and Fogelholm C.-J. (1999): *Papermaking science and Technology, Book 6. Chemical pulping,* Fapet Oy, Helsinki, Finland.

Hansson, P. and Fransson, P. (2004): Color and shape measurement with a three color photometric stereo system, *Applied Optics*, Vol. 43, No. 20, pp. 3971-3977.

Hansson, P. and Johansson, P. Å. (2000): Topography and reflectance analysis of paper surfaces using a photometric stereo method, *Optical Engineering*, Vol. 39, No. 9, pp. 2555-2561.

Hecht E. (2002): *Optics, fourth edition*. Addison Wesley, USA.

Heikkilä, J. and Silven, O. (1997): A Four-step Camera Calibration Procedure with Implicit Image Correction, *Proceedings of IEEE Computer Society Conference on Computer Vision and Pattern Recognition*, San Juan, Puerto Rico,1997.

Hermans, M. A. and Hada, F. S. (2004): Modified conventional wet pressed tissue machine, U.S. Patent 6921460 (Issued March. 17, 2004).

Hindle, P.H., and Smith, C.R.R. (1994): Ultra-fast web thickness and coating measurement with true, two-dimensional control, *proceedings from the NIR '94 Conference*, Lorne, Australia, 1994.

Hollmark, H. (1972): Study of the creping process in an experimental paper machine, *STFI (Swedish Forest Products Laboratory) Research Report No. 144*, Series B, 1972.

Hollmark, H. and Ampulski, R.S. (2004): Measurement of tissue paper softness: A literature review, *Nordic Pulp and Pap. Res. J.*, Vol. 19 No. 3, pp. 345-353.

Howe, R. D. and Cutkosky, M. R. (1992): Touch Sensing for Robotic Manipulation and Recognition, *The Robotics Review 2*., (Kutib O. et. al., ed.), MIT Press, pp. 55-112.

Howe, R. D. and Cutkosky, M.R. (1993): Dynamic Tactile Sensing: Perception of Fine Surface Features with Stress Rate Sensing, *IEEE Trans, Robotics and Automation*, Vol. 9, No. 2, p. 140.

I'Anson, S. J., Constantino, R. P. A., Hoole, S. M. and Sampson, W. W. (2008): Estimation of the profile of cross-machine shrinkage of paper, *Measurement Science and Technology*, Vol. 19, No.1 pp. 1-11.

I'Anson, S. J. (1995a): Identification of periodic marks in paper and board by image analysis using two-dimensional fast Fourier transforms: part 1. The basics, *Tappi J.,* Vol. 78, No. 113.

I'Anson, S. J. (1995b): Identification of periodic marks in paper and board by image analysis using two-dimensional fast Fourier transforms: part 2. Forming and press section marks, *Tappi J.,* Vol. 78, No. 97.

Ihalainen, H., Marjanen, K., Mäntylä, M. and Kosonen, M. (2012): Developments in camera based on-line measurement of paper, *Control systems 2012*, New Orleans, USA, 2012.

ISO 11475 (2004): Paper and board -- Determination of CIE whiteness, D65/10 degrees (outdoor daylight)

ISO 2471 (2008): Paper and board -- Determination of opacity (paper backing) -- Diffuse reflectance method

Johnson, B.C. (1972): Circular Aperture Diffraction Limited MTF: Approximate Expressions, *Applied optics*, Vol. 11, No. 8.

Kawabata, S. (2002): Testing the tactile properties of tissue and nonwovens. *Handb. of physical test. of pap.* (Borch, L., Habeger, M., ed.), Vol 2, pp. 505-530.

Kjaer, A.P., Heath, W.P. and Wellstead, P.E. (1995): Identification of cross-directional behavior in web production: techniques and experience, *Control Engineering Practice*, Vol. 3, No. 1, pp. 21-29.

Keller, D.S, Pawlak, J.J., Kellomäki, M., Hagglund, J.-E. and Johansson, N. (2004): Three storage phosphor systems for beta-radiographic imaging of paper, *Nordic Pulp and Pap. Res. J.*, Vol. 19, No. 2, pp. 170-175.

Keller, D.S. and Pawlak, J.J. (2001): β-Radiographic imaging of paper formation using storage phosphor screens, *Journal of pulp and paper science*, Vol. 27, No. 4, pp. 117-123.

Kim, S.J and Pollefeys, M. (2008): Robust radiometric calibration and vignetting correction, *IEEE Transaction on Pattern Analysis and Machine Intelligence*, Vol. 30, No. 4, pp. 562-576.

Komppa, A. and Ebeling, K, (1981): Correlation between the areal mass and optical densities in paper, *Trans. 7nd Fund. Res. Symp*., Cambridge, 1981, (Brander, J., ed.), FRC, UK, pp. 603-632, 1961.

Komulainen, P. (2004): Method for measuring porosity of moving web-line paper, WO Patent 2005024394 A1, (Issued Sep 8, 2004).

Kropholler, H.W., Clarke, B. and Gorres, J. (1981): Investigating paper structure using image analysis, *Trans. 7nd Fund. Res. Symp*., Cambridge, 1981, (Brander, J., ed.), FRC, UK, pp. 603-632, 1961.

Kubelka, P. (1948): New contributions to the optics of intensely light-scattering materials. Part I: Nonhomogeneous layers, *J. opt. soc. Am.*, Vol. 38, No.5, pp. 448-457.

Kubelka, P. (1954): New contributions to the optics of intensely light-scattering materials. Part II: Nonhomogeneous layers, *J. opt. soc. Am.*, Vol. 44, No.4, pp. 330-334.

Kuo, L.-S. and Cheng, Y.-L. (1997): A novel method of testing surface softness of household papers - CK method, *J. Expt. Forest of NCHU*, Vol. 19, No. 1, pp. 53-61.

Kuparinen, T. (2008): *Reconstruction and analysis of surface variation using photometric stereo*, PhD Thesis, Lappeenranta University of Technology, Lappeenranta, Finland, 2008.

Kuusela, R. (1990): *Infrared moisture measurement of paper, board and pulp*, PhD Thesis, University of Kuopio, Kuopio, Finland, 1990.

Lambert, J. (2001): *Photometry, or, on the measure and gradiations of light, colors, and shade: translation from the Latin of photometria, sive, de mensura et gradibus luminis, colorum et umbrae*, Illuminating engineering society of North America, New York, USA.

Land, E.H. (1951): Some aspects of the development of sheet polarizers, *J. opt. soc. Am.*, Vol. 41, No. 12, pp. 957-963.

Lang, D. W. (2012): Experiences with online measurement of tissue weight using infrared technology, *Control systems 2012*, New Orleans, USA, 2012

Leiviskä, K. (ed.) (2009): *Papermaking science and Technology, Book 14, Process and maintenance management*, Fapet Oy, Oulu, Finland.

Leppänen, T. (2007): *Effect of fiber orientation on cockling of paper*, PhD Thesis, University of Kuopio, Kuopio, Finland, 2007.

Lim, J.S. (1990): *Two-dimensional signal and image processing*, Prentice Hall, USA.

Linder, T. and Löfqvist, T. (2012): Anisotropic light propagation in paper, *Nordic Pulp and Pap. Res. J.*, Vol. 28 No. 2, pp. 500-506.

Luner, P., Kärnä, A.E.U. and Donofrio, C.P. (1961): Studies in interfibre bonding of paper. The use of optical bonded area with high yield pulps, *Tappi*, Vol. 44, No. 6, pp. 409-414.

Madsen, B. K. and Simms, R. J. (1979): Apparatus and method for measuring the consistency of a pulp suspension, U.S. Patent 4171916 A, (Issued Oct 23, 1979).

Marjanen, K., Ihalainen, H. and Yli-Fossi, T. (2009): Measuring paper quality by texture analysis, *Paper research symposium*, Kuopio, Finland, 2009.

McConnel, W. (2004): The science of Creping, *Tissue world Americas*, Miami, USA, September 21-23, 2004

Meijer, R., Tixier, S., Haran, F., Lantz, K. and MacHattie, R. (2012): IR vs nuclear fiber weight measurement – field trial results on tissue, *Control systems 2012*, New Orleans, USA, 2012.

Mercer, P.G. (1987): Selective on-line measurement of filler components in paper, U.S. Patent 4845730 A, (Issued Dec 18, 1987).

Metso IQ (2012): Metso IQ, paper quality measurement and control, Available at: http://www.metso.com/Automation/pp_prod.nsf/WebWID/WTB-110817-2256F-9B12E?OpenDocument&tab=3 (visited May 1, 2013).

Metso IQ (2013): Metso IQ, surface measurement , Available at: http://www.metso.com/Automation/pp_prod.nsf/WebWID/WTB-120904-2256F-C465D?OpenDocument (Visited May 30, 2013).

Metso IQInsight (2013): Metso IQInsight, web-wide moisture measurement , Available at: http://www.metso.com/mp/marketing/Vault2MP.nsf/BYWID2/WID-091117-2256E-D9200/$File/PM091116_IQInsight_profile_measurement_datasheet.pdf?openElement (Visited Nov 1, 2013).

Mettänen, M. (2010): *Measurement of print quality: joint statistical analysis of paper topography and print defects*, PhD Thesis, Tampere University of Technology, Tampere, Finland, 2010.

Middleton, S.R. and Scallan, A.M. (1992): The optical properties of bleached kraft pulps, *Nordic Pulp and Pap. Res. J.*, Vol. 7, No. 1, pp. 22-24.

Mikhail, E.M., Bethel, J.S. and McGlone, J.C. (2001): *Introduction to modern photogrammetry*, John Wiley & Sons Inc., USA.

Naidu, P.S. (2001): *Sensor array Signal processing*, CRC press, USA.

Nasa (2014): Electromagnetic spectrum, Available at: http://imagine.gsfc.nasa.gov/docs/science/know_l1/emspectrum.html (Visited April 25, 2014).

Neimo, L. (ed.) (1999): *Papermaking science and technology, book 4a*, *Papermaking chemistry*, Fapet Oy, Helsinki, Finland.

Niskanen, K. (ed.) (1998): *Papermaking science and technology, Book 16, Paper Physics*, Fapet Oy, Jyväskylä, Finland.

Nordman, L. and Uggla, R. (1977): Adhesion between fibre webs and metal surfaces during drying, Fibre-water interactions in paper making, *Trans 6th Fund Res Symp*, Oxford, FRC, UK, pp. 459-473, 1977.

Norman, B. and Wahren, D. (1974): The measurement of Mass Distribution in Paper Sheets Using a Beta Radiographic Method, *Svensk Papperstidning*, Vol. 77, No. 10, pp. 397-406.

Oliver, J. (1980): Dry-creping of tissue paper – a review of basic factors, *TAPPI J.*, Vol. 63, No. 12, pp. 91-95.

Paavilainen, L. M. (1991): Influence of morphological properties of softwood fibers on sulfate pulp fiber and paper properties, *Proc. Tappi 1991 International paper physics conference*, Atlanta, USA, 1991.

PAPTAC standard E.1 (1990): Brightness of pulp, paper and paperboard.

Parker. J. (1972): *The sheet-forming process*, Special Technical Association publication, Atlanta, USA.

Patterson, T. (2013): Evaluating and enhancing tissue softness, *PaperCon 2013 conference*, Atlanta, USA, 2013.

Paulapuro, H. (2008): *Papermaking science and Technology, Book 8, Papermaking Part 1, Stock Preparation and Wet End*, Fapet Oy, Helsinki, Finland.

Paulapuro, H. (2008): *Papermaking science and technology, book 18, Paper and board grades*, Fapet Oy, Helsinki, Finland.

Pauler, N. (2002): *Paper optics*, Elanders tofters, Sweden.

Pawlak, J. J. and Elhammoumi, A. (2011): Image Analysis Technique for the Characterization of Tissue Softness, *International Paper Physics conference*, Graz, Austria, 2011.

Pfeifer, R.J., Williams, P. and Holmes, R. (1998): System Considerations for a Fullsheet Imaging System, *Proceedings from the TAPPI Process Control Electrical & Information Conference*, Vancouver, Canada, 1998.

Philips-Invernizzi, B., Dupont, D. and Caze, C. (2001): Bibliographical review for reflectance of diffusing Media, *Optical engineering*, Vol. 40, No. 5, pp. 1082-1092.

Polak, E. (1997): *Optimization, Algorithms and Consistent Approximations*, Springer-Verlag, New York, USA.

Ramasubramanian, M.K. (2011): Modeling and simulation of the creping process, *PaperCon 2011 conference*, Cincinnati, USA, 2011.

Ramsay H.L. (1966): Simplified calculation for predicting optical properties of coated board, *Tappi*, Vol. 49, No. 12, pp.116A-118A.

Raunio, J.-P. (2006): *Estimation of shrinkage profile based on wire marking*. Master's thesis, Tampere University of Technology, Tampere, Finland, 2006.

Raunio, J.-P. and Ritala, R. (2009): Estimation of basis weight of paper: light transmittance measurements over eight orders of magnitude of spatial scale, *The 2009 XIX IMEKO World Congress*, Lisbon, Portugal, 2009.

Raunio, J.-P. and Ritala, R. (2012): Variability of Crepe Frequency in Tissue Paper; Relationship to Basis Weight, *Control systems 2012*, New Orleans, USA, 2012.

Saito, M., Sato, Y., Ikeuchi, K. and Kashiwagi, H. (1999): Measurement of surface orientations of transparent objects using polarization in highlight*, Proceedings of IEEE Conference on Computer Vision and Pattern Recognition*, pp. 381–386, 1999.

Sara, H. (1978): *The characterization and measurement of paper formation with standard deviation and power spectrum*, PhD Thesis, Helsinki University of Technology, Helsinki, Finland, 1978.

Bendtsen method (1967): *Scandinavian Pulp, Paper and Board Testing Committee*, Paper and board — Determination of roughness Bendtsen method, SCAN-P21:67 standard.

Sadovnikov, A. (2010): *Computational evaluation of print unevenness according to human vision*, PhD Thesis, Lappeenranta University of Technology, Lappeenranta, Finland, 2010.

Sarimveis, H. and Retsina, T. (2000): Tissue softness prediction using neural network methodologies, *Paptac, 86th Annual Meeting*, pp. 27 –30, Montreal, Canada, 2000.

Scallan, A.M. and Borch, J. (1972): An interpretation of paper reflectance based upon morphology. I: initial considerations, *Tappi*, Vol. 55, No. 4, pp. 583-588.

Shakespeare, J., Paavola, A. (2009): Online measurement of surface fiber orientation, *Proc. Papermaking Research Symposium*, Kuopio, Finland, 2009.

Shakespeare, J. (2007): Measuring fiber orientation by detecting dispersion of polarized light, U.S. Patent 7164145 B2 (Issued Jan. 16, 2007).

Shapiro, S., Vyse, R., and Hagart-Alexander, C. (1998): New wet end weight measurement system opens papermaking optimization opportunities, *proceedings from the Joint Tappi Process Control, Electrical and Engineering Conference and ISA PUPID 38th Annual Symposium*, Vancouver, Canada, 1998.

Simchony, T., Chellappa, R. and Shao, M. (1990): Direct analytical methods for solving Poisson equations in computer vision problems, *IEEE transactions on pattern analysis and machine intelligence,* Vol. 12, No. 5, pp. 435-446.

Smith, M.L. and Smith L.N. (2005): Dynamic Photometric Stereo - A New Technique for Moving Surface Analysis, *Image and Vision Computing*, Vol. 23, No. 9, pp. 841-852.

Sonka, M., Hlavac, V. and Boyle, R. (1998): *Image processing, analysis, and machine vision*, PWS, California, USA.

Starr, R.E. and Young R. H. (1984): A study of limitations involved in the determination and use of Kubelka-Munk constants for paper coating formulations, *1984 Air Knife Coating seminar*, Atlanta, USA, 1984.

Stenius, P. (2000): *Papermaking science and technology, Book 3, Forest products chemistry*, Fapet Oy, Helsinki, Finland.

Stitt, J. (2007): Set characteristics of Yankee dryer coatings, *Tissue world*, Nice, France, 2007

Sturm, S.P. (1984): Measuring the percentage or fractional moisture content of paper having a variable infrared radiation scattering characteristics and containing a variable amount of a broadband infrared radiation absorber, U.S. Patent 4577104 A, (Issued Jan 20, 1984).

Sun Z. (2000): *Debonding and buckling of a thin short-fiber nonwoven bonded to a rigid surface and its application to the creping process*, Ph.D. Thesis, NC state University, North Carolina, USA, 2000.

Sundholm, J. (1999): *Papermaking science and technology, Book 5,* Mechanical pulping, Fapet Oy, Helsinki, Finland.

Taylor, C.J. and Nixon, R.N. (1981): Image analysis applied to fibre images, *Trans. 7nd Fund. Res. Symp*., Cambridge, 1981, (Brander, J., ed.), FRC, UK, pp. 603-632, 1961.

Williams, P., Domin, T., Green, E.S. and Holmes, R.A. (1996): Measurement/control of sheet material using at least one sensor array, U.S. Patent 5563809 (Issued Nov. 8, 1996).

Yu, W. (2004): Practical anti-vignetting methods for digital cameras, *IEEE Transactions on Consumer Electronics*, Vol. 50, No. 4, pp. 975-983.

Welch, P.D. (1967): The use of fast Fourier transform for the estimation of power spectra: a method based on time averaging over short, modified periodograms, *IEEE transactions on audio and electroacoustic*, Vol. 15, No. 2, pp. 70-73.

Vartiainen, J. (2007): *Measuring irregularities and surface defects from printed patterns*, PhD Thesis, Lappeenranta University of Technology, Lappeenranta, Finland, 2007.

Viitaharju, P.H. and Niskanen K.J. (1993): Dried-in shrinkage profiles of paper webs, *Tappi J.*, Vol. 76, No. 8, pp. 129-134.

Wolff, L. B. (1990): Surface orientation from two camera stereo with polarizers, *Proceedings of Conference of Optics, Illumination and Image Sensing for Machine Vision IV*, vol. 1194 of Proceedings of SPIE - The International Society for Optical Engineering, pp. 287–297.

Woodham, R.J. (1994): Gradient and curvature from photometric-stereo method including local confidence estimation, *J. opt. soc. Am.,* Vol. 11, No. 11, pp. 3050-3068.

Woodham, R. J. (1978): Method for determining surface orientation from multiple images, *SPIE Proc*, 1978.

Ylisaari, J., Ritala, R., (2010): Web-wide transmittance imaging measurement variability analysis, *International Control systems Program 2010*, Stockholm, Sweden, 2010.

Zhang, Z. (1999): Flexible camera calibration by viewing a plane from unknown orientations, *International Conference on Computer Vision*, Corfu, Greece, 1999.

Publications

Publication I

Raunio, J.-P. and Ritala, R. (2009): Analysis of paper structure based on light transmittance and basis weight measurements, *In CD-Proceedings of Papermaking Research Symposium 2009*, Kuopio, Finland, 2009, 11 pages.

ANALYSIS OF PAPER STRUCTURE BASED ON LIGHT TRANSMITTANCE AND BASIS WEIGHT MEASUREMENTS

J-P. Raunio[1], R. Ritala[2]

[1] Tampere University of Technology, Department of Automation Science and Engineering, P.O. Box 527, FI-33101 Tampere, Finland. E-mail: jukka-pekka.raunio@tut.fi
[2] Tampere University of Technology, E-mail: risto.ritala@tut.fi

Abstract. This paper studies the structure of paper based on light transmittance and basis weight measurements. In this paper the analysis of paper structure is based on the similarities and differences between the small-scale transmittance and basis weight variations. The data comprises 2D basis weight and light transmittance measurements on uncoated and coated papers. The relationship between the basis weight and light transmittance in point-wise aligned 2D measurements is studied through scale – dependence of linear correlation coefficient. It was observed that in small scales the correlation between basis weight and light transmittance measurements in coated papers is positive in contrast to negative correlation in uncoated papers. However, in large scales the correlation is negative for both paper types. This behavior is due to small scale structure properties of coating, which was analyzed with layered Kubelka-Munk theory for light transmittance in paper.

Keywords: Paper structure, transmittance, basis weight, measurement

1 Introduction

The optical properties and the basis weight of paper web are important for quality management. This paper studies the structure of paper based on light transmittance and basis weight measurements. The optical properties, such as gloss, color, opacity, and brightness affect to light transmittance but obviously not to basis weight or how it is measured. However, it is well-known that light transmittance is related to basis weight. In this paper the analysis of paper structure is based on the similarities and differences between the two paper properties in small scale. The structure of both uncoated and coated papers is studied.

The relationship between the basis weight and light transmittance in point-wise aligned 2D measurements is studied with linear correlation and how it depends on spatial scale. In this work the data is low pass filtered to reduce of spatial resolution. Based on the behavior of paper measurements a model for paper structure which depends on spatial scale is obtained. The model is tested by computing the correlation dependency between the light transmittance and basis weight values in theory. The theoretical light transmittance is determined with Kubelka-munk theory. The Kubelka-Munk equations divide the coated paper to layers which corresponds to coatings and base paper. Now the estimation of light transmittance is possible even the paper is coated. The Kubelka-Munk theory is used previously in an estimation of light transmittance of uncoated and coated

paper and it has been noticed that the theory give information of optical structure of material although it does not describe the behavior of light perfectly.

This paper is organized as follows. In Section 2 the data analyzed in this study is presented. Data is composed of basis weight and light transmittance of paper, and must be pre-processed before the analyses. Section 3 introduces the Kubelka-Munk theory and how it is applied to coated paper. Also, the relationship between basis weight and light transmittance is shortly described. Section 4 reports the main results and shows how the structure of paper is estimated. Section 5 concludes about the usability of estimate of paper structure and discusses the future measurement applications of paper.

2 The measurements

The data comprises 2D basis weight and light transmittance measurements. The two paper properties were measured from 20 paper samples; 6 papers were coated and 14 were uncoated. The Figure 1 and Figure 2 show examples of uncoated paper and coated paper.

2.1 Basis weight measurements

The basis weight measurement is based on transmittance of beta radiation. The paper was measured at 0.05 mm/pixel resolution. The size of the measured basis weight image was 12 cm in CD and 12 cm in MD. Figure 1 and Figure 2 show examples of basis weight images. The basis weight images were aligned with transmittance images at subpixel resolution before the analyses with the method presented in [4]. The resolution of images after the alignment was 0.1 mm/pixel and the size of the images was 8 cm in CD and 8 cm in MD. The average basis weights of uncoated and coated papers were 40 g/m^2 and 80 g/m^2.

2.2 Light transmittance measurements

The light transmittance measurement is based on light transmittance of paper. In this work the transmittance of light is measured with scanner. The light source is on the opposite side of paper to the image sensor. The sensor imaging the sample obviously measures light transmittance of paper. Figure 1 and Figure 2 show examples of transmittance images. The resolution of images is 0.1 mm/pixel and the size of the images is 8 cm in CD and 8 cm in MD. The mean of transmittance image was removed and the variance scaled to 1, and the light transmittance image is inverted because of the negative correlation for easier visual comparison.

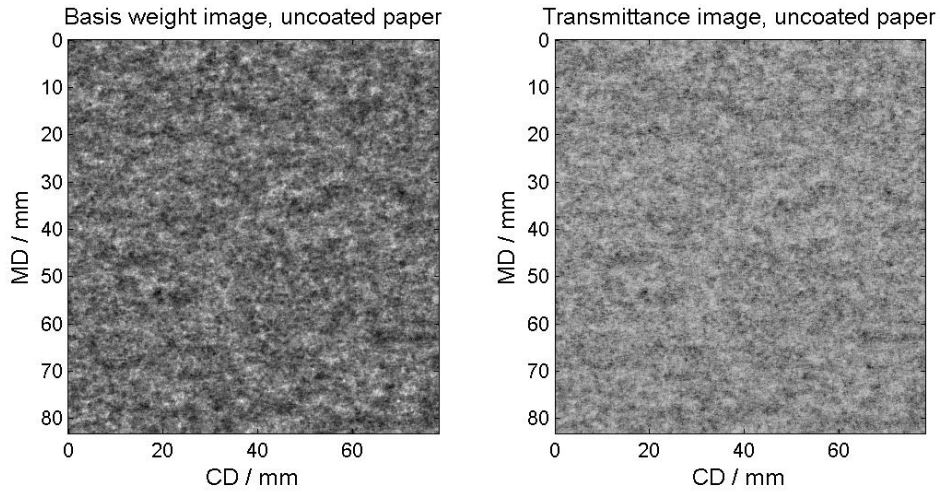

Figure 1: The basis weight and light transmittance images from uncoated paper. The resolution of images is 0.1 mm/pixel and the size of the images is 8 cm in CD and 8 cm in MD. The images are aligned at subpixel resolution.

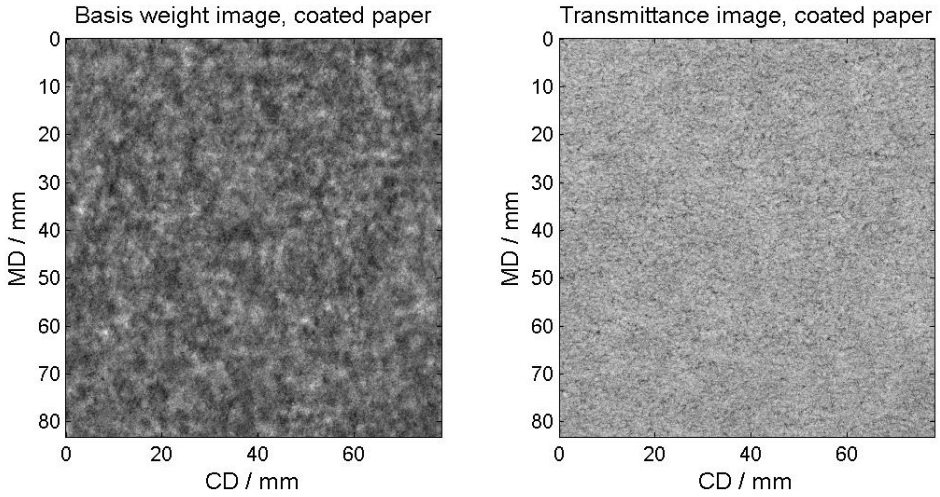

Figure 2: The basis weight and light transmittance images from coated paper. The resolution of images is 0.1 mm/pixel and the size of the images is 8 cm in CD and 8 cm in MD. The images are aligned at subpixel resolution.

3 Theoretical background

This chapter analyzes theoretically how the structure of paper may affect the small scale correlation between light transmittance and the basis weight of coated and uncoated paper. First, the relationship between the light transmittance and basis weight is shortly described.

In this paper the light transmittance of paper is denoted as T and the basis weight value is denoted as W. The basis weight and light transmittance are assumed to be linearly related as follows

$$W = aT + b + N \tag{1}$$

where *a* and *b* are regression coefficients which define the transformation from transmittance to basis weight [7]. *N* is the sum of noise effects specific for basis weight and light transmittance measurements.

3.1 Estimation of light transmittance

The optical properties of paper can indirectly characterize the sheet structure. In this work the estimation of light transmittance is determined theoretically by studying the behavior of light in separate papers. It is known that light both scatters from material and is absorbed to it. Kubelka-Munk theory gives tools for characterize the paper with these optical parameters. In this work the light transmittance is determined theoretically as a function of paper thickness.

3.1.1 Kubelka-Munk theory

Kubelka-Munk theory defines the light scattering and absorption coefficients of material. These parameters give information of structure of material although it does not describe the behavior of light perfectly. The Kubelka-Munk theory is usually applied in a transform from reflectances R_0 and R_∞ to light scattering and absorption coefficients [2],[5]. In this work the light scattering *S* and absorption *K* are assumed to be known and the reflectances R_0 and R_∞ are determined as follows

$$R_\infty = 1 + \frac{K}{S} - \sqrt{\frac{K^2}{S^2} + 2\frac{K}{S}} \tag{2}$$

$$R_0 = \frac{e^{Sd\left(\frac{1}{R_\infty} - R_\infty\right)} - 1}{\frac{1}{R_\infty} e^{Sd\left(\frac{1}{R_\infty} - R_\infty\right)} - R_\infty} \tag{3}$$

where *d* is the thickness of material [5]. The light transmittance of material can be determined the same way by using light absorption and scattering coefficients and equation (1) [2],[5].

$$T = \frac{\left(1 - R_\infty{}^2\right) e^{-\frac{1}{2}Sd\left(\frac{1}{R_\infty} - R_\infty\right)}}{1 - R_\infty^2 e^{-Sd\left(\frac{1}{R_\infty} - R_\infty\right)}} \tag{4}$$

Now the light transmittance is obtained as a function of thickness *d*. Equation (3) is sufficient for homogenous materials, such as uncoated paper sheets, but with coated papers the coating layers must be considered separately from the base paper. Coated paper consists of two coating layers and one base paper layer. The light transmittance for multilayer coated papers can be obtained from Stokes equations [3]. The light transmittance for a three-layer construction coating(A)-base paper(B)-coating(C) can be determined as follows

$$T_{ABC} = \frac{T_{AB}T_c}{1 - R_{0BA}R_{0C}} \tag{5}$$

where T_c is the light transmittance of coating layer C, R_{OC} is the reflectance of coating layer C and T_{AB}, R_{0BA}, are obtained as follows in equations (5), (6)

$$T_{AB} = \frac{T_A T_B}{1 - R_{0A}R_{0B}} \tag{6}$$

$$R_{0BA} = R_{0B} + \frac{R_{0A}T_B^2}{1 - R_{0A}R_{0B}} \tag{7}$$

where T_A and T_B are light transmittances of layers A and B [3],[6]. Similarly, R_{0A} and R_{0B} are reflectances of layers A and B. Now the transmittance of coated paper is determined as a function of thicknesses of layers A(coating), B(base paper), and C(coating).

3.2 Estimation of basis weight

The estimation of basis weight is straightforward. It is known that the basis weight is the product of density and thickness of paper. In uncoated papers the basis weight is determined as $W=\varrho d$. In coated papers the coating layers and the base paper layer must be considered separately and the basis weight is determined to three layered coated paper ABC as follows

$$W_{ABC} = \rho_A d_A + \rho_B d_B + \rho_C d_C \tag{8}$$

where ρ_A, ρ_B, ρ_C are the densities of coating layers and the base paper layers. The thicknesses of layers are describes as d_A, d_B, and d_C. The densities are known, so the basis weight of paper is obtained as function of paper thickness.

4 The results

This chapter studies the structure of coated and uncoated papers. First, the correlation dependency is studied between the basis weight and light transmittance measurements. Next, the behavior of correlation dependency in theory is studied. The theoretical light transmittance value is estimated with Kubelka-Munk equations. The behavior of coated paper is explained with model which varies in a function of measurement scale. This means that in small scale the model of paper structure differs from the model of paper structure in large scale.

4.1 Correlation dependency between basis weight and light transmittance measurements

The correlation dependency of resolution in uncoated and coated is studied from paper sheet images. Images are low pass filtered with elliptic filter to simulate the reduction of resolution. Choosing the elliptic filter is based on small order of the filter, adjustable ripple in pass and stop bands, and sharp edge between the pass and stop band [1].

The reduction of resolution is simulated evenly from 0,1 mm/pixel to 20 mm/pixel and the cross correlation between the signals for all simulated resolutions is computed. The correlation curve is computed for all 14 uncoated paper sheets, and by averaging of curves the generalized behavior is found. Figure 3 shows the averaged dependency between the correlation and resolution in uncoated papers. From Figure 3 can be seen that the correlation is significant and the maximum correlation is achieved at 6 mm/pixel resolution. After that the correlation starts to decrease slightly. This suggests some paper structure variations at length scales of 10 mm and higher affecting the parameter a and b in (1).

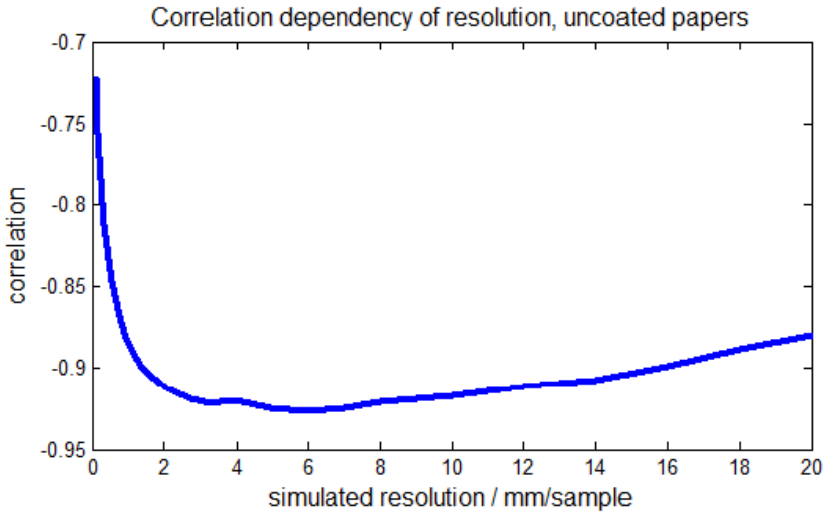

Figure 3: Correlation between basis weight and light transmittance as a function of resolution in uncoated papers

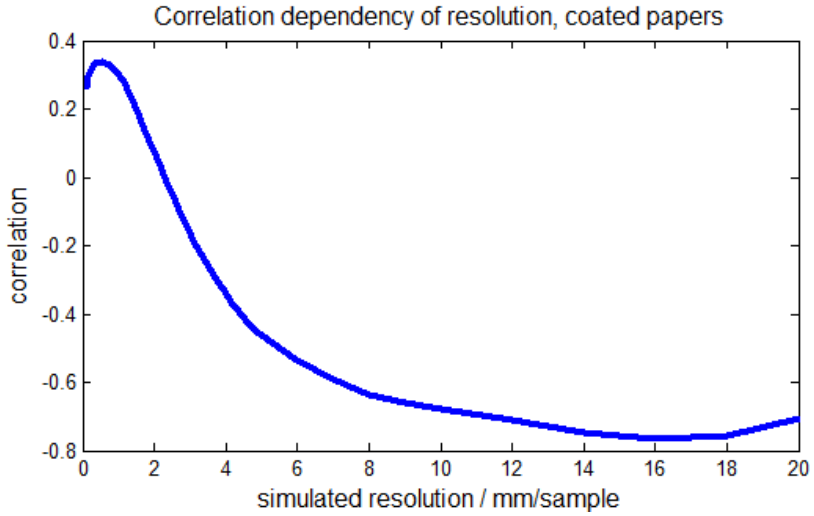

Figure 4: Correlation between basis weight and light transmittance as a function of resolution in coated papers

Also, the correlation curve for all 6 coated paper sheets is computed and the generalized behavior is found. Figure 4 shows the averaged dependency between the correlation and resolution in coated papers. It can be seen that the correlation is positive in small scales in contrast to uncoated papers. However in larger scale the correlation is positive

similarly as that of uncoated papers, and the maximum correlation is achieved at 16 mm/sample resolution. It can be seen that the correlation depends on measurement scale in both paper cases.

4.2 The structure of uncoated paper

The Figure 3 shows that the correlation dependency is significant between the two paper properties in uncoated papers. The correlation dependency is also studied in theory. The light transmittance is computed with Kubelka-Munk equation (4), and the basis weight with $W=\varrho d$ equation. The thickness of paper assumes random values from normal distribution. The mean of distribution is 0.06 mm and standard deviation is 0.006 mm. The density of paper is assumed to be 650 kg/m^3. This means that basis weight of theoretical uncoated paper is 40 g/m^2 such as in true measurements. The Figure 5 shows the joint distribution between theoretical basis weight and light transmittance values. The light absorption of uncoated paper assumes value 0.5 m^2/kg and light scattering assumes value 50 m^2/kg [5]. Also, the noise is added to both theoretically computed paper properties for easier visual observation.

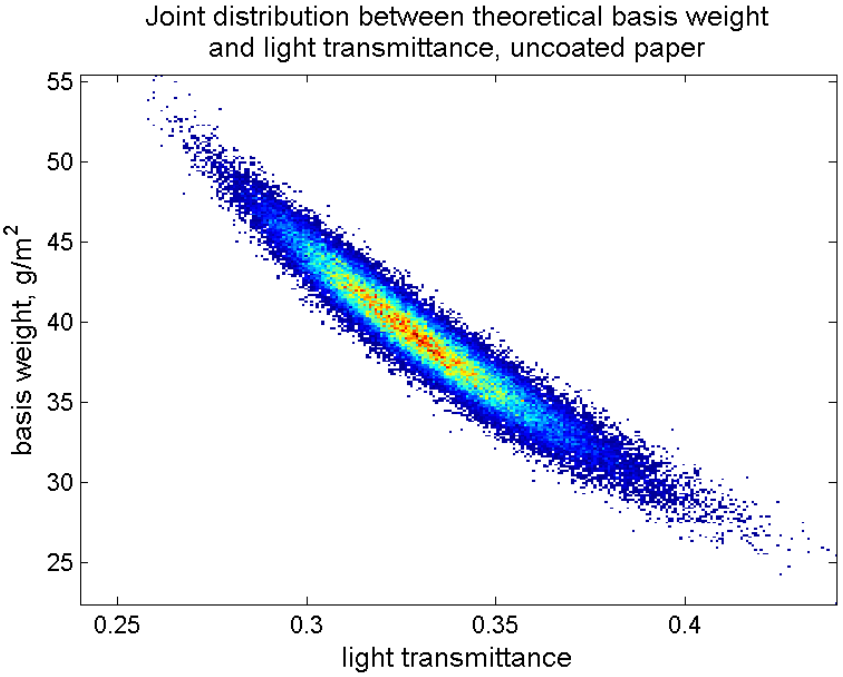

Figure 5: Joint distribution between theoretical basis weight and light transmittance in uncoated paper. The light scattering was 50 m^2/kg and light absorption was 0.5 m^2/kg.

The joint distribution shows that the correlation between the theoretical basis weight and light transmittance is significant such as in true measurements (Figure 3). It can be say based on the results and measurements that the light transmittance of paper is a good estimate for basis weight of paper. Especially, if the examined resolution is lower than the highest imaging resolution the light transmittance images can be low pass filtered to wanted resolution to achieve more advantageous estimation.

4.3 The structure of coated paper

The theoretical light transmittance of coated paper was computed with layered Kubelka-Munk theory (5). It was noticed that the correlation between the two paper properties depends on the measurement scale of coated paper. Therefore, the structure of coated paper is also explained with model which depends on the length scale. The model is expressed as follows

$$d = d_A + d_B + d_C, \quad d_A = d_C \tag{9}$$

where d_A, d_C are thicknesses of coatings and d_B is the thickness of base paper layer. The d describes the whole thickness of paper. The thicknesses of coating layers and the optical properties of coating layers are assumed to be equal.

It is assumed that the thicknesses of coatings d_A and d_C are constant and equal in large scale (20 mm). In small scale (0.1 mm) the thicknesses of coatings d_A and d_C are not constant anymore, and the shape of coating layer is opposite as to the base paper layer. This means that more coating goes to small scale valleys as to the small scale hills of base paper. The deviation of coating varies from zero (large scale) to 0.002 mm (small scale).

The joint distribution between theoretical basis weight and light transmittance values for large and small scale is computed. The thickness of base paper assumes random values from normal distribution. The mean of distribution is 0.085 mm and the standard deviation is 0.006 mm. In large scale the thickness of coating is constant $d_1 = d_3 = 0.00835$ mm. In small scale the deviation of coating is 0.002 mm and the thickness of coating varies depending on the thickness of base paper. The densities of base paper and coating assume value 650 kg/m^3 and 1500 kg/m^3. Hence, the basis weight of theoretical coated paper is 80 g/m^2 such as in true measurements. The Figure 6 and Figure 7 show the joint distributions between the theoretical basis weight and light transmittance values. Figure 6 shows the values computed in large scale and Figure 7 shows the values computed in small scale. The light absorptions and scatterings for base paper and coating are: $K_{A,C}$ = 1 m^2/kg $S_{A,C}$ = 150 m^2/kg K_B = 0.5 m^2/kg and S_B = 50 m^2/kg [5],[6]. Also, the noise is added to both theoretically computed paper properties for easier visual observation.

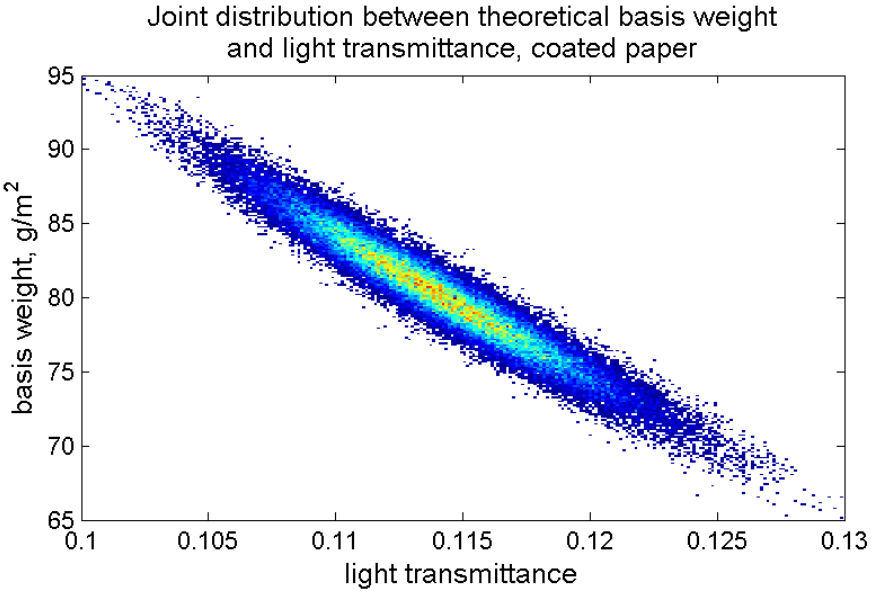

Figure 6: Figure shows the joint distribution between two paper properties when the structure of coated paper is described in large scale (20 mm). The light absorptions and scatterings for base paper and coating are: $K_{A,C}$ = 1 m²/kg $S_{A,C}$ = 150 m²/kg K_B = 0.5 m²/kg and S_B = 50 m²/kg

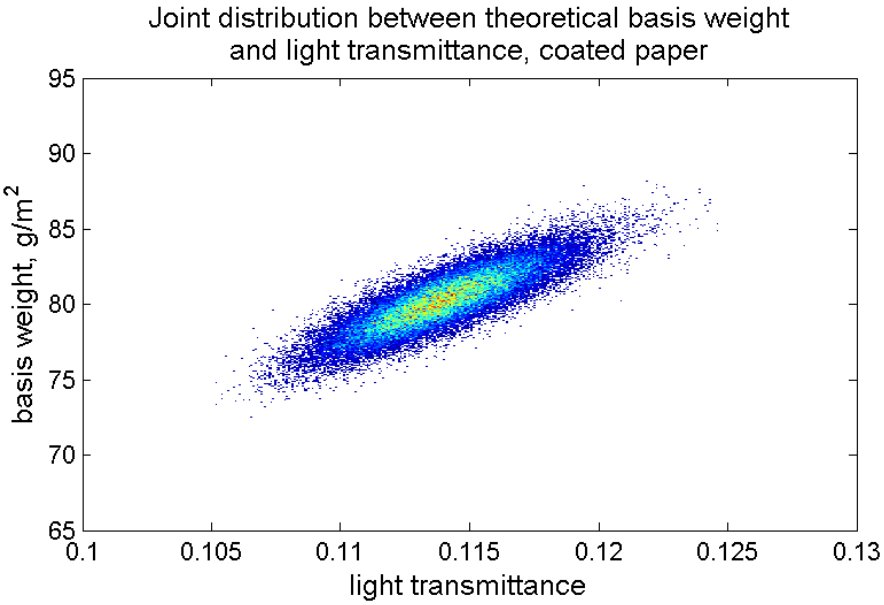

Figure 7: Figure shows the joint distribution between two paper properties when the structure of coated paper is described in small scale (0.1 mm). The light absorptions and scatterings for base paper and coating are: $K_{A,C}$ = 1 m²/kg $S_{A,C}$ = 150 m²/kg K_B = 0.5 m²/kg and S_B = 50 m²/kg.

It was noticed that the correlation dependency changes from positive to negative while the resolution decreases such as in true measurements. The correlation coefficients between the two paper properties from length scale 0.1 mm to length scale 20 mm are shown in Figure 8. In Figure 8 the model of structure changes in function of resolution such as presented at the beginning of chapter.

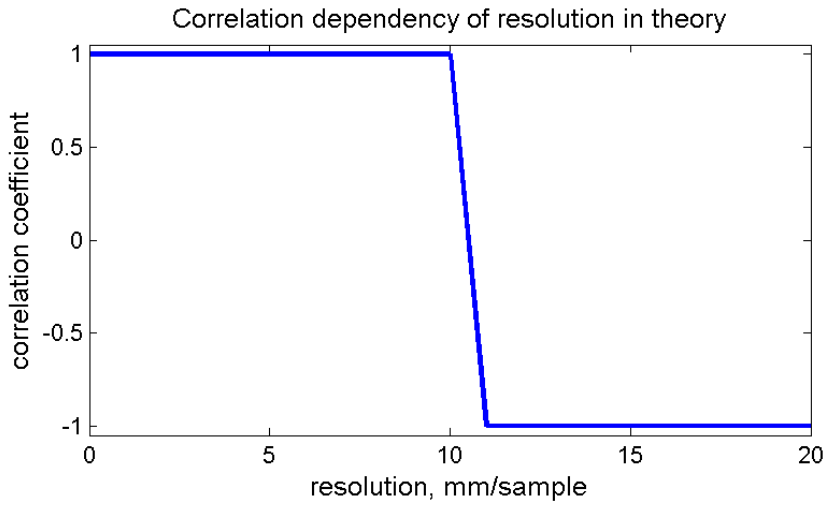

Figure 8: Correlation dependency of resolution. The model of structure changes in a function of resolution. The deviation of coating is zero in small scale (0.1 mm) and 0.02 mm in large scale (20 mm).

It can be seen from Figure 8 that the two paper properties are either significantly negatively correlated or significantly positively correlated. The model cannot simulate smooth translation from positive to negative correlation such as in true measurement (Figure 4). One reason for that is the lack of measurement noise in theoretically computed values. Also, the resolution when the sign of correlation changes is not the same such as in true measurement. This occurs because the presented small and large scale models are not ideal for 0.1 mm and 20 mm resolutions such as it was assumed in this work.

5 Conclusion

The correlation results indicate that the light transmittance is a good estimate for basis weight between the measurement scales 0.1 mm and 20 mm in uncoated papers. However, the quality of estimate depends on the measurement scale and therefore the resolution must take into account in basis weight estimation and light transmittance measurements.

In coated papers the correlation coefficients were depending significantly on the measurement scale. In small scale the correlation was positive between the two paper properties, and in large scale the correlation was negative. The behavior of measurements of coated paper was simulated by explaining the structure of paper with model which depends on measurement scale. It was noticed that the model presented in this work determine the rough structure of coated paper, and more study is needed to find more advantageous model. With complete model for example the basis weight of coated paper can be estimated from light transmittance images.

References

[1] Gustafsson F.: Determining the initial states in forward-backward filtering. IEEE Transactions on Signal Processing, **44**(4):988-992 (1996)

[2] Kubelka P.: New Contributions to the Optics of Intensely Light-Scattering Materials. Part I: Nonhomogeneous Layers. Journal of the Optical Society of America, **38**(5):448-457 (1948)

[3] Kubelka P.: New Contributions to the Optics of Intensely Light-Scattering Materials. Part II: Nonhomogeneous Layers. Journal of the Optical Society of America, **44**(4):330-334 (1954)

[4] Lähdekorpi M., Ihalainen H., Ritala R.: Using image registration and alignment to compare alternative 2D measurements. XVII IMEKO world congress, Rio de Janeiro (2006)

[5] Niskanen K.: Paper Physics, Fapet Oy, Jyväskylä (1998)

[6] Pauler N.: Paper Optics, AB Lorentzen & Wettre, Östervåla (2002)

[7] Sara H.: The characterization and measurement of paper formation with standard deviation and power spectrum. Ph.D. thesis, Helsinki University of Technology (1978)

Publication II

Raunio, J.-P., Tirronen, V., Ritala, R., Nironen, I., Rossi, T. and Kärkkäinen, T. (2010): Web-wide diagnostics of paper properties based on fault detector system images, *In CD-Proceedings of Tappi Papercon2010*, Atlanta, USA, 2010, 13 pages.

Publication III

Raunio, J.-P. and Ritala, R. (2010): 2D basis weight estimation based on light transmittance imaging, *In CD-Proceedings of Control Systems 2010*, Stockholm, Sweden, 2010, 6 pages.

2D BASIS WEIGHT ESTIMATION BASED ON LIGHT TRANSMITTANCE IMAGING

Jukka-Pekka Raunio[1], Ville Tirronen[2], Risto Ritala[3], Ilkka Lehtoranta[4]

[1)]Tampere University of Technology, Tampere, Finland, jukka-pekka.raunio@tut.fi
[2)]Jyväskylä University, Jyväskylä, Finland, ville.tirronen@jyu.fi
[3)]Tampere University of Technology, Tampere, Finland, risto.ritala@tut.fi
[4)]Viconsys Inc., Jyväskylä, Finland, ilkka.lehtoranta@viconsys.com

ABSTRACT

At present, the cross and machine directional (CD, MD) control of paper machine is based mainly on scanning on-line basis weight measurements. However, the uncertainty in such a basis weight measurement is rather high, in particular at high resolution in CD and MD. During the last few years, paper web inspection systems based on digital imaging consisting of 10-30 cameras imaging the whole paper web in CD and MD have been installed to paper machines. The imaging systems are measuring light transmittance. The quality of images is sufficient so that a 2D light transmittance map can be formed both in large and small scale by appropriate correction for variations in illumination and geometric distortions. There is a useful correlation between the CD profiles of light transmittance and basis weight measurements. Thus web-wide light transmittance measurement can be used for 2D basis weight estimation and advanced basis weight control of paper machine. The paper discusses the relationship between transmittance and basis weight based on CD profile estimates obtained with imaging, scanner measurement, and off-line web analyzer.

INTRODUCTION

Basis weight of paper web is an important property for quality management and control. At present the online web-wide estimate of basis weight is obtained on the basis of scanning measurement with a sensor travelling across the paper web. The online control of basis weight in CD has been based on such a scanning measurement. However, variations faster in MD than the scan time as well as residual variation in paper web are invisible to scanning measurement causing uncertainty to basis weight estimation. Web analyzers can be used to measure basis weight variations off-line, but as being off-line measurement it cannot be used for control. Furthermore web analyzer measurements are rather expensive. During the last few years, camera and illumination technology have become affordable and capable to enable web-wide high-resolution online imaging. The imaging systems at paper machines measure the light transmittance of paper.

In this work the relationship between light transmittance images and paper properties measured with scanner is studied. The paper discusses how the online light transmittance images can be used in analysis of variations in paper properties. A transformation from optical transmittance to true basis weight would be most useful both in formation and large scale. This transformation was studied on the basis of CD profiles.

This paper is organized as follows. In Section 2 the data analyzed in this study is presented. Data is composed of on-line and off-line basis weight and light transmittance measurements of paper, and must be pre-processed before the analyses. Section 2 also discusses the usability of web-wide images. Section 3 introduces how basis weight and light transmittance are related and shows how the CD profiles are computed. Section 3 discuss about the usability of light transmittance based basis weight estimation in real-life application.

THE DATA

The data consists of on-line light transmittance images captured with web inspection system (WIS), on-line measurements from quality control system (QCS) scanner, and off-line measurements from paper web analyzer. The data were measured simultaneously from both measurement systems. The data were aligned based on the time stamps in the data. The reliability of time stamps is not perfect and there might be a few second misalignment of time between the on-line measurements in MD. The misalignment of time between on-line and off-line measurements might be even higher as much as minutes.

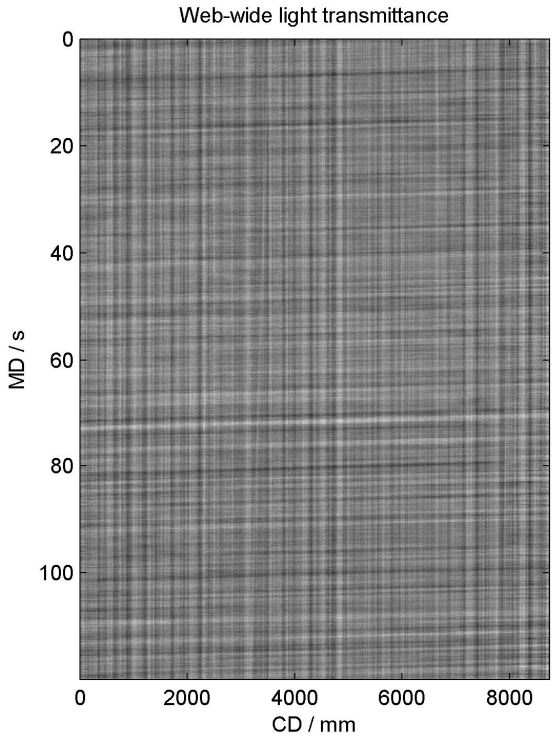

Figure 1. Web-wide light transmittance data. The transmittance was measured for 120 seconds corresponding to 3200 meters of paper.

On-line light transmittance measurement

The web inspection system (manufactured by Viconsys Inc) consists of 18 parallel VGA digital cameras and LED light panels. The imaging fields of the cameras are overlapping, so that the whole paper is captured in CD. The imaging frequency varies depending on the speed of paper web so that the images overlap also in MD.

In our example the paper was imaged continuously for up to for 120 seconds, which corresponds to 3200 meters of paper in MD. The resolution of images was 0.83 mm/pixel in both CD and MD, and the size of the image sensor was 640 x 128 pixel (CD x MD). Thus, the size of the single image was 531 mm x 105 mm. The maximum length of data can be up to 20 seconds in MD.

The WIS is mainly for detecting faults from paper and therefore the each image are not stored. Thus, WIS can store only limited amount of data at full resolution. Therefore, part of the transmittance data was captured with decreased resolution. The information of a single WIS image was averaged in MD providing larger length of data in MD. The result is vector size of 1 x 640 pixels. Now, the resolution of each vector is 0.83 mm (CD) x 105 mm (MD) and the maximum length of data can be up to 120 seconds in MD.

To be able to analyse the paper properties from WIS images the individual WIS images must be pre-processed and stitched together to form 2D web-wide image. First, the variation of illumination was removed. The calibration images were unavailable, so the illumination variation was removed with low-pass filters. This is not an ideal compensation of illumination and thus this method produce distortion especially to larger wavelengths. Overlap between the adjacent and consecutive images was obtained with point-wise cross correlation. The point-wise cross correlations were computed to all possible shifts between the consecutive images. The maximum correlation reveals the amount of the overlap between the images. Finally, the geometric distortions of each camera were obtained based on the overlap area of consecutive cameras. The corresponding points in overlap area determine the projective transform between the images [2],[4]. Figure 1 shows an example of web-wide image.

On-line QCS scanning measurement

Quality control system (QCS) scanner measures the basis weight, moisture, caliber, dry weight, and ash content of paper. The scanner travels across the paper web once every 30 seconds and resolution of such system is 14 mm / sample in CD. The value of the basis weight estimate is held in MD until the new estimate is measured so the resolution varies in MD. The raw data of scanner was inaccessible. The single estimate value in scanner measurement is low-pass filtered in MD by averaging the current and preceding scans. The exact details of filtering were not available. Figure 2 shows an example of web-wide basis weight data measured with QCS scanner.

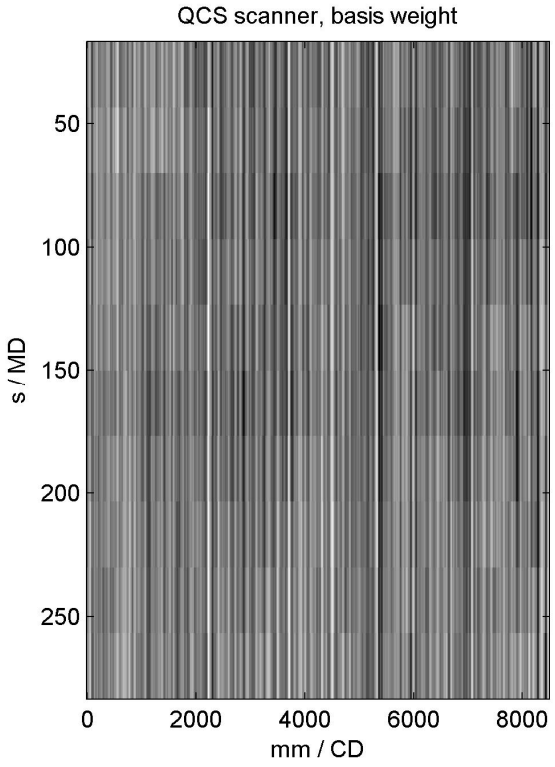

Figure 2. Web-wide basis weight data. The data was measured for 300 seconds corresponding to 8 000 meters of paper. The basis weight data was filtered in QCS by averaging the current and preceding scans.

Off-line paper web analyzer measurements

The properties of paper web were measured off-line with the paper web analyzer. The web analyzer measures basis weight, light transmittance, gloss, and ash content. The CD samples were taken from the top of a machine reel. Single measurement sample covers 30 CD strips. The resolution is 12 mm/sample in CD and the distance between the strips in MD is 11m; meaning the resolution is 11m/sample in MD and the length of the measured sample is 330 meter in MD

Usability of WIS Images

The paper properties are usually measured in paper laboratories from small areas using high resolution. The offline paper analyzer can measure the paper properties from CD strips but the size of the area in MD is usually less than one meter. Several CD strips can be taken and measured in MD but this method is inconvenient and being off-line it cannot be used for control. The online measurement system such as QCS scanner measures the paper continuously in CD and MD. The resolution of such system in CD is sufficient to control the paper machine. However, the resolution in MD is insufficient to detect all consistency variations in headbox. The WIS images provide information never seen before. Figure 3 shows an example of web-wide light transmittance image captured during 10 seconds. The tilted waves which are most likely produced in headbox because of the consistency variations can be seen in web-wide

image. These phenomena are invisible to QCS scanner because of the low MD resolution.

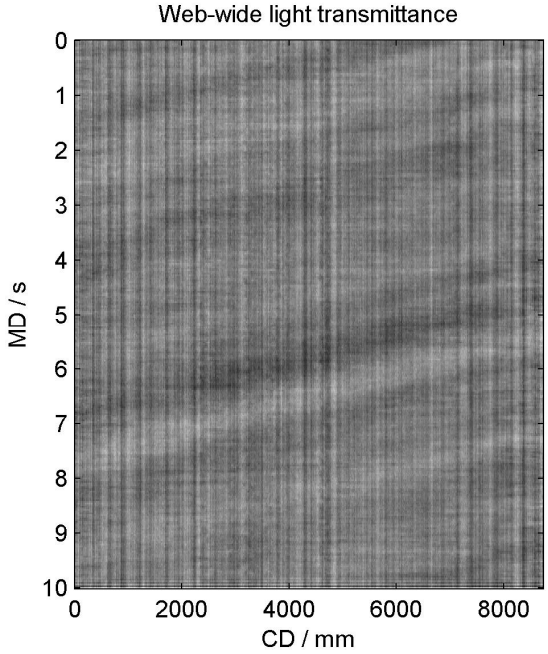

Figure 3. Light transmittance image captured with WIS. Image covers 10 seconds of paper.

The tilted waves can be analyzed with directed sensor array principle [5], which provides a tool to separate the headbox effects from web-wide image. Removal of the tilted waves and the analysis of irregular 2D residual variation are studied in [6]. The article [6] shows that the large scale MD variations that can be seen in WIS images (see fig. 4) are produced mainly from variations seen in tilted directions. Fig. 4 shows also the MD variation where variation of tilted waves is removed. Fig. 4 and [6] indicate that MD variation measured with QCS scanner is heavily averaged and doesn't provide accurate information of MD profile to control the paper machine reliably in smaller scale. The WIS images provide information also to control the paper machine in two dimensions (2D control). In 2D control the CD and MD components are not separated from each other and the control is solely based on the 2D map [7],[8].

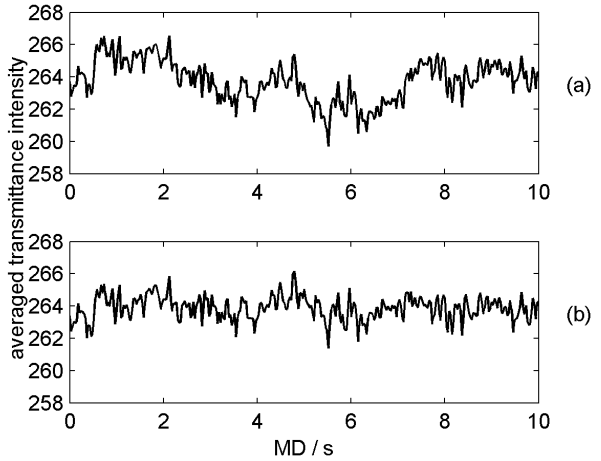

Figure 4. Original MD variation (a) of paper calculated from web-wide transmittance image. MD variation after the effect of tilted waves are removed (b).

THE RELATIONSHIP BETWEEN QCS, WIS, AND OFF-LINE PAPER WEB ANALYZER MEASUREMENTS

The relationship between on-line basis weight (QCS) and on-line transmittance (WIS) is impossible to study in two dimensions. The averaging of QCS scans removes the small scale variation and thus the finding of corresponding points between light transmittance and basis weight data is impossible. Also, the imperfect compensation of illumination variation removes and distorts large wavelengths from transmittance images. Therefore the relationship between QCS measurements, WIS measurements, and off-line paper web analyzer measurements are studied on the basis of CD profiles. Figure 5 shows CD profiles computed from on-line transmittance, on-line basis weight, off-line basis weight, and off-line transmittance measurements.

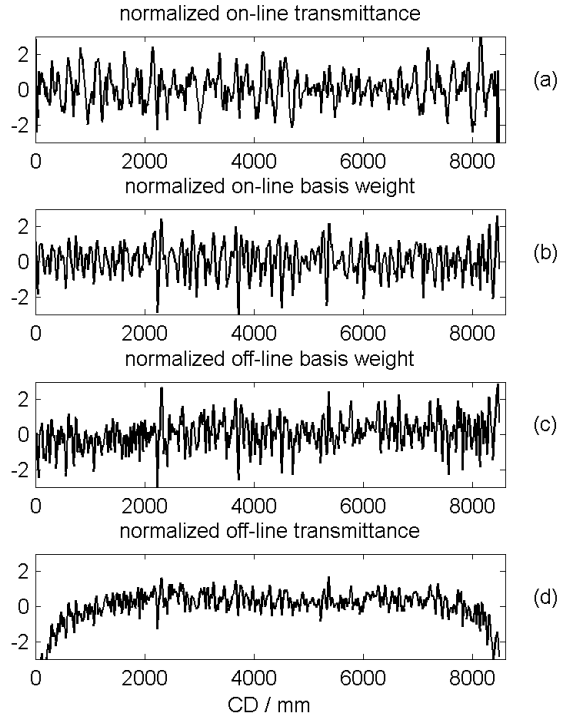

Figure 5. Figure shows an example of CD profiles of on-line light transmittance (a), on-line basis weight (b), off-line basis weight (c), and off-line transmittance (d).

The CD profiles from 2D maps of QCS, WIS, and off-line web analyzer measurements are computed by simple averaging of the measurements in MD. The CD resolution of on-line transmittance profile and off-line measurement profile were resampled to QCS scanner data resolution to be able to analyze the profiles point-wise. The resolution of resampled profiles was 14 mm in CD and the CD profiles were aligned uniformly in CD according to maximized correlation. The mean of the profiles has been removed and the variances scaled to 1 before the analyses. The basis weight and

transmittance profiles correlate negatively so the transmittance profile was multiplied by minus one to get the positive correlation between measurements.

The relationship between the measurements was studied with cross-correlation between the CD profiles. The correlation between on-line transmittance and on-line basis weight was rather low $\rho = 0.27$. The correlation should be higher based on earlier studies [2],[3]. Therefore, the profiles were analyzed in frequency domain to find the frequencies which disturbs the correlation between the CD profiles.

Frequency analysis of CD profiles

The lack of calibration images in WIS produces unwanted errors to the formed web-wide image. Especially, low frequencies may be distorted because of the imperfect removal of illumination variations. The distribution of frequencies in CD profiles is studied to reveal the frequencies which are most reliable in estimation of basis weight from light transmittance images.

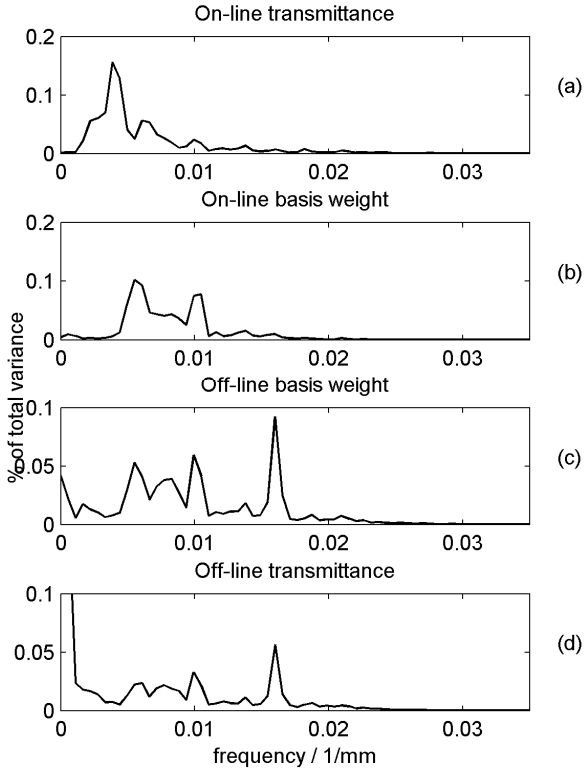

Figure 6. The Welch spectra computed from the light transmittance (a), on-line basis weight (b), off-line basis weight (c), and off-line transmittance.

The spectra of on-line transmittance (a), on-line basis weight (b), off-line basis weight (c), and off-line transmittance (d) are shown in Fig 6. The spectrum of on-line transmittance profile confirms the fact that low frequencies are distorted in pre-processing of images. In the spectrum of on-line transmittance profile the intensity of frequencies between 0.002-0.005 1/mm is higher than in basis weight and off-line transmittance measurements. This could be caused by imperfect forming of the web-wide image.

It can be seen from Fig. 6 that frequencies are not distributed similarly between the measurements. Therefore, the uncertainty in various frequencies between the measurements is studied. The profiles are band-pass filtered and the correlation between the profiles in certain frequencies is computed. The width of the pass-band was 0.004 1/mm in frequency domain. The Butterworth filter was chosen because of the monotonicity in the pass- and stop bands [11]. The pass band was moved continuously from zero frequency to cut-off frequency which is half of the sampling frequency and the moving correlation between the profiles was computed separately in each pass-band frequency.

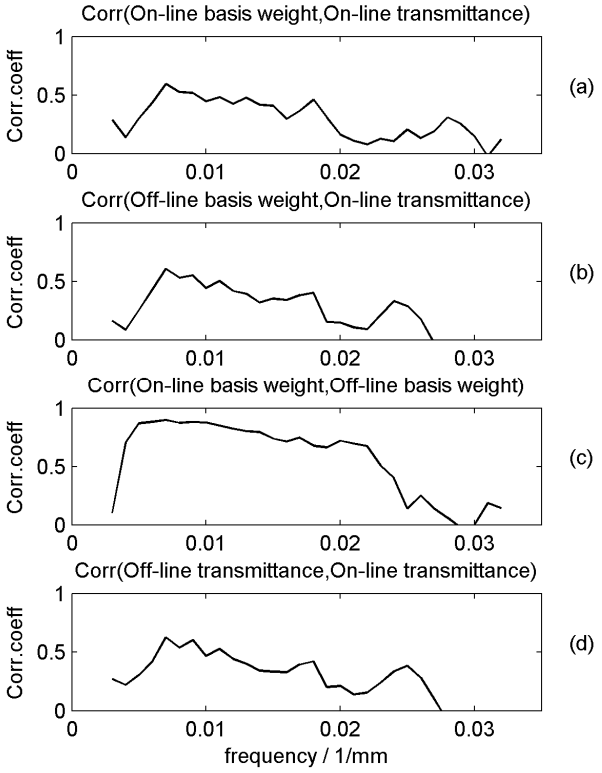

Figure 7. The moving correlation between the on-line basis weight and on-line transmittance (a), between the on-line transmittance and off-line basis weight (b), between the on-line basis weight and off-line basis weight (c), and between the off-line transmittance and on-line transmittance (d)

Fig. 7 (a) shows the magnitude of correlation in each frequency at between the measurement profiles. It can be seen that in low frequencies (= lower than 0.007 1/ mm, wavelength higher than 170 mm) the correlations is low in (a), (b), and (d). This was assumed previously to be caused by the imperfect removal of illumination variation. However, it does not explain the low correlation between on-line and off-line basis weight profiles (c) in low frequencies. It seems that there are phenomena in the paper that only the off-line measurement can detect. It is also notable that

correlation between the on-line transmittance and other profiles is low between the frequencies 0.018 1/mm and 0.024 1/mm which could be also caused by imperfect pre-processing of images.

To remove the effect of inadequate pre-processing of WIS images from large and small wavelengths the certain frequencies are removed from profiles with band-pass filter. Such action removes the low frequencies completely so the results must be interpreted carefully if such information is used in control of paper machine. The frequency limits for band-pass filter were adjusted to 0.007 1/mm and 0.018 1/mm corresponding to wavelengths between 58 mm and 143 mm. The band-pass limits were chosen based on the correlation curve in Fig. 7 and also the spectra of profiles in Fig. 7. Figure 8 shows example of band-pass filtered and non-filtered profiles captured from 1600 mm – 3200mm in CD.

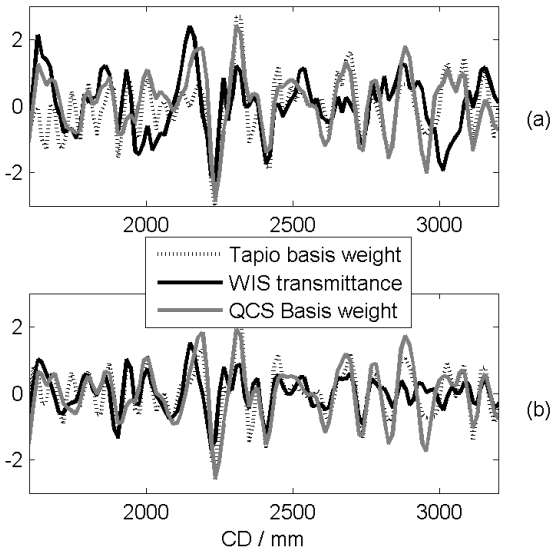

Figure 8. Non-filtered (a) and filtered profiles (b). In filtered profiles the wavelengths larger than 143 mm and smaller than 58 mm are filtered out.

Next, the improvement of estimation after filtering is analyzed.

Correlation analysis between on-line transmittance, on-line QCS scanner and off-line measurements

It was assumed in the previous chapter that low frequencies are distorted because of the inadequate compensation of illumination variation and therefore the profiles were band-pass filtered. The correlations between the filtered CD profiles are presented in table 1. It can be seen that the correlation between the off-line basis weight and on-line transmittance is still rather low ($\rho = 0.48$) although the profiles are filtered. The reason for that is discussed next.

The high correlation between off-line basis weight and the off-line transmittance ($\rho = 0.94$) reveals that ash content variation does not significantly disturb the relationship between the two paper properties. The last portion which cannot be explained occurs mostly because of the different behaviour of light and beta radiation in paper. The correlation between the off-line and on-line basis weight is $\rho = 0.81$. The reduced correlation is partly due to moisture, partly due to that time alignment is not accurate and the CD profiles are not stable such it was assumed, and partly due to deficiencies and differences in the two measurement systems.

Table 1. The covariance matrix for filtered CD profiles

	On-line transmittance	On-line basis weight	Off-line basis weigh	Off-line transmittance
On-line transmittance	1.00	0.51	0.48	0.49
On-line basis weight		1.00	0.81	0.76
Off-line basis weight			1.00	0.94
Off-line transmittance				1.00

It is impossible to determine the exact relative contributions of these three factors. However, the on-line moisture correlates significantly ($\rho = 0.88$) with the on-line basis weight and it can be assumed that the moisture effect is not the dominating one. The stability of basis weight profile as a function of time is studied with autocorrelation function (see Fig. 9). Autocorrelation is obtained by correlating the first QCS scan to preceding scans. It can be seen that the basis weight profile is not stable. The magnitude of correlation drops rapidly to values $\rho = 0.80 \ldots 0.85$ which is about as high as the correlation between the on-line and off-line basis weight profiles ($\rho = 0.81$). The autocorrelation function also shows that if the alignment between off-line and on-line data is not accurate the correlation $\rho = 0.80 \ldots 0.85$ is the best that can be achieved. Based on the results it can be assumed that the misalignment of CD profiles in MD and instability of basis weight profile are the main factors that decrease the correlation most between the off-line and on-line basis weight profiles.

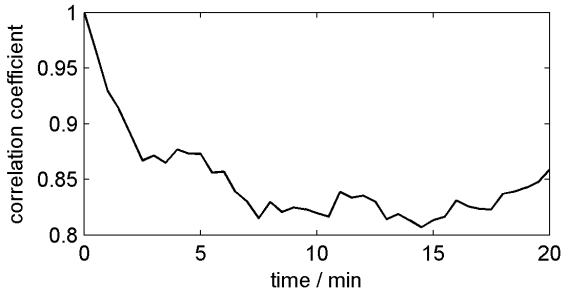

Figure 9. The autocorrelation function of preceding QCS scans.

The correlation between on-line basis weight profile and off-line transmittance profiles is $\rho = 0.76$. The drop from correlation ($\rho = 0.81$) is due to the differences between measurements. It can be said conversely that ρ

= 0.76 is the best correlation between the on-line transmittance and off-line basis weight profiles in these data. However, the correlation between on-line transmittance profile and the off-line basis weight profile is lower than it was expected (ρ = 0.48). The correlation between on-line basis weight and on-line transmittance was slightly higher (ρ = 0.51). The inaccuracy in time alignment was higher between the off-line and on-line measurements which may explain the higher correlation value between the on-line measurements. The small increase reveals that misalignment of time does not decrease the correlation significantly.

It was assumed previously that imperfect compensation of illumination variation affects mainly low frequencies. Therefore, the profiles were band-pass filtered. Evidently, the compensation of illumination variation produces distortion in all frequencies of the transmittance profile not the low frequencies alone. This assumption was studied by identifying a linear model where both the on-line and off-line basis weight profiles were explained by on-line transmittance profile. The prediction errors of the two models were calculated and the correlation between the model errors was computed. The correlation was high (ρ = 0.75) showing that there are common features in the two basis weight variations that the on-line transmittance is not capable of explaining. This result and also the high correlation between off-line transmittance and basis weight profiles (ρ = 0.94) confirm the assumption that the compensation of illumination variation produces distortion in all frequencies but with lower frequencies distorted more.

The existence of calibration images would improve the pre-processing of WIS images and thus the correlation between on-line transmittance and other measurements would increase significantly. Therefore, the importance of calibration images is emphasized in future studies and measurements.

CONCLUSION

At present the paper machine is controlled based on the basis weight measured with QCS scanner. However, the variations faster in MD than scan time are invisible to such a measurement causing uncertainty to basis weight estimation. For example, the tilted waves which produce mainly the MD variation are invisible to QCS system because of the low speed of scanning. Web inspection systems measure the web-wide light transmittance in purpose to find the imperfections from paper. The resolution of such system is more accurate than QCS scanner and tilted waves can be detected and analyzed.

In this work the relationship between the basis weight and light transmittance was studied. The relationship was studied on the basis of CD profiles because the averaging of CD scans was removing the small scale variation from 2D basis weight map. The correlation between on-line transmittance and on-line basis weight was poor (ρ = 0.27). Therefore, the profiles were analyzed in frequency space. The frequency analysis revealed that low and part of high frequencies are somewhat distorted in pre-processing of WIS images most probably in compensation of illumination variations. Therefore, the profiles were band-pass filtered to remove the effect of imperfect preprocessing. The correlation of band-pass filtered CD profiles between on-line basis weight and on-line transmittance was higher (ρ = 0.51). However, the correlation between off-line transmittance and on-line basis weight was ρ = 0.76 which can be assumed to be the highest possible correlation between on-line transmittance and off-line basis weight. The gap between the correlation values ρ = 0.51 and ρ = 0.76 is probably caused by inadequate compensation of illumination variation.

The lack of calibration images means that the calibration was done with mathematic methods such as low-pass filters. Such calibration is not sufficient and the importance of calibration images is emphasized in future studies. However, it was noticed based on the current data that in smaller wavelengths the correspondence between the basis weight and transmittance CD profiles was rather good. Thus, 2D web-wide transmittance map can be used in 2D control of paper machines. However, the results must be interpreted carefully because of the large disturbance in large wavelengths.

REFERENCES

[1] Sara, H., " The characterization and measurement of paper formation with standard deviation and power spectrum", dissertation, Helsinki University of Technology, Helsinki, Finland, 1978.

[2] Raunio, J.-P., and Ritala, R., "Estimation of basis weight of paper: light transmittance measurements over eight orders of magnitude of spatial scale", proceedings from the 2009 XIX IMEKO World Congress, Lisbon, Portugal, 2009

[3] Raunio, J.-P. and Ritala, R., "Analysis of Paper Structure Based on Light Transmittance and Basis Weight Measurements, proceedings from the 2009 Papermaking Research Symposium, Kuopio, Finland, 2009

[4] Sonka, M., Hlavac, V., Boyle, R., *Image processing, analysis, and machine vision*, PWS, California, 1998

[5] Naidu, P. S., "Sensor Array Signal Processing", CRC Press, USA, 2001

[6] Ylisaari, J., Ritala, R., "Web-wide transmittance imaging measurement variability analysis", will be presented in Control systems 2010, Stockholm, 2010

[7] Wellstead P. E., Heath W. P., "Two-dimensional control systems: application to the CD and MD control problem", *Pulp & Paper Canada*, Vol.95(2), p. 48-51, 1994

[8] Duncan S. R., "Two-dimensional control systems: Learning from implementations", *Journal of Electronic Imaging*, Vol.10(3), p. 661-668, 2001.

[9] Hayes, M., "Statistical Digital Signal Processing and Modeling", John Wiley & Sons, USA, 1996.

Publication IV

Raunio, J.-P. and Ritala, R. (2012): Simulation of creping pattern in tissue paper, *Nordic Pulp and Pap. Res. J.*, Vol. 27, No. 2, pp. 375-381.

Publication V

Raunio J.-P., Tirronen, V., Lehtoranta, I. and Ritala, R. (2013): Web-wide imaging of paper; Analyzing the potential of on-line light transmittance measurement in quality control and diagnostics of paper, *Nordic Pulp and Pap. Res. J.*, Vol. 28, No. 1, pp. 137-146.

Publication VI

Raunio, J.-P. and Ritala, R. (2013): Potential of full-web imaging in measuring web structure on-line, *J-For*, Vol. 3, No. 1, pp. 10-16.

POTENTIAL OF FULL-WEB IMAGING IN MEASURING WEB STRUCTURE ON-LINE

JUKKA-PEKKA RAUNIO, RISTO RITALA*

ABSTRACT

This paper presents on-line analysis methods to estimate the microscopic structure of paper. The structural characteristics are estimated from web inspection system (WIS) images. A WIS is primarily designed for detecting paper defects, and therefore the images need to be pre-processed to obtain structural measurements. The macroscopic 2D maps constructed from the microscopic estimates computed from WIS images reveal phenomena in the paper-making process which cannot be observed with present on-line measurement systems. The results of this study indicate that characteristics estimated using WIS images give useful information for improving the uniformity and control of paper quality on paper machines.

INTRODUCTION

There is structural variability in paper from sub-millimetre scale (fibres, fillers) to scales of tens of kilometres in the running direction of the paper machine (machine direction, MD). The variability from sub-millimetre scale to roughly ten centimetres is called microscopic variation in this paper. At microscopic scale, the magnitude of paper formation variations, the length scale of formation variations, the anisotropy of fibre orientations, and the dominant orientation of fibres are normally the properties of interest. The larger macroscopic variations are typically divided into three components: MD variation, variation in the cross-direction of the paper machine (CD), and residual variation [1]. Residual variation has zero mean in both the CD and MD directions. At macroscopic scale, for example, the CD and MD basis weight profiles and the CD shrinkage profile of paper are the properties of practical interest for paper machine control.

At macroscopic scale, optimal control of the paper machine requires various quality measurements from the paper sheet. At present, paper properties can be measured using the on-line scanner which forms part of the quality control system (QCS) and which travels over the running paper web in typically 30 seconds [1], [2]. However, the uncertainty of quality estimates based on such a measurement is large due to the poor representativeness of the points actually measured. Furthermore, the travel time of the furnish flow inside the headbox manifold from one edge of the headbox to the other is only approximately 2–3 seconds. Therefore, any consistency variation in the furnish flow creates a quality variation as waves diagonal to the machine direction. The scanners cannot observe these variations. Diagonal waves can be observed through off-line measurements, but these measurements are slow, and the detection of irregular basis-weight variations comes too late from a control—and often from a diagnostic—perspective.

At microscopic scale, the paper is studied mainly using off-line measurements, which mean that the results cannot be used for paper machine control. Microscopic structure estimation for diagnostics and control requires a fast web-wide high-resolution measurement device, for which imaging is a high-potential technology. Therefore, the usability of 2D images has been widely studied based on off-line studies during the last decade. Imaging technology is being used in the analysis of formation [3], paper roughness [4], fibre orientation [5], and CD web shrinkage [6], [7]. Furthermore, measurement devices which estimate the orientation of fibres and the anisotropy of paper fibre orientation on-line have been studied and

RISTO RITALA
Tampere University of Technology, Tampere, Finland

JUKKA-PEKKA RAUNIO
Tampere University of Technology, Tampere, Finland
*Contact: jukka-pekka.raunio@tut.fi

patented [8]. However, such on-line measurement systems do not cover the entire web width and therefore suffer from the same problems as the QCS scanner.

On-line web-wide imaging has been widely studied over the past two decades [9], [10]. During the last few years, the performance of cameras and illumination sources has reached a level which enables on-line web-wide high-resolution imaging of paper at a reasonable price. The technology is in use in web inspection systems (WIS), which detect and classify defects such as holes and dirt particles in the paper web. WIS on paper machines have light-emitting diode (LED) panels for illumination and digital cameras to measure the light transmittance of paper. The potential of WIS for characterizing the macroscopic variability of paper basis weight and CD shrinkage profiles was earlier assessed by the authors in [11], [12].

This paper presents characterization methods for microscopic variability of paper computed from the WIS image. Light transmittance describes basis weight rather well in a newsprint grade studied in this work [11], [13]. Paper formation is defined as small-scale variability in basis weight and is commonly summarized by its length scale and magnitude [14]. Even paper has a small magnitude of formation. A small length scale of variation means grainy paper (the opposite being cloudy paper). The in-plane orientation distribution of a fibre network is characterized by the anisotropy of fibre orientation and the dominant fibre orientation direction, i.e., the direction of highest probability. The microscopic fibre orientation direction, i.e., the direction of highest probability. The microscopic characteristics of paper structure are estimated either directly from WIS images or through its 2D Fourier power spectrum. Furthermore, this paper analyzes the macroscopic 2D maps constructed from the microscopic estimates. The 2D maps are divided into CD, MD, and residual variations using variance component analysis (VCA). The sensor array principle is used to separate the diagonally oriented variability from other variability.

This paper is organized as follows. Chapter 2 presents the high-resolution image data studied in this work and its pre-processing. Chapter 3 introduces the microscopic and macroscopic characterization methods used. Chapter 4 presents the macroscopic 2D maps of paper characteristics and describes the use of VCA to divide the variability according to its potential origin. Chapter 4 also reports the correlations between the 2D maps, between the strictly MD profiles, and between the diagonal profiles. Chapter 5 summarizes conclusions and discusses the future possibilities of web-wide imaging.

THE WIS IMAGES

The paper grade studied in this work was newsprint which was manufactured at the speed of 25 m/s with a width of 8.5 m. The entire width of the web was imaged with a WIS installed permanently on the paper machine. The system consisted of 18 parallel video graphics array (VGA) standard cameras with 640x128 (CDxMD) pixels and LED panels. The imaging areas of adjacent cameras and the areas of consecutive images of a single camera over time overlapped, so that the entire web was captured in CD and MD. Image resolution was 0.81 mm/pixel in both CD and MD. The pixel values were represented by eight bits each, meaning that the data rate was 608 Mbytes/s. The length of the imaging period available for this work was 10 seconds in MD, corresponding to 240 metres of paper web. The image data consisted of 59400 images in a matrix of 18 images in CD and 3300 images in MD. Individual images were 80 mm (0.003s) in MD and 500 mm in CD.

Pre-processing for microscopic properties

The quality of the images as acquired was not sufficient for analysis of microscopic paper properties (see Fig. 1, top). Uneven illumination caused variation in local intensity and in the local intensity variance. These variations must be removed before paper properties can be estimated.

Each image is acquired through an optical system consisting of a LED panel, paper, and camera. This system causes geometric and intensity distortion. Furthermore, the camera distortion and LED panel intensity vary camera-to-camera and LED-to-LED. The geometric and inten-

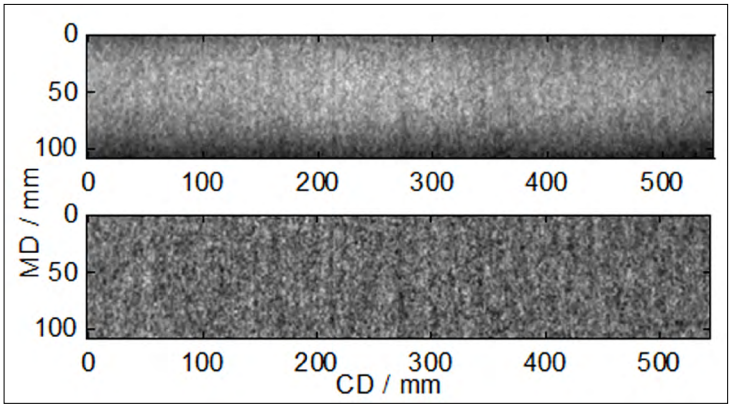

Fig. 1 - VGA image captured with WIS (top) and the image divided by an average image (bottom).

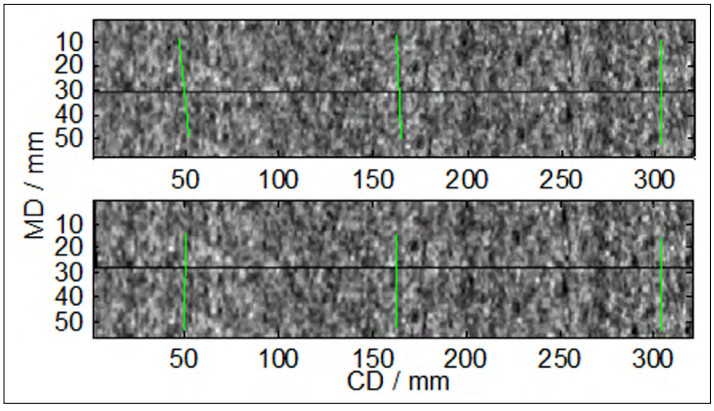

Fig. 2 - Effect of perspective transformation. Overlapping areas of consecutive images before (top) and after (bottom) projective transformation. The green lines illustrate the geometric distortion.

sity distortions can be modelled and compensated for reliably using a reference image (see, for example, [15]). However, no such reference image was available for this work. Therefore, models of intensity and geometric distortions were estimated directly from the image data. It was assumed that the unevenness of illumination was constant at the time scale of the data and that the paper web transmittance was the only cause of temporal variations in detected light intensity. The static texture due to illumination effects and CD transmittance profile can be determined simply by computing the MD average image of the N=3300 images for each camera located in the WIS. Each original image was divided pixel-by-pixel by the average image to enhance dynamic phenomena (see Fig. 1, bottom). This action was applied for data from each camera separately.

Camera orientation causes perspective distortion to images. It was assumed that the camera orientation did not change during the imaging period. Therefore, the perspective projection can be determined by studying the overlap areas of the images. Consecutive images in MD overlapped by 20%. This is sufficient to estimate the perspective distortion of the cameras reliably. The perspective distortion can be corrected by planar projective transformation [16]. The top part of Fig. 2 shows an example of an image pair for which overlapping areas are stitched together from consecutive uncorrected images, and the bottom part of Fig. 2 shows the perspective-corrected images.

The simplest approximation for paper structure is a randomly distributed two-dimensional network of fibres. The basis weight of fibres is normally 5–10 g/m^2, which means that typical newsprint has 10–20 layers of fibres. The resolution of WIS light-transmittance images is insufficient to detect individual fibres, but the light-transmittance pixel value gives an average estimate of the number of fibre layers in a certain unit area. The discrete number of fibre layers in the thickness direction of paper is Poisson distributed [17]. The mean and variance of the Poisson distribution are correlated, and the standard deviation of the Poisson distribution is proportional to the square root of the expected value of Poisson-distributed data [18]. The correlation between these two statistical properties can be removed from images using the square-root function [18], and therefore the correlation computed between the light transmittance and the variance does not contain the relation arising from the properties of the Poisson distribution.

Pre-processing for macroscopic properties

Pre-processing of WIS images compensates for the illumination and removes the geometric distortion at microscopic scale. However, the focus differences between the cameras have a significant impact on the variance of transmittance, as can be seen in Fig. 3 (top), which shows the macroscopic map of the magnitude of formation variation (standard deviation of pixels). The microscopic paper structure characteristics estimated from the standard deviation of pixels and from the power spectrum may be affected by the focus of the camera. Therefore the camera-to-camera CD profiles were removed from these 2D macroscopic maps before analysis. Fig. 3 (bottom) shows the magnitude of formation map from which the camera-to-camera CD profile has been removed.

CHARACTERIZATION OF PAPER STRUCTURE

This chapter presents the methods used to characterize structural variability in paper based on WIS images. The estimation methods for light transmittance, magnitude of formation, length scale of formation, anisotropy of fibre orientations, and dominant fibre orientation are described.

Characterization methods for microscopic variability

The pixel size of the WIS images (0.8 mm) is not sufficient to detect small-scale constituents such as individual fibres. Therefore, the microscopic characteristics describe the behavior of fibre-network elements with diameters larger than 0.8

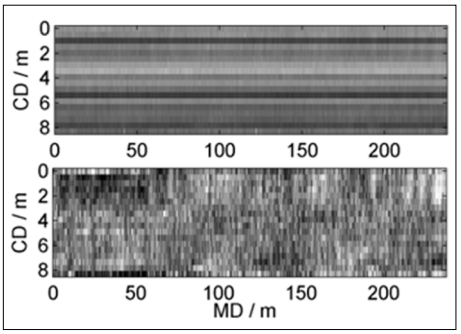

Fig. 3 - Original 2D macroscopic magnitude of formation map (top) and the map from which the camera-to-camera CD profile has been removed (bottom). The resolution of the map is 18x3300 (CD x MD).

mm. The intensity of light transmittance for each image is computed by averaging the pixel values of a pre-processed image:

$$\mu_{m,n} = \frac{1}{N_{cd} N_{md}} \sum_{i=1}^{N_{cd}} \sum_{j=1}^{N_{md}} x_{m,n;i,j} \,, \quad (1)$$

where N_{cd} and N_{md} are the number of pixels in the CD and MD, i and j describe the location of pixels in a single image, and m and n describe respectively the CD and MD location of the image in the 2D matrix. The average pixel value represents the average light transmittance in the image. The magnitude of formation for each image is estimated by computing the standard deviation of pixel values from a pre-processed image as follows:

$$\sigma_{m,n} = \sqrt{\frac{1}{N_{cd} N_{md}} \sum_{i=1}^{N_{cd}} \sum_{j=1}^{N_{md}} (x_{m,n;i,j} - \mu_{m,n})^2} \,, \quad (2)$$

where $\mu_{m,n}$ is the average intensity of light transmittance determined in Eq. (1).

The length scale of formation, anisotropy of fibre orientation, and dominant fibre orientation can be estimated from the power spectrum of a light-transmittance image. A two-dimensional Fourier transform converts the spatial image into frequency space. The Fourier transform of $f(\mathbf{x})$, denoted as $F(\mathbf{k})$, describes the amplitude, orientation, and phase by sinusoidal terms, so that summing the sinusoids reproduces $f(\mathbf{x})$. Let $\mathbf{x}$ be the point (x_{CD}, y_{MD}) in 2D spatial space, and let $\mathbf{k}$ be the point (k_{CD}, k_{MD}) in 2D frequency space.

Then

$$F(\mathbf{k}) = \int_{\Re^2} f(\mathbf{x}) \exp(-i2\pi(\mathbf{x}\cdot\mathbf{k}))d\mathbf{x}. \quad (3)$$

The power spectrum, which is the squared amplitude of each sinusoidal term, is

$$S(\mathbf{k}) = |F(\mathbf{k})|^2. \quad (4)$$

The power spectrum computed from a single sample image retains a significant amount of noise, and the estimates derived from it are therefore uncertain. To reduce this uncertainty, the 2D Welch power spectrum estimate was computed by averaging 30 consecutive power spectra in MD and by taking their average as the spectrum estimate [19]. Before computing the power spectrum, each image was Hamming windowed [20]. This decreases the image edge effects that produce spectral side lobes in finite-sample Fourier transforms. Figure 4 shows an example of a 2D Welch power spectrum.

There are small higher-intensity areas in the power spectrum on the left of Fig. 4. These spectral peaks are due to periodic transmittance variations in paper, which may be caused by structures in felts, wires, or rolls on the paper machine. When the characteristics of paper are analyzed, these peaks must be removed from the power spectrum because they are not properties of the forming process, but rather of dewatering and drying processing elements. The locations of the peaks in the power spectrum can be determined as follows. First, the power spectrum is 2D median filtered [16]. Then the point-wise ratio of the initial spectrum to the median-filtered spectrum is computed. In this ratio, the peak intensities are exaggerated so that their areas can be identified by thresholding. The exact peak locations are estimated by fitting a second-order 2D polynomial to each identified peak area in the original spectrum and detecting the location of the maximum of the polynomial. Finally, the spectrum value at each peak area is replaced by the value of the spectrum in its neighborhood. The power spectrum with peaks removed is presented on the right in Fig. 4.

The 2D power spectrum is computed in the Cartesian coordinate system. However, estimation of some paper characteristics is easier in the polar coordinate system, where (k_{CD}, k_{MD}) of elements are represented as pairs of angle ϕ and distance k from the origin. ϕ describes the angular displacement [-90…+90] compared to the MD. Figure 5 shows the power spectrum shown in Fig. 4 (right) transformed into the polar coordinate system.

It can be seen that a significant amount of the variation is oriented in the MD (meaning that the paper is anisotropic). The length scale of formation is estimated from the probability function of frequency. The probability function is computed by summing the power spectrum values in the polar coordinate system over angle direction and dividing the resulting vector by the sum of power spectrum values as follows:

$$p(k) = \frac{\sum_{\phi} S_{Polar}(\phi, k)}{\sum_{k,\phi} S_{Polar}(\phi, k)}, \quad (5)$$

where $S_{Polar}(\phi,k)$ is the power spectrum in the polar coordinate system. The average wavelength, which describes the length scale of the formation characteristics, is computed as the inverse of the expected value of the probability function of frequency $p(k)$ determined as follows:

$$E[\lambda]_{m,n} = E[k]^{-1}_{m,n} = \frac{1}{\sum_{k} p(k)k}. \quad (6)$$

The anisotropy of fibre orientation is determined as the ratio of average wavelengths in CD and MD. A value of 1 corresponds to paper which is isotropic and a value of 0 to anisotropic paper where all the flocs are oriented in the MD. The average wavelengths are estimated from the CD and MD spectra. The CD and MD spectra are computed by summing the values of a 2D spectrum over the MD and CD respectively:

$$S(k_{MD}) = \sum_{k_{CD}} S(k_{CD}, k_{MD}), \quad S(k_{CD}) = \sum_{k_{MD}} S(k_{CD}, k_{MD}) \quad (7)$$

The average wavelength is the inverse of the expected value of the probability distribution. Therefore, the anisotropy of fibre orientation is

$$\frac{E[\lambda_{CD}]_{m,n}}{E[\lambda_{MD}]_{m,n}} = \frac{E[k_{CD}]^{-1}_{m,n}}{E[k_{MD}]^{-1}_{m,n}} = \frac{(\sum_{k_{CD}} S(k_{CD})k_{CD})^{-1}}{(\sum_{k_{MD}} S(k_{MD})k_{MD})^{-1}}. \quad (8)$$

The dominant fibre orientation can be estimated from the angle probability function. This probability function can be computed by summing the power spectrum values in the polar coordinate system over the frequency direction and dividing

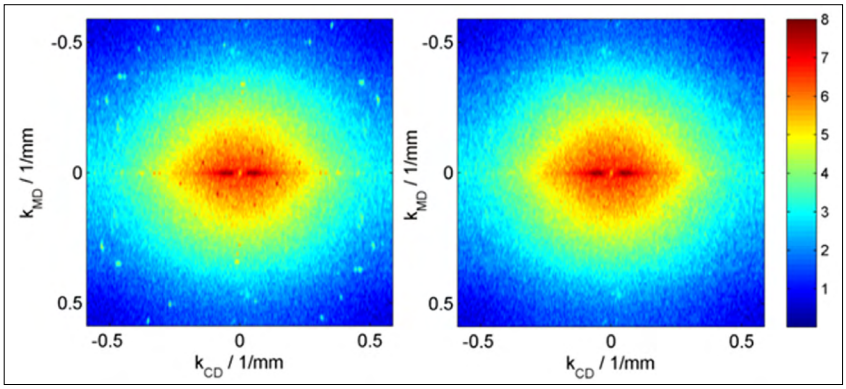

Fig. 4 - Averaged power spectrum computed over 30 power spectra on the left. The power spectrum with spectral peaks removed on the right.

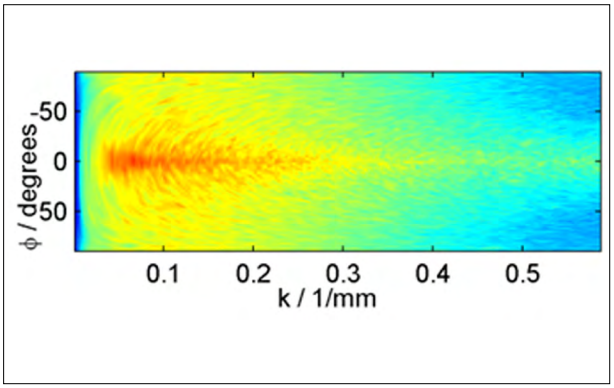

Fig. 5 - Power spectrum transformed to polar coordinate system.

the resulting vector by the sum of the power spectrum values:

$$p(\phi) = \frac{\sum_{k} S_{Polar}(\phi, k)}{\sum_{k,\phi} S_{Polar}(\phi, k)}. \quad (9)$$

The dominant fibre orientation is determined as in [21]:

$$\theta_{m,n} = \arg\left(\sum_{\phi=0}^{2\pi} \exp(i\phi) p(\phi)\right) = \arg\left(\sum_{\phi=0}^{2\pi} \cos(\phi) p(\phi) + i \sum_{\phi=0}^{2\pi} \sin(\phi) p(\phi)\right). \quad (10)$$

Characterization methods for macroscopic variability

The two-dimensional variation of paper (e.g., light transmittance = *I*) can be separated into machine-directional, cross-directional, and residual components as follows:

$$I_{m,n} = I_n^{(MD)} + I_m^{(CD)} + I_{m,n}^{(RES)}, \quad (11)$$

where $Im^{(CD)}$ is zero because the CD profile was removed from the 2D map to suppress the effects of nonuniform illumination profile. The variability can further be characterized by the variances of the three components under the assumption that residual variation is statistically independent of machine-directional variations:

$$\sigma_{tot}^2 = \sigma_{CD}^2 + \sigma_{MD}^2 + \sigma_{res}^2. \quad (12)$$

This separation of variances into components is called variance component analysis (VCA) [22]. The consistency variation in the headbox inflow forms diagonal waves which are part of the residual variation. Therefore, VCA was applied to the original 2D maps and to 2D maps from which the 2D map variation from various angles had been removed. Using this approach, variation distributed in various orientations can be studied. The removal of variance was based on the directed sensor array principle [23], in which the delay of a wave between adjacent cameras and the angle of the wave are related through trigonometry as:

$$\tau = \frac{d}{c}\sin(\theta), \quad (13)$$

where **T** is the delay in seconds, d is the distance between adjacent cameras, c is the speed of the paper web, and θ is the angle of the diagonal wave. Figure 6 (top) shows the 2D light-transmittance map computed from the pre-processed WIS images, and Fig. 6 (bottom) shows the same map after the diagonal waves have been removed.

TABLE 1 *CD, MD, and residual variations computed using VCA. Variances from the original 2D maps and from 2D maps from which the variations oriented at the angle of the diagonal waves have been removed (wr) are shown. μ is light transmittance, σ is magnitude of formation, E[λ] is length scale of formation, $E[\lambda_{CD}]/E[\lambda_{MD}]$ is anisotropy of fibre orientation, and θ is dominant fibre orientation.*

	CD (% of total)	MD (% of total)	Res. (% of total)	Tot. var(σ^2)
μ	-0.02	80.12	0.000231	
μ (wr)	0.20	15.43	75.62	0.000061
σ	0.06	19.96	87.49	0.001344
σ (wr)	0.16	7.56	86.95	0.001231
E[λ]	0.21	8.03	76.50	0.001786
E[λ] (wr)	0.30	19.02	82.07	0.001509
$E[\lambda_{CD}]/E[\lambda_{MD}]$	0.66	13.05	56.56	0.000029
$E[\lambda_{CD}]/E[\lambda_{MD}]$(wr)	2.73	39.62	78.93	0.000018
θ	0.11	13.93	88.20	0.230820
θ (wr)	0.29	6.76	90.23	0.196934

RESULTS

Figure 7 shows macroscopic 2D maps of light transmittance, magnitude of formation, length scale of formation, anisotropy of fibre orientation and dominant fibre orientation. The zero angle in Fig. 7(e) means that the features are oriented strictly in the MD. A positive angle means a counter-clockwise rotation.

The diagonal waves, which are obvious in the light-transmittance map in Fig. 7(a), can also be seen in the maps of dominant fibre orientation angle (e), anisotropy of fibre orientation (d), and length scale of formation (c), although the relative magnitude is much smaller.

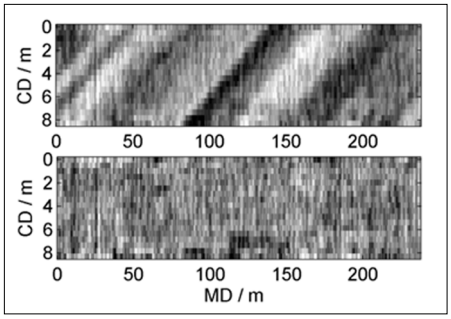

Fig. 6 - Macroscopic light-transmittance map (top) and light-transmittance map from which the variation of diagonal waves has been removed (bottom).

Variance component analysis of 2D paper characteristic maps

Table 1 shows the variances of the 2D maps separated into CD, MD, and residual variances. Furthermore, the table shows the variances of 2D maps from which the variation oriented at the angle of the diagonal waves (see Fig. 7(a)) has been removed.

The CD variances are insignificant because the CD profiles were removed from the 2D maps. The proportion of

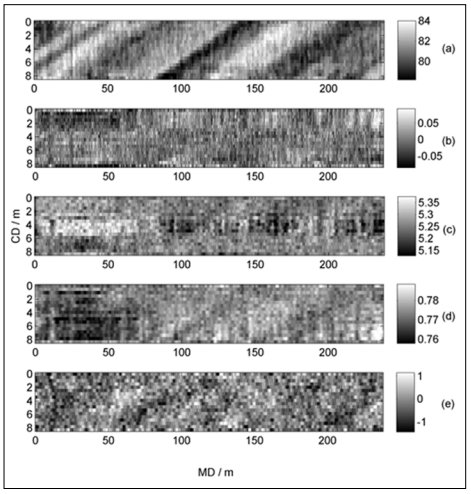

Fig. 7 - 2D macroscopic maps estimated based on the methods presented above: light transmittance (a), magnitude of formation (b), length scale of formation (c), anisotropy of fibre orientation (d), and dominant fibre orientation (e). Gray-level values represent the pixel values (a), standard deviation of pixel values (b), mm (c), anisotropy (d), and degrees (e).

MD variation is higher than 15% for light transmittance, length scale of formation, and anisotropy of fibre orientation, whereas for other characteristics, the residual variation overwhelmingly dominates. The reduction in total variance after diagonal wave removal shows the proportion of variance oriented in the direction of the diagonal waves. For light transmittance, the diagonal waves constituted almost three-quarters of the total variance, whereas for other characteristics, their effect was less than 30%. Figure 8 presents the variances (%) with varying delays (see Eq. 13) between the front and the back end of the wave in the MD. Zero corresponds to a strictly machine-directional variation.

It can be seen from Fig. 8(a) that in the distribution of variance of light transmittance, the local maximum occurs at a delay of 2.2 s, which is well in accordance with the travel time of a pulp consistency variation from the back to the front of the headbox. The diagonal waves in the anisotropy of fibre orientation and in the dominant orientation indicate a relation to consistency variation before the headbox. However, anisotropy variation oriented strictly in the MD is also high, which is consistent with the fact that the main reason for fibre orientation anisotropy is the MD speed difference between the wire and the jet and the turbulence in the jet [24], [14]. This turbulence prevents flocculation in the headbox, which leads to low magnitude of formation and small length scale of formation [14].The variation of length scale of formation is oriented more in the MD than at a diagonal angle, which indicates that such variation visible in 2D maps is formed in or after the headbox. The variation in magnitude of formation does not show any clear MD or diagonal phenomena because more than 90% of the variance is residual variation.

Correlation coefficients between the MD profiles

The MD profiles from 2D macroscopic maps were computed by averaging the 2D maps over the CD. Table 2 shows the correlation coefficients between the 1D MD profiles computed from the 2D maps and Table 3 the correlation coefficients between the profiles oriented at the same angle as the diagonal waves (see Fig. 7(a)).

The correlation coefficients in both tables are rather small, which indicates that although the cause of the variation is the same (e.g., the consistency variation), the influence on estimated paper characteristics is independent. However, it can be seen that anisotropy of fibre orientation and length scale of formation correlate significantly between the MD profiles (-0.74) and that this correlation is smaller (-0.5) in Table 3. This observation, together with the results of VCA, leads one to assume that the main reason for variation of these two properties is the same and is oriented in the MD. Furthermore, the negative correlation indicates that larger length scale of formation means smaller anisotropy.

CONCLUSIONS

This paper has studied the potential of a web-inspection system for evaluating the microscopic structural characteristics of paper. The structural characteristics were estimated from WIS images. The WIS is primarily designed for detecting paper defects, and therefore the images were pre-processed before structural analysis. It was observed that the macroscopic 2D maps constructed from the microscopic estimates computed from WIS images revealed diagonal variation in the papermaking process which cannot be observed by present on-line measurement systems.

The directed sensor array principle was used to study the possible causes of diagonal variation. It was observed that the delay between the front and the back end of the diagonal variation in MD was in

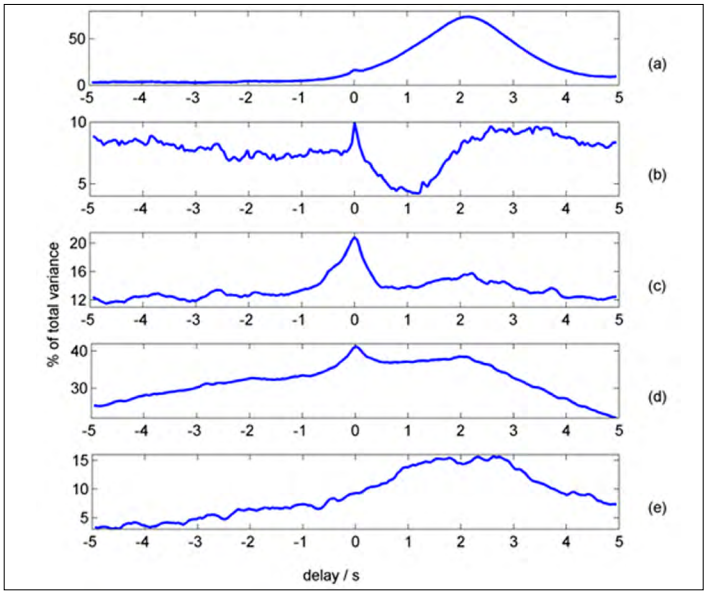

Fig. 8 - Distribution of variance for various delays: light transmittance (a), magnitude of formation (b), length scale of formation (c), anisotropy of fibre orientation (d), and dominant fibre orientation direction (e).

TABLE 2 *Correlation coefficients between the MD profiles*

	μ	σ	E[λ]	$E[\lambda_{CD}]/E[\lambda_{MD}]$	θ
μ	1	0.02	0.11	-0.17	0.20
σ		1	-0.34	0.30	0.01
E[λ]			1	-0.74	-0.21
$E[\lambda_{CD}]/E[\lambda_{MD}]$				1	0.18
θ					1

TABLE 3 *Correlation coefficients between the profiles oriented at the same angle as the diagonal waves*

	μ	σ	E[λ]	$E[\lambda_{CD}]/E[\lambda_{MD}]$	θ
μ	1	-0.22	-0.27	0.25	-0.01
σ		1	-0.14	-0.07	0.01
E[λ]			1	-0.50	-0.13
$E[\lambda_{CD}]/E[\lambda_{MD}]$				1	0.18
θ					1

accordance with the travel time of a pulp consistency variation from back to front in the headbox. Furthermore, the variability of structural characteristics at various delays was studied. The variability in light transmittance and in dominant fibre direction was mainly oriented in the diagonal direction (the reason might be consistency variations), whereas the variability in length scale of formation is strictly oriented in the MD (attributable to the properties of the jet or the speed difference between wire and jet).

Current on-line measurement systems for paper characteristics do not cover the entire web width, and therefore diagonal variation caused by consistency variations entering the headbox cannot be detected. The results of this study indicate that characteristics estimated using WIS images give useful web-wide information for improving the uniformity and control of paper quality on paper machines. Furthermore, the structural characteristics can be estimated from WIS images as such, and the novel analysis method requires only the ability to download the raw images from WIS. The drawback in using downloaded images is the increased delay from measurement to results. However, the characteristics could be estimated in the CPU of the WIS, which would speed up the analytical process and decrease delay.

REFERENCES

1. Ritala, R., "Managing Paper Machine Operation", in: Leiviskä, K. (ed.), Process and Maintenance Management, Fapet Oy, Oulu, Finland (2009).
2. Kjaer, A.P., Heath, W.P., and Wellstead, P.E., "Identification of Cross-Directional Behavior in Web Production: Techniques and Experience", Control Engineering Practice, 3(1):21-29 (1995).
3. Marjanen, K., Ihalainen, H., Yli-Fossi, T., "Measuring Paper Quality by Texture Analysis", Paper Research Symposium, Kuopio, Finland (2009).
4. Kuparinen, T., "Reconstruction and Analysis of Surface Variation Using Photometric Stereo", PhD Thesis, Lappeenranta University of Technology, Lappeenranta, Finland (2008).
5. Shakespeare, J., "Measuring Fibre Orientation by Detecting Dispersion of Polarized Light", Honeywell International, U.S. Patent 7164145 B2 (Issued Jan. 16, 2007).
6. I'Anson, S.J., Constantino, R.P.A., Hoole, S.M., and Sampson, W.W., "Estimation of the Profile of Cross-Machine Shrinkage of Paper", Measurement Science and Technology, 19(1) (2008).
7. Raunio, J.-P., "Estimation of Shrinkage Profile Based on Wire Marking", Master of Science Thesis, Tampere University of Technology, Tampere, Finland (2006).
8. Shakespeare, J., Paavola, A., "Online Measurement of Surface Fibre Orientation", Paper Research Symposium, Kuopio, Finland (2009).
9. Chen, S.-C., Subbarayan, R., Kristinsson, K., and Snyder, R., "Paper Machine Applications with Full-Sheet Imaging Measurement", Control Systems '98 Conference, Porvoo, Finland (1998).
10. Ferguson, K.H., "Full-Sheet Imaging System Becomes Control Reality", Pulp & Paper, 71(10):75-81 (1997).
11. Raunio, J.-P., Ritala, R., "2D Basis Weight Estimation Based on Light Transmittance Imaging", International Control Systems Conference, Stockholm, Sweden (2010).
12. Ylisaari, J., Ritala, R., "Web-Wide Transmittance Imaging Measurement Variability Analysis", International Control Systems Conference, Stockholm, Sweden (2010).
13. Raunio, J.-P., Ritala, R., "Estimation of Basis Weight of Paper: Light Transmittance Measurements over Eight Orders of Magnitude of Spatial Scale", Proceedings, 19th IMEKO World Congress, Lisbon, Portugal (2009).
14. Niskanen, K., Kajanto, I., Pakarinen, P., "Paper Structure", in: Niskanen, K. (ed.), Paper Physics, Fapet Oy, Jyväskylä, Finland (1998).
15. Yu, W., "Practical Anti-Vignetting Methods for Digital Cameras", IEEE Transactions on Consumer Electronics, 50(4), pp. 975-983 (2004).
16. Sonka, M., Hlavac, V., Boyle, R., Image Processing, Analysis, and Machine Vision, 2nd ed., PWS, Pacific Grove, California, USA (1998).
17. Corte, H., Kallmes, O.J., "Statistical Geometry of a Fibrous Network", Transactions of the 2nd Fundamental Research Symposium (Bolam, F., ed.), Oxford, UK, 1961, pp. 13-46 (1961).
18. Draper, N.R., Smith, H., Applied Regression Analysis, John Wiley, New York, USA, 292-293 (1998).
19. Welch, P.D., "The Use of Fast Fourier Transform for the Estimation of Power Spectra: A Method Based on Time Averaging over Short, Modified Periodograms", IEEE Transactions on Audio and Electroacoustics, 15(2), pp. 70-73 (1967).
20. Lim, J.S., Two-Dimensional Signal and Image Processing, Prentice-Hall, New Jersey, USA (1990).
21. Fisher, N.I., Statistical Analysis of Circular Data, Cambridge University Press, England (1993).
22. Dunn, O.J., Clark, V.A., Applied Statistics: Analysis of Variance and Regression, Wiley, New York (1974).
23. Naidu, P.S., Sensor Array Signal Processing, CRC Press, Boca Raton, Florida, USA (2001).
24. Parker, J., "The Sheet-Forming Process", STAR No. 9, TAPPI, Atlanta (1972).

Publication VII

Raunio, J-P and Ritala R. (2013): Method for detecting free fiber ends in tissue paper, *Meas. Sci. Technol.*,Vol. 24, No. 12, pp. 1-6. 125206

Meas. Sci. Technol. **24** (2013) 125206 (6pp) doi:10.1088/0957-0233/24/12/125206

Method for detecting free fiber ends in tissue paper

Jukka-Pekka Raunio and Risto Ritala

Tampere University of Technology, Automation science and engineering, Korkeakoulunkatu 3, FI-33720, Tampere, Finland

E-mail: jukka-pekka.raunio@tut.fi

Received 1 August 2013, in final form 16 September 2013
Published 1 November 2013
Online at stacks.iop.org/MST/24/125206

Abstract
Softness is one of the major properties of tissue paper. Tissue softness can be divided into bulk and surface softness. The bulk softness can be measured quite reliably by measuring the thickness and elasticity of a sheet. However, the measurement of surface softness is not straightforward. One significant factor influencing surface softness is the fibers extending from the surface of the tissue paper. This paper presents a novel imaging method to detect the amount of such fibers on the tissue paper. The method is based on the detection of shadows caused by the free fiber ends. The shadows cannot be detected as such from the reflectance image of the sheet because of the wavy surface of tissue paper. Thus, the 3D information of the surface was estimated based on the photometric stereo, and the intensity variations caused by the wavy surface were filtered out. The method has the advantages over previous methods of improved accuracy and the possibility of implementation in a running paper machine.

Keywords: tissue paper, detection of fibers, photometric stereo, imaging system

1. Introduction

Tissue paper is the general name for toilet paper, paper towel, facial tissues, napkins and other soft paper products. Tissue paper is a sheet-like product manufactured continuously at speeds as high as 35 m s^{-1}. The width of the manufactured paper web in a tissue paper machine can be up to 6 m and the thickness of the paper web is of the order of 50 μm. The tissue paper consists of a random arrangement of wood fibers [1] and smaller particles such as minerals, and chemicals [2]. Tissue products have promising future markets due to their sustainable raw material and lack of competing materials. Therefore it is expected that tissue manufacturing will continue to increase, which increases the financial significance of understanding the phenomena in the tissue-making process.

The most common type of tissue machine is the dry crepe machine in which the sheet is dried on only one drying cylinder, called the Yankee cylinder. The tissue sheet adhere to the Yankee cylinder and is then detached from the surface with a blade [3]. As a result, a strong microstructure—crepe folds—is generated on the paper web. The detaching, known as creping, generates high softness [4] and also stretches the sheet in the machine direction. Although the tissue-making process is quite well known, the final tissue product may not meet the required softness quality of the end-user. One reason for suboptimal quality control is the difficulty of measuring the softness of the tissue paper reliably [4, 5]. The softness of tissue paper is usually studied with softness panel tests in which people evaluate the softness of tissue paper subjectively. Furthermore, several measurement devices have been developed with the goal of correlation with the rating by softness panels [6–8]. However, the instrumental measurements often conflict with panel test results. This is partly because of the uncertainty of factors affecting subjective feeling of softness and partly because the current devices measure the forces that are not on the same sensitivity scale as what humans perceive.

Tissue softness can be divided into two categories: bulk and surface softness. The bulk softness can be estimated reliably by measuring the stiffness and the thickness of the sheet. However, the surface softness is a complex combination of roughness, friction and elasticity of the surface. The fibers extending from the surface of tissue, called free fiber ends, affect such surface properties significantly [5, 9–12]. At present the measuring of free fiber ends is based on a laboratory device that captures an image of a paper folded over the edge [9, 11, 13]. Hollmark and Ampulski [4] suggested that

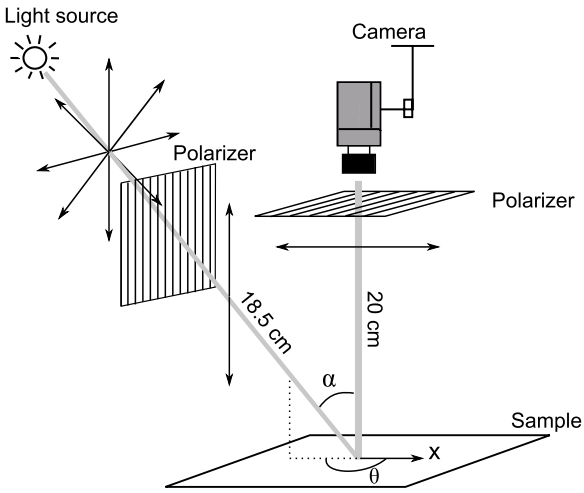

Figure 1. The imaging arrangement of the camera system. The polarizers block the light that is specularly reflected from the surface of the sample. The arrows show the polarization of light.

the artificial robotic fingers studied in medical applications [14, 15] could also be applied in measuring the surface softness of tissue paper. However, implementing such measurements methods in online conditions at a running paper machine would not be realistic.

In this paper we introduce an imaging method that detects fibers extending from the surface of tissue paper based on the shadows of the fibers. The surface of tissue paper is wavy because of the creping process and therefore the shadows of fibers cannot be detected as such from reflectance images of the tissue surface. The detection method presented in this work utilizes the photometric stereo method in which the target is illuminated from 12 directions and the surface normal of each image pixel is estimated [16, 17]. Furthermore, Lambert's law [18] is applied inversely to reconstruct the reflectance image from the estimated surface normals. This action filters discontinuities in the reflectance image such as the shadows of fibers. Finally, the shadows are detected from the difference of the reconstructed reflectance image and the original reflectance image. We demonstrate the method in laboratory conditions. Photometric stereo applications for surface topography measurement have recently been commercialized online [19]. Thus the method presented in this paper, being based on photometric stereo, can be readily implemented online.

This paper is organized as follows. In section 2 the measurement system in this work is presented. Section 3 summarizes the theory of photometric stereo and presents how it is applied in this work: the shadow detection method. Section 4 evaluates the quality of the results based on the results with a reference measurement system. Section 5 concludes the results and discusses the potential and possibilities to apply the measurement system online in a paper machine.

2. The measurement system

The measurement system created during this work is a laboratory device that consists of a digital camera, an LED and the sample holder. The digital camera used in this work had a macro 105 mm lens. The geometric distortion and vignetting caused by the objective was minor so calibration of the camera system was not required. The size of the image sensor was 5184 × 3456 pixels and pixels of each color from the 2 × 2 Bayer matrix (red, green, and blue (RGB)) were applied in this analysis because the color of the LED was white. The pixel values were represented with 14 bits. The size of the imaging area was 21 × 14 mm^2, corresponding 4.1 × 4.1 μm^2 pixels.

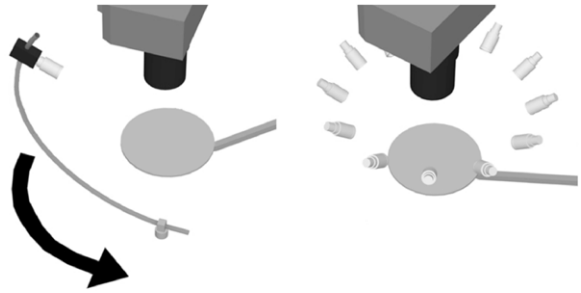

Figure 2. Schematic drawing of the measurement device. The device consists of a digital camera, an LED and the sample holder. The each location of the LEDs during imaging is drawn on the same image on the right.

The origin of the imaging system is set at the center point of the image on the surface of the sample. The distance between the LED and the origin of the imaging system was 18.5 cm and the distance between the CCD (charge-coupled device) sensor of the camera and the origin was 20 cm. The vertical angle between the LED and the surface normal was $\alpha = 30^\circ$ and the horizontal angle between the LED and the x-axis is marked by θ (see figure 1).

Figure 2 shows a schematic drawing of the measurement device and the measurement procedure. The LED was attached to a supporting arm that can rotate around the sample. In this work the sample was illuminated from 12 locations in a horizontal plane and the image was captured in each illumination condition. The horizontal angle between the LED locations was 30° ($\theta = 0^\circ, 30^\circ, 60^\circ, 90^\circ, \ldots, 330^\circ$).

The surfaces can be divided roughly into specular and diffuse surfaces based on the reflection of the target. The photometric stereo method assumes that the reflection of the target is diffuse [16]. The surface of tissue paper is nearly diffuse. However, the wood fibers and mineral pigments in the paper may produce specular reflections and distort the estimation of surface normals. Therefore the unwanted effect of specular reflection was reduced by crossing at 90° two linear polarizers placed in front of the LED and in front of the camera lens [20, 21] (see figure 1). Light that passes the first polarizer is blocked at the second polarizer if the light is specularly reflected. Both polarizers were attached to a supporting arm so the polarizer in front of the camera lens was rotating and thus the orientation between the polarizers was constant during measurement.

The shape of the beam pattern of the LED on the target surface depends on the location and the beaming of the LED. The location of the LED is known accurately in our measurement system. However, the beaming includes uncertainties and therefore the center of the LED beam is not

necessarily located at the origin of the measurement system. Thus the intensity variation on a sample surface caused by the beam pattern of the LED is compensated by a 2D second-order polynomial fitted to the reflectance image. The selection of the second-order polynomial was based on the assumption that the intensity of the light reflected from the sample decreases quadratically when the distance from the center of the LED beam increases. The 2D fitting problem can be defined in matrix form as follows:

$$[\mathbf{1}\ \mathbf{x}\ \mathbf{y}\ \mathbf{xy}\ \mathbf{x^2}\ \mathbf{y^2}][a\ b\ c\ d\ e\ f]^{\mathrm{T}} = i\,, \tag{1}$$

where **x** and **y** are the vectors containing the x and y coordinates of each pixel in the image. The vector i contains the intensity of the image pixels of the original image. The symbols from a to f are the coefficients of polynomial terms that are solved in the least squares sense. The polynomial was fitted to each Bayer matrix color layer separately.

The computation of surface normals with photometric stereo is based on the variation of reflected intensity of the sample surface. The photometric stereo theory assumes that the light arriving at the sample surface is collimated [16]. However, this is not the case in our measurement system because the distance between the light source and the sample is small and the physical size of the LED light source is small. Therefore the orientation of the light beam arriving from the LED varies between the locations of the sample surface. Thus the pixel intensity values must be compensated by computing the distances between each image pixel and the light source. The height of the light source z_{light} is finally divided by the distance as follows:

$$\mathrm{cosSigma} = \frac{z_{\mathrm{light}}}{\sqrt{\sum(\mathbf{x}_{\mathrm{light}} - \mathbf{x}_{\mathrm{sample}})^2}}, \tag{2}$$

$\mathbf{x}_{\mathrm{light}}$ is the (x, y, z)-vector containing the coordinates of the light source. $\mathbf{x}_{\mathrm{sample}}$ is the $(x, y, 1)$-vector containing the coordinates of the sample in the homogeneous coordinates [22]. The compensation result is called cosSigma because it is the cosine of the angle of two vectors. Finally, the original image was multiplied pointwise with the cosSigma-matrix and divided pointwise by the 2D polynomial.

The free fiber end produces a shadow at a certain location on the paper depending on the vertical and horizontal angle of illumination. These shadows are detected to estimate the density of free fiber ends in paper.

2.1. Compensating the variation of illumination of the surface with photometric stereo

In photometric stereo two or more images are captured from a surface illuminated from different directions (see figure 2) [16]. The photometric stereo method estimates the surface normals of a Lambertian surface. A Lambertian (matt) surface is defined as one in which the reflected intensity is independent of the viewing direction [18]. Lambert's law represents the pixel intensity i at the point (x, y) as follows:

$$i = \rho E \mathbf{l}^{\mathrm{T}}_{3\times1}\mathbf{n}_{3\times1}, \tag{3}$$

where ρ is the surface albedo describing the reflectivity of the surface, E is the intensity of the light source, **n** is the unit normal of the surface and **l** is the unit vector toward the light source. In our measurement setup $\mathbf{l}^{\mathrm{T}}$ is

$$\mathbf{l}^{\mathrm{T}} = \begin{pmatrix} \cos(\theta)\sin(\alpha) \\ \sin(\theta)\sin(\alpha) \\ \cos(\alpha) \end{pmatrix}, \tag{4}$$

where θ and α determine the orientation of the LED (see figure 1). The **l** vector must be computed for each image pixel separately because the orientation of the unit vector toward the light source depends on the location of the point on the sample. The ρEn can be solved from equation (3) because the camera measures the pixel intensities (i) and the location of the light source is known (**l**). However, the albedo depends on the spatial location so the unit normal of the surface cannot be solved. Woodham suggested that three light sources is enough to determine the unit normal and the albedo from equation (3) [16]. This technique is also applied in this work. Furthermore, the equally bright light source illuminating from 12 directions are applied to decrease the uncertainty of the estimate. Now Lambert's law can be represented in matrix form as follows:

$$\mathbf{i}_{k\times1} = \rho E \mathbf{L}_{k\times3}\mathbf{n}_{3\times1}, \tag{5}$$

where k is the number of light sources, **i** is the intensity vector of the pixels for each light source, **L** is the matrix consisting of 1×3 unit vectors toward each LED location, **n** is the unit normal of the surface and k is the number of light sources ($k = 12$). The problem is overdetermined for a single pixel with 12 light sources and scaled unit normal **m** (scaled by the albedo) and can be solved by minimizing the square of error with pseudoinverse as

$$\rho E\mathbf{n} = \mathbf{m} = (\mathbf{L}^{\mathrm{T}}\mathbf{L})^{-1}\mathbf{L}^{\mathrm{T}}\mathbf{i}. \tag{6}$$

The equation is applied for each image pixel separately and this results in a scaled unit normal for each point on the surface represented by pixels.

The photometric stereo method squeezes the information from 12 reflectance intensities into three point vector (= surface normals) and thus averages out any outliers caused by, e.g., the shadows. Next Lambert's law (3) was applied inversely to reconstruct the reflectance intensities from the estimated surface normals. The reconstructed reflectance intensities were subtracted from the original reflectance intensities and the shadows were detected from the difference. Figure 3 shows the small portion of the original reflectance image illuminated from the direction of the lower edge (a) and the reconstructed reflectance image from the same area computed with the method described above (b). The figure also shows the difference image (c) between the original and the reconstructed reflectance images. The mean was removed from the images and the variance scaled to unity before the subtraction. Furthermore, spatial variations larger than 0.3 mm were removed from the difference image with a linear 2D Bessel high-pass filter [23].

It can be seen that the shadow caused by the fiber is extremely faint in the original reflectance images (see figure 4(a)) but the difference image (figure 4(c)) reveals the shadows more clearly. The maximum distance between the shadow and the fiber is 80 μm in the y-direction ($\theta = -90^{\circ}$), indicating that the difference in height between the fiber end

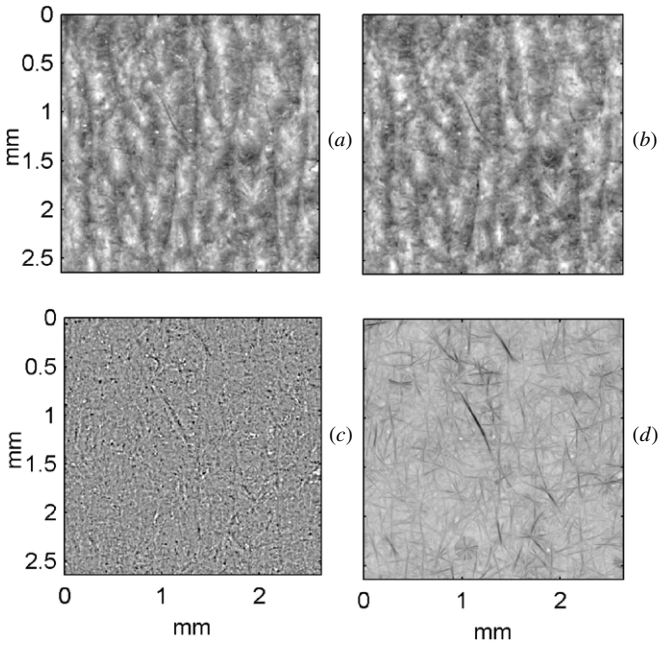

Figure 3. Close-up of the original image (*a*), the reconstructed image (*b*), the difference between the images (*c*) and the processed image $O(x, y)$ which amplifies the shadows (*d*).

and the tissue paper surface is $\tan(60^\circ) \times 80\ \mu\text{m} \approx 140\ \mu\text{m}$. However, in most cases the fiber causing the shadow is invisible to the camera or difficult to detect. Therefore only the number of free fiber ends on the surface is obtained in this work, not the orientation or the height.

2.2. Detection of shadows

The shadows caused by the fibers can be seen as faint dark curves in the difference image (see figure 4(*c*)). In this work the detection of shadows is based on a line detection method called 'orientated means' in which the mean is computed for each pixel location and orientation of the line [24]. The method reinforces the shadows, making their detection easier. The typical width of the wood fibers in tissue paper is 20 μm and the length of fibers varies typically from 200 μm to 1000 μm [2]. However, the length of the shadows varies depending on the angle and the extent of the free end of the fiber in the paper surface being usually shorter than the length of the fiber. Therefore objects longer than 100 μm are reinforced from the difference image. Let $I(x, y)$ be a continuous function representing the image intensities given in a two-dimensional domain. The mean of an object at orientation θ is denoted as follows [24]:

$$F(x_0, y_0, L, W, \theta) = \frac{1}{WL}\int_{-W/2}^{W/2}\int_{-L/2}^{L/2} I(x_0 + x\cos\theta - y\sin\theta, y_0 + x\sin\theta + y\cos\theta)\,\mathrm{d}y\,\mathrm{d}x \quad (7)$$

where L is the length of the object (= 100 μm) and W is the width of the object (= 20 μm). The mean is computed for several orientations. The shadows are darker than the rest of the variation in paper and thus the minimum orientation value is selected for the resulting image. The minimum mean for several orientations can be denoted as follows:

$$O(x, y) = \min_{\theta\in[0,\pi]}(F(x, y, L, W, \theta)), \quad (8)$$

where $O(x, y)$ is the resulting image presented in figure 3(*d*).

The shadow objects can be detected from $O(x, y)$ by thresholding. First, the histogram which shows the distribution of pixel values was computed. The threshold limit was set to 0.2%. The threshold limit was selected based on the fiber counts of the reference measurement system introduced in the next section. From the binary image only objects whose length is larger than 100 μm are accepted. Furthermore, the shape of the object should be elongated. Therefore the lengths of the minor and major axes of an ellipse fitted to the each object were calculated. The ellipse fitting algorithms are based on the 2D normal distribution fitted to the coordinate points [25]. The covariance matrix (Σ) of the 2D normal distribution can be written in terms of the standard deviations σ_x and σ_y and correlation ρ between the x and y coordinates of the object as follows:

$$\Sigma = \begin{pmatrix} \sigma_x^2 & \rho\sigma_x\sigma_y \\ \rho\sigma_x\sigma & \sigma_y^2 \end{pmatrix}. \quad (9)$$

The eccentricity of the corresponding ellipse is given by

$$e = \left(\frac{2\left(\left(\sigma_x^2 - \sigma_y^2\right)^2 + \rho^2\sigma_x^2\sigma_y^2\right)^{1/2}}{\sigma_x^2 + \sigma_y^2 + \left(\left(\sigma_x^2 - \sigma_y^2\right)^2 + \rho^2\sigma_x^2\sigma_y^2\right)^{1/2}}\right)^{1/2}. \quad (10)$$

In this work objects whose major axis was at least five times longer than the minor axis, i.e. those with eccentricity larger than $2\sqrt{6}/5$, are accepted in the final binary image. Figure 5 shows the threshold binary image (*a*) and the final binary image

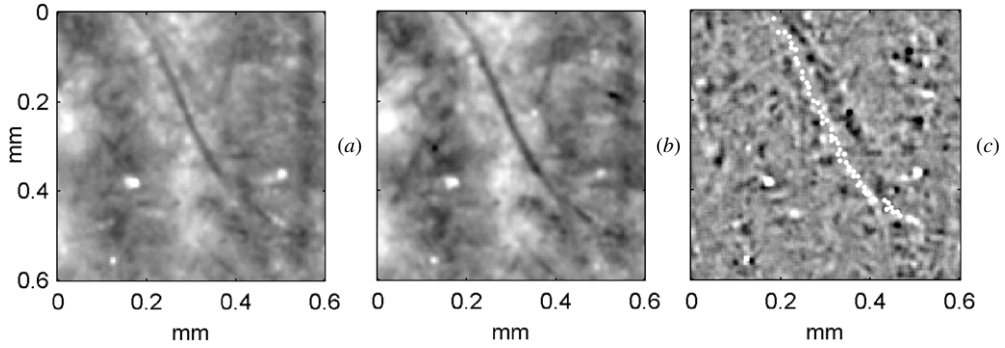

Figure 4. A further close-up from the location of the dark fiber in the middle of the images presented in figures 3(*a*)–(*c*). The white dots (*c*) show the location of the dark fiber as estimated from the original reflectance image (*a*).

Table 1. The averages and standard deviations of free fiber end densities estimated with the reference measurement system and the novel imaging system (36 samples per grade).

	Kitchen towel	High-quality facial tissue	Low-quality facial tissue	High-quality toilet paper	Low-quality toilet paper
Avg_{ref}	42.4	124.8	71.6	90.9	41.5
Std_{ref}	19.7	25.5	19.8	16.2	18.0
Avg_{img}	52.0	127.5	64.1	93.9	43.8
Std_{img}	14.6	7.9	7.8	11.1	15.2

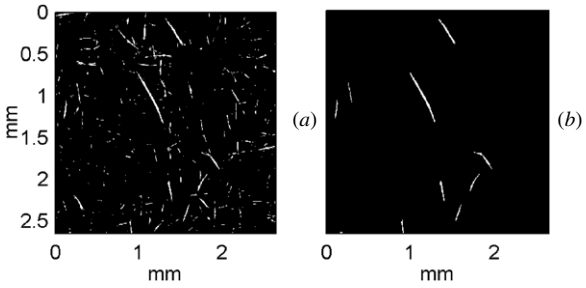

Figure 5. The threshold binary image (*a*) and the binary image from which the circular objects are removed (*b*).

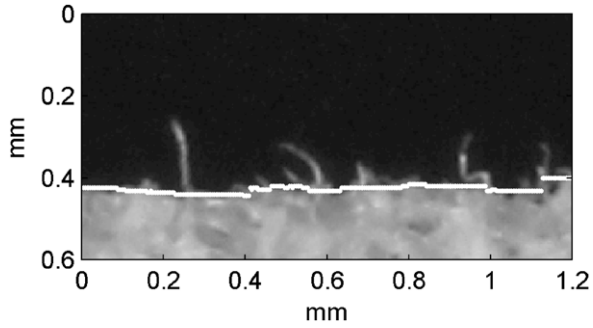

Figure 6. Close-up of the surface of folded tissue paper. The estimated surface boundary is drawn on the image with white dots.

in which the objects having eccentricity larger than $2\sqrt{6}/5$ are presented (*b*).

The objects detected from the binary image may not be shadows of fibers but, for example, color variations in paper or shadows of crepe folds. Thus the uncertainty of detection was decreased by estimating two difference images, detecting the shadows from both images, and computing the average of counts. Furthermore, the direction of illumination in reflection images from which the difference image was estimated was perpendicular to the propagation of the creping pattern, decreasing the probability of detecting shadows caused by crepe folds.

3. Evaluating the performance of the imaging system

The performance of the imaging method presented in this paper was evaluated with a reference measurement similar to the one introduced in [9, 13]. The measurement procedure is as follows: the tissue paper sample was folded over an edge and the image of the folded edge of the tissue paper was captured with a digital camera. Figure 6 shows an example of the folded tissue paper. The long fibers extending from the surface can be seen clearly. The exact surface boundary in the tissue paper sample is difficult to determine. Therefore only the free fiber ends that extend from the assumed surface boundary of the tissue paper by more than 50 μm are counted. The surface boundary was estimated by computing the difference of the pixel vector in the *y*-direction for each *x* location. The maximum difference in *y*-direction was obtained and the mean value from the neighboring surface boundary points in the *x*-direction was computed. Figure 6 shows an example of the estimated surface boundary (white dots) superimposed on the folded edge image. Fibers whose location was more than 50 μm above the estimated surface boundary were considered to be free fiber ends. The width of the folded edge was approximately 2 mm and this width was used to estimate the density of free fiber ends per area. The adjustable parameters in the novel imaging method—the length of shadows considered to be shadows of the free fiber ends and the threshold level in conversion from grayscale to binary image—were chosen to minimize the difference between the two independent measurements.

The results of the reference and the imaging method were compared for five widely manufactured tissue grades. The samples were collected from commercial tissue machines in North America. The grades were kitchen towel, low-quality facial tissue, high-quality facial tissue, low-quality toilet paper and high-quality toilet paper. The tissue paper samples were cut on the top of a machine reel so that the embossing, printing or other converting processes had not affected the structure of tissue paper samples. Densities of free fiber ends (fibers cm^{-2}) in each grade were measured in 36 samples with a reference measurement system and with our imaging system (see table 1). The fibers were counted from the side of the tissue paper that had been in contact with the Yankee cylinder, which is usually the softer side of the tissue paper.

It can be seen that the results of the novel imaging method follow the results of the reference method. The amount of fibers was highest in high-quality facial tissue, second highest in high-quality toilet paper, third highest in low-quality facial tissue and smallest in kitchen towel and low-quality toilet paper. Furthermore, the magnitudes of the standard deviation are significantly smaller in the novel imaging method, which is because of the larger measurement area that decreases the uncertainty. The surprisingly small standard deviations in high-quality and low-quality facial tissues could be explained with the more stable tissue-making process. However, it can be seen that the fiber counts of our imaging method differ slightly from the results of the reference measurement system

in each grade. The count difference can be explained with the different measurement technique: the reference method counts particularly the extending fibers whereas the novel imaging method counts the shadows of fibers. It is possible that the slant angle of a fiber is so small that the reference method ignores the fiber in its count whereas the novel imaging method may still detect the shadow of such a tilted fiber. Furthermore, the folding of tissue paper may straighten up certain fibers that otherwise lie flat on the surface, and thus cause the difference in the counts.

4. Conclusions

Softness is one of the major properties of tissue paper. Softness can be divided to bulk and surface softness. One significant factor affecting the surface softness is the density of free fiber ends. In this work the planar measurement method based on digital images, which measures the density of such fibers on the surface of tissue paper, was presented.

The imaging method presented in this paper was compared to a commonly used reference method which detects the fiber reliably but cannot be applied in online conditions at the paper machine. The novel imaging method does not require any additional folding of paper and the images can be captured from above the paper surface. Thus by applying high-speed cameras and fast LED pulsing the measurement system could be used at a running paper machine. Woodham [17] extended the photometric stereo to a moving surface by using an RGB camera and light sources with distinct colors. At the moment the topography of a paper surface can be measured with a commercial online device that is based on three colors of light and an RGB camera [19]. Thus the development of an online system consisting more than three colors of light is possible but requires multiwavelength cameras, or extremely short exposure times, short light pulses and highly accurate alignment of images.

It was noticed that the results of the novel free fiber end counting method follow the results of the reference method and that the standard deviation in fiber counts in the novel imaging method was significantly smaller, indicating good repeatability of measurement. The results of this work provide a good starting point for developing an online free fiber end measurement system.

References

[1] Corte H and Kallmes O J 1961 Statistical geometry of a fibrous network *Trans. 2nd Fund. Res. Symp. (Oxford, 1961)* ed F Bolam (London: British Papers and Board Makers' Association) pp 13–46

[2] Niskanen K 1998 Paper structure *Paper Physics* ed K Niskanen, I Kajanto and P Pakarinen (Jyvaskyla: Fapet) pp 13–53

[3] Oliver J 1980 Dry-creping of tissue paper a review of basic factors *Tappi J.* **63** 91

[4] Hollmark H and Ampulski R S 2004 Measurement of tissue paper softness: a literature review *Nord. Pulp Pap. Res. J.* **19** 345

[5] Patterson T 2013 Evaluating and enhancing tissue softness *Tappi, Papercon Conf. (Atlanta, GA)*

[6] Kawabata S 2002 Testing the tactile properties of tissue and nonwovens *Handbook of Physical Testing of Paper* vol 2 ed B Lyne and M Habeger p 505

[7] Kuo L-S and Cheng Y-L 1997 A novel method of testing surface softness of household papers—CK method *J. Exp. Forest NCHU* **19** 53

[8] Sarimveis H and Retsina T 2000 Tissue softness prediction using neural network methodologies *Paptac, 86th Annu. Meeting (Montreal, Canada, 2000)* pp 27–30

[9] Pawlak J J and Elhammoumi A 2011 Image analysis technique for the characterization of tissue softness *Int. Paper Physics Conf. (Graz, Austria)* pp 231–8

[10] Allen D B 1994 Development of a mechanical stylus based surface analysis system for soft paper products *Tappi, Nonwovens Conf. Proc. (Orlando, FL)* pp 133–8

[11] Carstens J E 1981 Layered paper having a soft and smooth velutinous surface, and method of making such paper *US Patent* 4300981

[12] Gallay W 1976 Textural properties of paper: measurements and fundamental relationships *The Fundamental Properties of Paper Related to its Uses* ed F M Bolan (London: British Papers and Board Makers' Association) pp 684–95

[13] Fibro Systems AB 2013 FRT1090 Fibre Rising Tester (www.fibro.se/download/FRT_1090.pdf) Accessed 12 Sep 2013

[14] Howe R D and Cutkosky M R 1992 Touch sensing for robotic manipulation and recognition *The Robotics Review* vol 2 ed O Kutib *et al* (Cambridge, MA: MIT Press) pp 55–112

[15] Howe R D and Cutkosky M R 1993 Dynamic tactile sensing: perception of fine surface features with stress rate sensing *IEEE Trans. Robot. Autom.* **9** 140

[16] Woodham R J 1980 Method for determining surface orientation from multiple images *Opt. Eng.* **19** 139

[17] Woodham R J 1994 Gradient and curvature from photometric-stereo method including local confidence estimation *J. Opt. Soc. Am.* **11** 3050

[18] Lambert J 2001 *Photometry, or, On the Measure and Gradiations of Light, Colors, and Shade: translation from the Latin of photometria, sive, de mensura et gradibus luminis, colorum et umbrae* (New York: Illuminating Engineering Society of North America)

[19] Metso Automation Inc Metso IQ fiber orientation measurement 2012 (www.metso.com/Automation/docs2.nsf/0/029E6268A706E086C2257A23003D8057/$file/E8935_EN_01%20IQ%20Fiber%20Orientation%20www.pdf) Accessed 3 May 2013

[20] Wolff L B 1990 Surface orientation from two camera stereo with polarizers *Proc. Conf. of Optics, Illumination and Image Sensing for Machine Vision IV* pp 287–97

[21] Saito M, Sato Y, Ikeuchi K and Kashiwagi H 1999 Measurement of surface orientations of transparent objects using polarization in highlight *CVPR'99: Proc. IEEE Conf. on Computer Vision and Pattern Recognition (23–25 June, Fort Collins, CO)* pp 381–6

[22] Sonka M, Hlavac V and Boyle R 1998 *Image Processing, Analysis, and Machine Vision* (Pacific Grove, CA: Brooks/Cole)

[23] Lim J S 1990 *Two-Dimensional Signal and Image Processing* (Englewood Cliffs, NJ: Prentice-Hall)

[24] Galun M, Basri R and Brandt A 2007 Multiscale edge detection and fiber enhancement using differences of orientated means *ICCV'07: IEEE 11th Int. Conf. on Computer Vision (14–21 Oct. 2007, Rio de Janeiro)* pp 1–8

[25] Fitzgibbon A, Pilu M and Fisher R B 1999 Direct least square fitting of ellipses *IEEE Trans. Pattern Anal. Mach. Intell.* **21** 476

Tampereen teknillinen yliopisto
PL 527
33101 Tampere

Tampere University of Technology
P.O.B. 527
FI-33101 Tampere, Finland

ISBN 978-952-15-3416-4
ISSN 1459-2045